



Government of **Western Australia**
Department of **Mines and Petroleum**

RECORD 2014/3

REGOLITH GEOCHEMISTRY AND MINERAL PROSPECTIVITY — THE SOUTHEAST YILGARN CRATON AND EAST ALBANY–FRASER OROGEN

by
AJ Scheib



Geological Survey of Western Australia



Government of **Western Australia**
Department of **Mines and Petroleum**

Record 2014/3

REGOLITH GEOCHEMISTRY AND MINERAL PROSPECTIVITY — THE SOUTHEAST YILGARN CRATON AND EAST ALBANY–FRASER OROGEN

by
AJ Scheib

Perth 2014



**Geological Survey of
Western Australia**

MINISTER FOR MINES AND PETROLEUM
Hon. Bill Marmion MLA

DIRECTOR GENERAL, DEPARTMENT OF MINES AND PETROLEUM
Richard Sellers

EXECUTIVE DIRECTOR, GEOLOGICAL SURVEY OF WESTERN AUSTRALIA
Rick Rogerson

REFERENCE

The recommended reference for this publication is:

Scheib, AJ 2014, Regolith geochemistry and mineral prospectivity — the southeast Yilgarn Craton and east Albany–Fraser Orogen:
Geological Survey of Western Australia, Record 2014/3, 50p.

National Library of Australia Card Number and ISBN 978-1-74168-550-3

Grid references in this publication refer to the Geocentric Datum of Australia 1994 (GDA94). Locations mentioned in the text are referenced using Map Grid Australia (MGA) coordinates, Zone 51. All locations are quoted to at least the nearest 100 m.

Disclaimer

This product was produced using information from various sources. The Department of Mines and Petroleum (DMP) and the State cannot guarantee the accuracy, currency or completeness of the information. DMP and the State accept no responsibility and disclaim all liability for any loss, damage or costs incurred as a result of any use of or reliance whether wholly or in part upon the information provided in this publication or incorporated into it by reference.

Published 2014 by Geological Survey of Western Australia

This Record is published in digital format (PDF) as part of a digital dataset on CD and is available online at <www.dmp.wa.gov.au/GSWApublications>.

Further details of geological products and maps produced by the Geological Survey of Western Australia are available from:

Information Centre
Department of Mines and Petroleum
100 Plain Street
EAST PERTH WESTERN AUSTRALIA 6004
Telephone: +61 8 9222 3459 Facsimile: +61 8 9222 3444
www.dmp.wa.gov.au/GSWApublications

Contents

Abstract	1
Introduction.....	2
Study area.....	2
Geology.....	2
Southeast Yilgarn Craton – Eastern Goldfields Superterrane.....	5
Albany–Fraser Orogen	5
Northern Foreland Zone.....	5
Biranup Zone.....	6
Fraser and Nornalup Zones.....	6
Recherche and Esperance Supersuites	6
Tectonic events.....	6
Metasedimentary units	6
Gunbarrel and Eucla Basins.....	7
Regolith.....	7
Formation of regolith carbonate.....	9
Regolith carbonate and Au	9
Mineral deposits and prospects	9
Methods – sampling and analyses.....	11
Regolith sampling	11
Analytical methods	11
Quality control	11
Statistical and spatial data analysis	14
Results – regolith geochemistry	14
Regolith matrix.....	14
Major element chemistry, LOI and pH	14
Assessing carbonate contents in regolith samples	14
Variation across regolith types	16
Relating the regolith matrix to the fine-fraction chemistry.....	19
Discussion of the regolith matrix	20
Trace element chemistry in the fine fraction.....	24
Gold.....	24
Assessment of digestion methods for the fine fraction	24
Multi-element associations and groupings in the fine fraction	30
Chalcophile index	30
Ferro-alloy index.....	31
Rare earth element index	37
Base metal index	37
Relationship of indices to regolith type	37
Discussion of trace element data.....	39
Gold in the fine-fraction of the regolith	39
Element extractability	39
Element associations.....	40
Summary and conclusions.....	40
References	41

Appendices

Appendix 1: Site coordinates for all GSWA samples collected in the study area.....	44
Appendix 2: List of analytical methods carried out for each sample collected in the study area	45
Appendix 3: Median concentrations of 52 trace elements in the fine fraction	48
Appendix 4: Bivariate plots of concentrations following TerraLeach and aqua regia digestions	49

Figures

1.	Map of the study area showing GSWA sample site locations, transport routes, topographic localities, homesteads and a selection of mineral deposits and prospects in the area	3
2.	Simplified bedrock geology of the study area derived from the 1:500 000 scale Interpreted bedrock geology map of Western Australia and the 1:500 000 Interpreted pre-Mesozoic bedrock geology of the east Albany–Fraser Orogen and southeast Yilgarn Craton	4
3.	Regolith map of the study area derived from the 1:500 000 scale regolith cover map of Western Australia	8
4.	Pictures of a sandy colluvium, a sandy soil with abundant ferruginous lag, a cross section through approximately 1 m of transported laterite and a view of the sandplain landscape at Mulga Rock	10
5.	Distribution of GSWA sample sites indicating the method and digestion applied as part of the analytical program	13
6.	Graduated colour dot map of loss on ignition (LOI) data for 151 regolith samples	17
7.	Graduated colour dot map of pH data for 151 regolith samples	17
8.	Graduated colour dot map of the SiO ₂ concentration in 151 regolith samples	18
9.	Graduated colour dot map of the CaO concentration in 151 regolith samples	18
10.	Graduated colour dot map of the CIA for 151 regolith samples	19
11.	Bivariate plots of the SiO ₂ to CaO ratio against LOI, pH; and the chemical index of alteration (CIA) for 151 regolith samples	20
12.	Box-and-whisker plots of CaO and SiO ₂ concentrations, LOI, and pH values in the coarse fraction for the six regolith types present in the study area	21
13.	Bivariate plot of extractable Ca concentrations following various digestions of the <50 µm fraction against total CaO concentrations in the <2 mm to >45 µm fraction	22
14.	Bivariate plots of the extractable Ca and total CaO concentration against LOI, SiO ₂ concentration, pH, and CIA	22
15.	Bivariate plots of the ratio of SiO ₂ to CaO concentrations in the coarse fraction against aqua regia (AR)-extractable concentrations of Sr and Rb, and the ratios of Rb to Sr and Rb to Ca in the fine fraction	23
16.	Box-and-whisker plot of Au concentrations determined using AR, TerraLeach (TL)9, TL7, and TL0 digestions, and fire assay (FA)	25
17.	Bivariate plots of AR-extractable Au concentrations against Au concentrations determined by FA, TL7, TL9, and TL0	26
18.	Graduated colour dot map of the AR-extractable Au concentrations in 151 regolith samples	27
19.	Bivariate plots of AR, TL7, TL9, and TL0-extractable Au concentrations against the AR-extractable Ca concentrations and the Rb to Ca ratio	28
20.	Box-and-whisker plots of the AR-extractable and FA Au concentrations grouped by the six regolith types in the study area	29
21.	Bivariate plot of total vs AR-extractable concentrations of Zn, Ba, and Zr in the fine fraction of 50 regolith samples	30
22.	Bar chart of contrast ratios for 48 elements calculated for extractable data of the fine fraction	31
23.	Distribution of the chalcophile index for 151 regolith samples across the study area	32
24.	Distribution of the ferro-alloy index for 151 regolith samples across the study area	33
25.	Distribution of the rare earth element index for 151 regolith samples across the study area	34
26.	Distribution of the base metal index for 151 regolith samples across the study area	35
27.	Bivariate plots of the chalcophile, ferro-alloy, rare earth element, and base metal indices against the AR-extractable concentrations of Ca, Rb/Ca ratio, Au, and Pb	36
28.	Box-and-whisker plots of the chalcophile, ferro-alloy, rare earth element, and base metal indices grouped by the six regolith types found in the study area	38

Tables

1.	List of GSWA 1:250 000 and 1:100 000 scale geology map sheets covering the study area with corresponding number of samples	5
2.	Regolith types and associated number of samples based on the 1:250 000 scale Fraser Range Regolith map and the 1:500 000 scale State regolith map	8
3.	List of analytical methods, sample number, size fraction, and determinants used in the study	12
4.	Major element total concentrations of eight regolith samples analysed by both ICP-MS and XRF	15
5.	Summary statistics of the total major element chemistry and values for LOI, pH, and chemical index of alteration (CIA) for the coarse fraction of 151 regolith samples	16
6.	Summary statistics of total CaO and extractable Ca concentrations determined by aqua regia, sodium pyrophosphate (TL9), hydrochloric acid (TL7), and deionized water (TL0) digestions	23
7.	Summary statistics of extractable Au concentrations from digestions using AR, TL9, TL7, and TL0, and Au concentration determined by fire assay (FA) in the coarse fraction	25
8.	Summary of Spearman ranked correlation coefficients between all extractable Au and Ca concentrations in the fine fraction and total CaO concentrations and loss on ignition (LOI) in the coarse fraction of 151 regolith samples	25

Regolith geochemistry and mineral prospectivity — the southeast Yilgarn Craton and east Albany–Fraser Orogen

by

AJ Scheib

Abstract

The prospectivity of the southeast Yilgarn Craton and east Albany–Fraser Orogen, a greenfields area in Western Australia, has been improved by the recent discoveries of the Nova Ni–Cu and Tropicana Au deposits. Surface anomalies detected by fine-fraction, low-density geochemical data from regolith may indicate additional buried mineralization in this region.

Multi-element geochemical data for 151 regolith samples from the southeastern Yilgarn Craton and east Albany–Fraser Orogen, following total and partial digestion, were used to assess the influence of grain size and sample digest on element concentrations. The relationship between regolith type and composition, in particular carbonate content, distribution of Au in regolith, effectiveness of various digests in relation to trace element concentrations in the fine fraction, and use of additive indices to examine trace element associations, were investigated.

The regolith geochemistry showed sampling and analysis should focus on the fine, <50 µm fraction using aqua regia as the preferred digest. All other digests yield much lower concentrations than aqua regia, with the exception of a hydrochloric acid leach, which seemed to work well for extracting rare earth elements. Lower concentrations were also determined for the <2 mm fraction, caused by dilution by commonly barren eolian sand.

In terms of the influence of carbonate in regolith, all of the Au datasets indicated only a weak and inconsistent relationship between Au and Ca, and between Au and loss on ignition (LOI) data. The exception is a series of colluvium and sandplain samples with anomalous Au concentrations of >13.8 µg/kg collected over Albany–Fraser Orogen meta-granitic and meta-mafic rocks of the Northern Foreland close to the Cundeelee Fault, which have a well-established carbonate signature.

Associations of chalcophile, ferro-alloy, and base metal elements show that anomalous samples are almost entirely related to transported regolith over the Albany–Fraser Orogen. However, in the Northern Foreland close to the Cundeelee Fault, northwest of Fraser Range homestead, and the Biranup Zone near Ponton Creek, north of Zanthus, the chemistry of transported regolith seems to be closely related to local bedrock and possibly bedrock-hosted mineralization. Regolith samples along Ponton Creek also have a strong signature of rare earth elements. Here, regolith samples are predominantly silicate-rich and carbonate-poor colluvium that is spatially related to outcrops of strongly foliated, garnetiferous granitic gneiss.

Regolith samples from the northern part of the study area do not indicate any anomalous elemental concentrations. This is probably due to thicker cover, in particular over the Gunbarrel Basin, and a higher proportion of recent, barren eolian material that is commonly found across the basin and the northeastern Albany–Fraser Orogen.

KEYWORDS: gold, greenfields, carbonate rocks, grain size, digestion, weathering, multi-element analysis

Introduction

Regolith geochemistry has been widely used to evaluate mineral prospectivity in areas dominated by residual regolith, although its usefulness in areas dominated by transported regolith is less certain. This Record demonstrates that regolith geochemistry can be used to see through transported cover in the southeast Yilgarn Craton and east Albany–Fraser Orogen, providing further evidence for expansion of mineral exploration across this greenfields area. This area is largely covered by transported regolith dominated by eolian sand and colluvium, with very little exposed bedrock. However, the mineral prospectivity of the area has been highlighted by the discovery of the Tropicana–Havana gold (Au) and the Nova nickel–copper (Ni–Cu) deposits. These discoveries have prompted work by GSWA to better understand the Albany–Fraser Orogen and its relationship to the Yilgarn Craton (Spaggiari et al., 2011). Such geological and geophysical mapping helps to understand and develop a geological framework, although it is important for mineral exploration to determine whether regolith geochemistry can be used to detect different bedrock types and bedrock-hosted mineralization.

Research and exploration for Au in regolith-dominated terrains indicated a relationship between secondary carbonate accumulations and anomalous Au concentrations. As a result, exploration efforts have concentrated on sampling the most carbonate-rich part of the regolith profile, particularly in parts of the Yilgarn Craton in Western Australia and the Gawler Craton in South Australia (Lintern and Butt, 1993, 1997; Lintern, 1997, 2001; Hill et al., 1998; Chen et al., 2002; Butt et al., 2005; McQueen, 2006). In Western Australia, regolith carbonate has been successfully used to detect buried mineralization not only at the Tropicana–Havana deposit, but also at the Aphrodite deposit (Joyce et al., 2005), the Kanowna Belle and Karari deposits (Anand and Dell, 2005; Gray et al., 2005), and the Panglo deposit (Scott and Howard, 2005). The recent discovery of the Nova Ni–Cu deposit followed drilling of an electromagnetic feature (Geoscience Australia, 2013) and a surface anomaly of Ni and Cu reported by Morris et al. (2000) in a sheetwash sample in the same area. Recent soil augering to the northwest of the Nova deposit also returned several large Au anomalies (Sirius Resources, 2013). In addition, Enterprise Metals Ltd (2012a,b) has announced several multi-element anomalies at its Fraser Range project, including one Au soil anomaly (named ‘Microwave’) some 35 km southeast of Nova, and one ‘Nova-style’ soil anomaly at Plato, southeast of the Fraser Range homestead. All these anomalies show that systematic regolith sampling may be a valid exploration tool.

This Record evaluates multi-element geochemical data from regolith of the southeastern Yilgarn Craton and east Albany–Fraser Orogen, with a particular focus on the relationship between Au and regolith carbonate. The data are also used to assess the multi-element chemistry of the fine and coarse fractions of the regolith in relation to the regional bedrock geology and related mineralization, and the effectiveness of various digestion methods in this sand-dominated greenfields area. The use of additive indices is also discussed.

Study area

The study area is located approximately 200 km east of Kalgoorlie (Fig. 1) and includes 151 samples collected between latitudes 33.2°S and 28.9°S and longitudes 122.1°E and 124.8°E (Fig. 1), some of which form part of two previous GSWA regional geochemical mapping programs of the Fraser Range region (Morris et al., 2000) and East Wongatha area (Morris, 2013a).

The study area is dominated by an arid to semiarid climate with an average annual rainfall of around 250 mm (Bureau of Meteorology (BOM) data for Fraser Range Station 12029 from 2011), which decreases from the southwest to the northeast. Annual potential evaporation is >2500 mm (Butt et al., 1977, 2005). Streams are ephemeral although some swamps, and gnamma holes retain water throughout the year, except in the driest months.

Samples collected in the study area extend over a southwest to northeast distance of approximately 500 km, taking in different vegetation zones. The southwestern part of the study area (extending north to the Trans-Australian Railway) corresponds to the biogeographic Coolgardie region and the northeastern half to the Great Victoria Desert region (Department of Environment, 2012).

The dominant vegetation types of the southwestern part comprise eucalypt woodlands, and mallee woodlands and shrublands (Department of the Environment and Water Resources, 2007). In the northeastern part, the vegetation changes into predominantly Hummock grasslands (spinifex) over the sandy and flat-lying desert environment of the Great Victoria Desert with some occasional acacia forests and shrublands.

The study area is fairly low-lying (200–300 m) and dominated by little relief, particularly over the Gunbarrel and Eucla Basins (Fig. 2). The Fraser Range, trending northeast across the central part of the study area, is the dominant topographic feature, comprising undulating hills and isolated low ridges with elevations above 300 m. Mount Pleasant, near Fraser Range homestead, is the highest peak at 579 m.

Geology

The geology of the study area includes granite–greenstones of the Archean Yilgarn Craton, Archean–Proterozoic metamorphic rocks of the Albany–Fraser Orogen, and Phanerozoic sedimentary rocks of the Gunbarrel and Eucla Basins (Fig. 2).

A summary of the regional geology is presented below, based on Cassidy et al. (2006), Spaggiari et al. (2011), and as shown in Spaggiari and Pawley (2012). An interpreted bedrock geology map is based on Tyler and Hocking (2008) and Spaggiari and Pawley (2012). More detailed lithological information at 1:250 000 and 1:100 000 scales can be extracted from the geological map series listed in Table 1, and from the digital Geological Exploration package (GSWA, 2011).



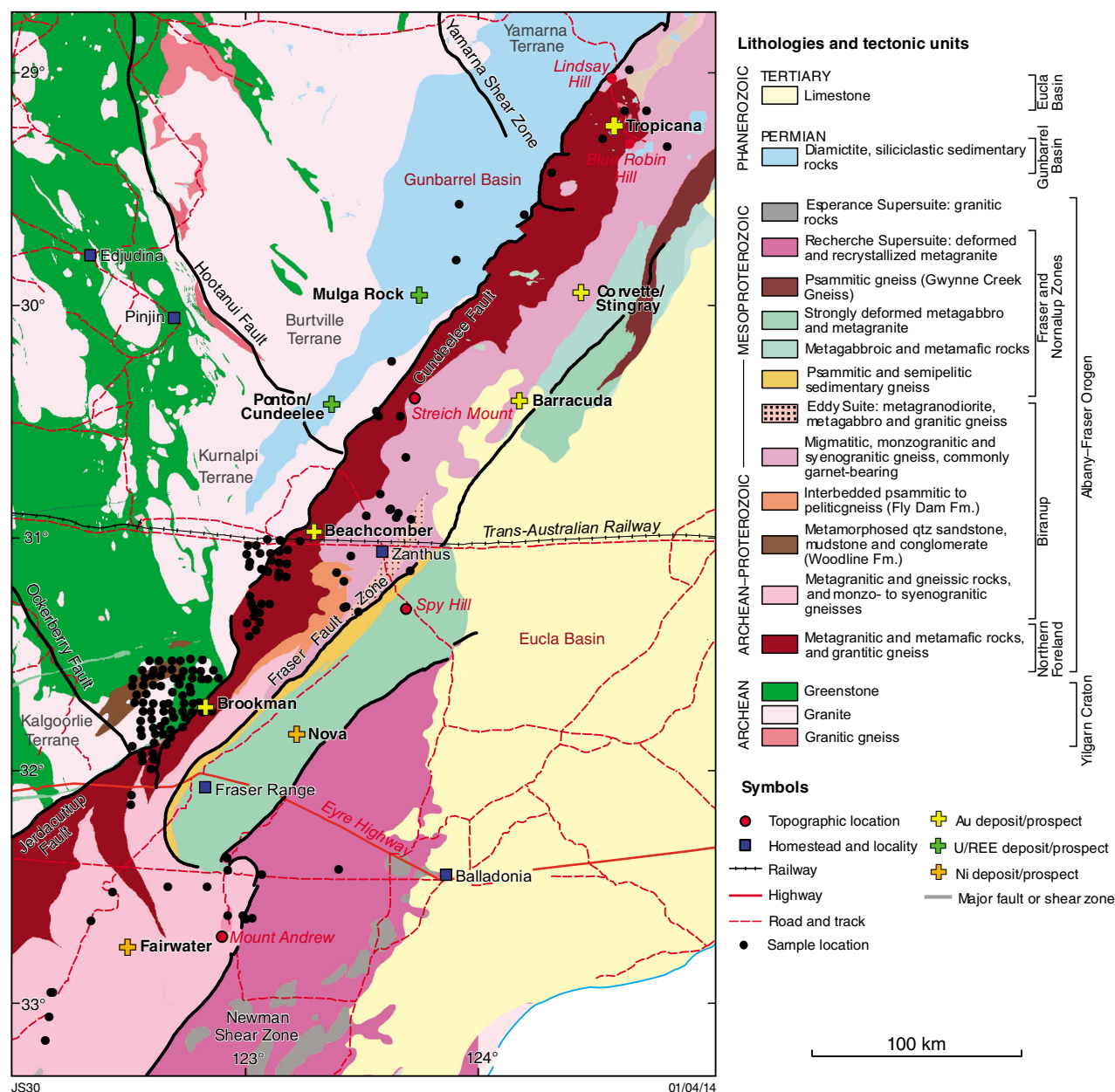


Figure 2. Simplified bedrock geology of the study area derived from the 1:500 000 scale Interpreted bedrock geology map of Western Australia (Tyler and Hocking, 2008) and the 1:500 000 Interpreted pre-Mesozoic bedrock geology of the east Albany–Fraser Orogen and southeast Yilgarn Craton (Spaggiari and Pawley, 2012); map also shows a selection of mineral deposits and prospects, and major fault and shear zones (Pawley et al., 2012; Spaggiari and Pawley, 2012)

Table 1. List of GSWA 1:250 000 and 1:100 000 scale geology map sheets covering the study area with corresponding number of samples

1:250 000 map sheet	1:100 000 map sheet	Number of samples
MINIGWAL	NARNOO	2
	KAKAROCK	1
PLUMRIDGE	MEINYA	1
	BARTLETT	5
CUNDEELEE	MOONYOORA	4
	YANDALLAH	8
ZANTHUS	ZANTHUS	1
	COONANA	(a)37
WIDGEMOOLTHA	YARDILLA	(a)73
NORSEMAN	FRASER RANGE	6
	COWALINYA	3
	MOUNT ANDREW	3
ESPERANCE	BURDETT	2
BALLADONIA	HARMS	2
	CHARLINA	1

NOTE: (a) samples from the Fraser Range regolith mapping program (Fig. 1; Morris et al., 2000)

Southeast Yilgarn Craton — Eastern Goldfields Superterrane

The Yilgarn Craton in the study area is within the Eastern Goldfields Superterrane (EGST), which comprises the Kalgoorlie, Kurnalpi, and Burtville Terranes (Cassidy et al., 2006). The EGST is largely composed of northwest-trending greenstone belts separated by extensive granite and granitic gneiss (Fig. 2; Cassidy et al., 2006). In the study area, the Kurnalpi Terrane is bounded by the Ockerberry Fault to the south and the Hootanui Fault to the north (Fig. 2). The Burtville and Kalgoorlie Terranes are to the northeast and southwest of the Kurnalpi Terrane, respectively.

The eastern part of the Kurnalpi Terrane includes c. 2.72 to 2.70 Ga mafic volcanic rocks, calc-alkaline rocks, and feldspathic sedimentary and mafic intrusive rocks. The western part includes c. 2.69 to 2.68 Ga bimodal rhyolite–basalt and felsic calc-alkaline complexes (Cassidy et al., 2006). The southernmost part of these greenstone associations comprise rocks of the Kurnalpi and Kalgoorlie Terranes, which are interpreted to have been tectonically interleaved with and overlain by a series of c. 2.66 Ga late basins associated with terrane amalgamation (Barley et al., 2003; Krapež et al., 2008). The Burtville Terrane to the north comprises slightly older 2.81 Ga intermediate and felsic volcanic rocks, mafic and ultramafic rocks (Barley et al., 2003), and granitic rocks.

More recently, Pawley et al. (2012) presented new geological mapping and geochronology for the northeast Yilgarn Craton and established a previously unrecognized, younger (<2.72 Ga) Yamarna Terrane in the northeast corner of the craton, redefining the extent of the Burtville Terrane. Bounded by the Yamarna Shear Zone to the southwest, the new Yamarna Terrane occurs only in the

northeastern-most corner of the study area (Fig. 2), where it is covered by sedimentary rocks of the Gunbarrel Basin. Pawley et al. (2012) also found that the Yamarna Terrane has a lithological affinity to the Kalgoorlie Terrane.

Albany–Fraser Orogen

The Albany–Fraser Orogen is dominated by variably deformed Paleo- and Mesoproterozoic metamorphic rocks and bounded along its western side by the Cundeelee and Jerdacuttup Faults to the southeastern margin of the Yilgarn Craton (Fig. 2). Rocks of the Albany–Fraser Orogen represent successive episodes of reworking along the Yilgarn Craton margin between approximately 1.8 and 1.1 Ga (Spaggiari et al., 2011). The orogen also contains reworked Archean Yilgarn Craton rocks, including isolated fragments within Paleoproterozoic rocks (Spaggiari et al., 2011).

The Albany–Fraser Orogen is divided into the Northern Foreland (dominated by reworked Yilgarn Craton) and the Paleo- to Mesoproterozoic Kepa Kurl Booya Province (representing the pre-amalgamation basement components). The latter province defines the crystalline basement of the Albany–Fraser Orogen (including the various components affected by, and possibly amalgamated during, Stage I tectonism) and is further divided into three fault-bound tectonic units comprising the Biranup, Fraser, and Nornalup Zones from northwest to southeast (Fig. 2; Myers, 1995; Spaggiari et al., 2009, 2011). These zones are intruded by Mesoproterozoic granitic rocks of the Recherche and Esperance Supersuites to the southeast (Myers, 1995; Spaggiari et al., 2011). The eastern extent of the orogen is overlain by the Cretaceous and Cenozoic sedimentary successions of the Eucla Basin (Lowry, 1970). Brief summaries of the Northern Foreland, Biranup, and Fraser and Nornalup Zones, and the Recherche and Esperance Supersuites, are given below. Two further sections describe the main tectonic events and remnant metasedimentary rocks that correspond to Proterozoic basin systems.

Northern Foreland Zone

Trending southwest to northeast, the Northern Foreland Zone is the part of the Yilgarn Craton that was reworked during the Albany–Fraser Orogen (Spaggiari et al., 2009). It consists of a series of metamorphosed (and partly deformed) granitic and mafic rocks. The degree of deformation in these rocks typically intensifies from northwest to southeast, and reflects lower strain conditions and metamorphic grade with increasing distance from the orogen (Spaggiari et al., 2009, 2011). However, in the northeastern part of the orogen the contact is much sharper, and is defined by the Cundeelee Fault (Spaggiari et al., 2011).

The Northern Foreland also includes the predominantly granitic gneiss of the Munglinup Gneiss, which is a reworked part of the Archean Yilgarn Craton, based on similar lithological ages of 2.8 to 2.6 Ga, and a similar Lu–Hf isotope signal (Spaggiari et al., 2009, 2011; Kirkland et al., 2011b). However, this unit only occurs in the far southwest of the study area without any sample points.

Biranup Zone

The Biranup Zone is dominated by a variety of intensely deformed granitic and gneissic rocks with ages ranging from c. 1.80 to 1.62 Ga (Spaggiari et al., 2011). The presence of fragments of Archean granitic rocks with ages typical of the Yilgarn Craton suggests that the Biranup Zone formed autochthonously along the Yilgarn Craton margin (Kirkland et al., 2011a; Spaggiari et al., 2011). One such fragment occurs in the Mount Andrew area (Fig. 2). At the northern end, the Biranup Zone contains remnants of strongly altered metagranites, which are likely to be part of a different crustal fragment of the Yilgarn, or more likely the Northern Foreland (Spaggiari et al., 2011).

Fraser and Nornalup Zones

The Fraser Zone contains the 1.31 to 1.29 Ga Fraser Range Metamorphics (pale green areas in Fig. 2), which are dominated by sheets of metagabbroic rocks interlayered with granitic material and layers of metasedimentary rocks of the Arid Basin (see 'Metasedimentary units', below). The latter are found along the northwestern side of the Fraser Zone and are typically intercalated with layers of mafic granulite and amphibolite that possibly relate to younger magmatic intrusions. Pelitic and semipelitic rocks (Oorschot, 2011; Spaggiari et al., 2011) dominate the metasedimentary component of the southernmost part of the Fraser Zone.

Most of the northeastern extent is masked by Cenozoic sediments of the Eucla Basin. However, geophysical data show that the Fraser Zone is a northeasterly trending fault-bound unit approximately 425 km long and 50 km wide (Spaggiari et al., 2011). Overall, the high-grade rocks of the Fraser Zone have strong, distinct geophysical features reflecting the high density of metagabbroic rocks (Smithies et al., 2013). Spaggiari et al. (2011) interpret the Fraser Zone as a structurally modified, mid- to deep-crustal 'hot zone' formed by the repeated intrusion of gabbroic magma into quartzofeldspathic country rock. Geochemical analysis of the Fraser Zone gabbroic rocks indicates that they formed in either a distal back-arc or an intercontinental rift setting (Smithies et al., 2013).

The Nornalup Zone is the southern- and eastern-most unit of the Albany–Fraser Orogen and is heavily intruded by the voluminous Recherche and Esperance Supersuites, which mask much of the original Paleoproterozoic basement (Spaggiari et al., 2011).

Recherche and Esperance Supersuites

The 1.33 to 1.28 Ga Recherche Supersuite and the 1.20 to 1.14 Ga Esperance Supersuite occur in the southern part of the study area (southwest of Balladonia in Fig. 2). They respectively mark two major magmatic events that coincide with the Albany–Fraser Orogen Stages I and II (Clark et al., 2000). Cenozoic carbonate-rich sedimentary rocks of the Eucla Basin mask these rocks to the east.

Both supersuites comprise variably metamorphosed igneous rocks. Those belonging to the Recherche

Supersuite are typically metamorphosed to amphibolite or granulite facies. They typically have a gneissic fabric and include synmagmatic mafic rocks. Igneous rocks of the Esperance Supersuite are typically unmetamorphosed, although may include rocks metamorphosed up to greenschist or amphibolite facies, and are overall less pervasively deformed than rocks of the Recherche Supersuite (Myers, 1995; Nelson et al., 1995).

Tectonic events

Three main tectonic events are recognized in the Albany–Fraser Orogen. The oldest, the Biranup Orogen, covers the period from 1.71 to 1.65 Ga and includes the c. 1.68 Ga Zanthus event (Kirkland et al., 2011a). However, dating of rocks of the Biranup and Nornalup Zones indicates magmatic activity occurred before the above period, marking the onset of modification along the Yilgarn margin from at least 1.8 Ga.

The Albany–Fraser Orogen is divided into two further tectonic events: Stage I (1345–1260 Ma) and Stage II (1215–1140 Ma; Clark et al., 2000; Bodorkos and Clark, 2004; Kirkland et al., 2011a). Stage I is likely to have been related to the collision of the West Australian Craton with the combined Mawson and South Australian Craton (Clark et al., 2000). Stage II is interpreted as intracratonic reworking (Clark et al., 2000). Stage I is predominantly related to mafic and felsic magmatism forming both the Recherche Supersuite and the magmatic rocks of the Fraser Zone (Fig. 2), accompanied by metamorphism and deformation. The intracratonic activities of Stage II include high-temperature metamorphism and juxtaposition of different tectonic units; there is also evidence of fold and thrust successions (Spaggiari et al., 2009, and references therein).

Metasedimentary units

Metasedimentary rocks of the Woodline Formation (Fig. 2) unconformably overlie granite–greenstones of the EGST west of Fraser Range homestead. They are the remnants of a much larger basin, the Barren Basin, which evolved between 1.8 and 1.6 Ga before and during the Biranup Orogen (also termed Cycle 1 sediments in Spaggiari et al., 2011). The younger Fly Dam Formation (Fig. 2) comprises a succession of higher grade, semipelitic and psammitic gneisses that appear to be the metamorphosed equivalents of interbedded sandstones and mudstones (Spaggiari et al., 2011). Remnants of the Barren Basin, such as the Fly Dam Formation, are found within the Biranup Zone southwest of Zanthus, and are interpreted as more distal and younger components of the Barren Basin Cycle 1 sediments deposited during the late stages of the Biranup Orogen (Spaggiari et al., 2011). Several successions of metasedimentary rocks (Gwynne Creek Gneiss (Fig. 2), the metasedimentary component of the Fraser Range Metamorphics, and the Malcolm Metamorphics) relate to Mesoproterozoic Cycle 2 sediments (remnants of the Arid Basin) and have been affected by Stage I tectonism (1345–1260 Ma; Spaggiari et al., 2011).

Gunbarrel and Eucla Basins

In the northwestern and southeastern parts of the study area, the Yilgarn Craton and Albany–Fraser Orogen are unconformably covered by sedimentary rocks of the Gunbarrel and Eucla Basins, respectively (Fig. 2). The Gunbarrel Basin is confined to the east by the Cundeelee Fault and comprises a Paleozoic to Mesozoic succession of sedimentary rocks and is floored by the Cambrian Table Hill Volcanic rocks, which were previously included in the Officer Basin (Hocking, 1994). These volcanic rocks are overlain by an up to 1.5 km-thick succession of Devonian, Upper Carboniferous to Lower Permian, and Cretaceous siliciclastic rocks (Hocking, 1994). The southern extent of the Gunbarrel Basin (also referred to as the Kingston Shelf; Hocking, 1994) shown in Figure 2 comprises largely Permian sedimentary rocks less than 1 km thick, which unconformably overlie the Yilgarn Craton. Not shown in Figure 2 is that large parts of the Gunbarrel Basin and northeastern Albany–Fraser Orogen are covered by post-Miocene sediments.

Overall, the thickness of cover across the Gunbarrel Basin is not well known. Data from a drillhole near Lake Minigwal (northwest of Mulga Rock; Fig. 1) recorded >400 m of sedimentary rocks capped by 8 m of regolith. At Mulga Rock itself, sedimentary rocks of the Permian Paterson Formation can reach thicknesses of >700 m and are overlain by 40 to 70 m of fluvial to lacustrine Cenozoic sediments (Douglas et al., 2003). Regolith of predominantly eolian sandplain makes up at least the upper 5 to 10 m.

The Eucla Basin to the east of the Fraser Zone (Fig. 2) comprises sedimentary rocks ranging from Early Cretaceous to Miocene age and consists broadly of mainly lacustrine to marine sediments (Lowry, 1970). The majority form a series of Middle Cenozoic carbonate-rich sedimentary rocks that correspond to three formations, which were deposited in cool to subtropical neritic conditions, and which partially filled the shallow and broad Eucla Basin. The Eocene Wilson's Bluff Limestone is a soft, poorly lithified cool-water carbonate (Miller, 2012). The overlying Oligocene to early Miocene Abakurrie Limestone is also a cool-water carbonate; however, it is somewhat more lithified than the Wilson's Bluff Limestone. The early to middle Miocene Nullarbor Limestone forms much of the Eucla Basin and may be the most extensive Cenozoic carbonate platform described to date (Miller, 2012). The extent of Phanerozoic sedimentary rocks beneath the Eucla Basin is unknown because of an almost total lack of subsurface data (Hocking, 1994). Mesozoic rocks of the Bight Basin, comprising lacustrine to shallow marine sandstone and siltstone, are present beneath the Eucla Basin over much of the area.

Regolith

A simplified regolith–landform map at 1:500 000 scale is shown in Figure 3 (Marnham et al., 2002). More detailed regolith maps have been compiled for the Fraser Range region (Morris et al., 2000) and the East Wongatha area (GSWA, 2010). The regolith classification system applied by GSWA is documented in Record 2013/7 (GSWA, 2013).

There are seven regolith units present in the study area, which is dominated by transported regolith. From the regolith geochemistry program of the Fraser Range region (Fig. 1), Morris et al. (2000) noted that only 6% of the area corresponds to exposed bedrock, which is likely to be even less for the remaining study area (Fig. 3). Nearly 65% of the Fraser Range region is covered by sandplain deposits, with colluvium accounting for 17%. The remaining alluvial, lacustrine, and sheetwash deposits account for approximately 12% (Morris et al., 2000). From the regolith geochemistry program of the East Wongatha area (Fig. 1), residual and eolian sandplain account for 70% of the regolith by area with a further 14% for colluvium (Morris, 2013a; Fig. 3). Sandplain is the most common regolith unit throughout the study area, and has been described by Morris et al. (2000) and Morris (2013a) as largely heterogeneous, comprising a mix of residual and eolian sand, silt, and clay, with locally developed carbonate and ferruginous material. This heterogeneity should be taken into account when interpreting geochemical data.

The 151 samples discussed here are from six regolith types (Fig. 3). Most samples are from sandplain ($n = 75$; Table 2) followed by colluvium ($n = 41$). Five samples are from areas of sheetwash and seven samples from alluvial regolith collected from south of the Trans-Australian Railway at Coonaanna Hill, west of Zanthus (Fig. 1). Table 2 lists 15 samples as exposed bedrock. However, these samples of regolith are close to exposed bedrock; they are mainly outcrops of Archean granites and greenstones within the Kurnalpi Terrane northwest of Fraser Range homestead and Coonaanna Hill. Sample locations corresponding to lacustrine deposits are found only south of the Trans-Australian Railway.

One extensive area of calcrete is located to the northeast of Zanthus (Fig. 3), although none of the 151 regolith samples are from this area. However, Morris et al. (2000) found that across the Fraser Range region, calcrete clasts were common in almost all samples, particularly in the heterogeneous sandplain deposits.

The origins of sandplain deposits across Western Australia are still not fully understood, although their formation is thought to relate to processes such as in situ development over bedrock, eolian transport of carbonate-rich material, or local derivation with limited transport. It is likely that in many cases, all three processes contributed to sandplain development. Newsome (2000), for example, concludes that most sandplain deposits in Western Australia relate to in situ weathering. Morris et al. (2000) suggest a strong influence from the underlying or nearby bedrock on the regolith composition, including sandplain deposits and colluvium.

Across the study area, the thickness of cover, including regolith and barren sedimentary rocks overlying basement rocks, is poorly understood because relatively few drill data are available or accessible. Morris et al. (2000) describe the regolith of the Fraser Range region (Fig. 1) as commonly thin. To the north, around Mulga Rock for example, recent eolian surface sand (sandplain) is 5 to 10 m thick and overlies more than 700 m of sedimentary rocks of the Gunbarrel Basin (Fig. 2). To the northwest,

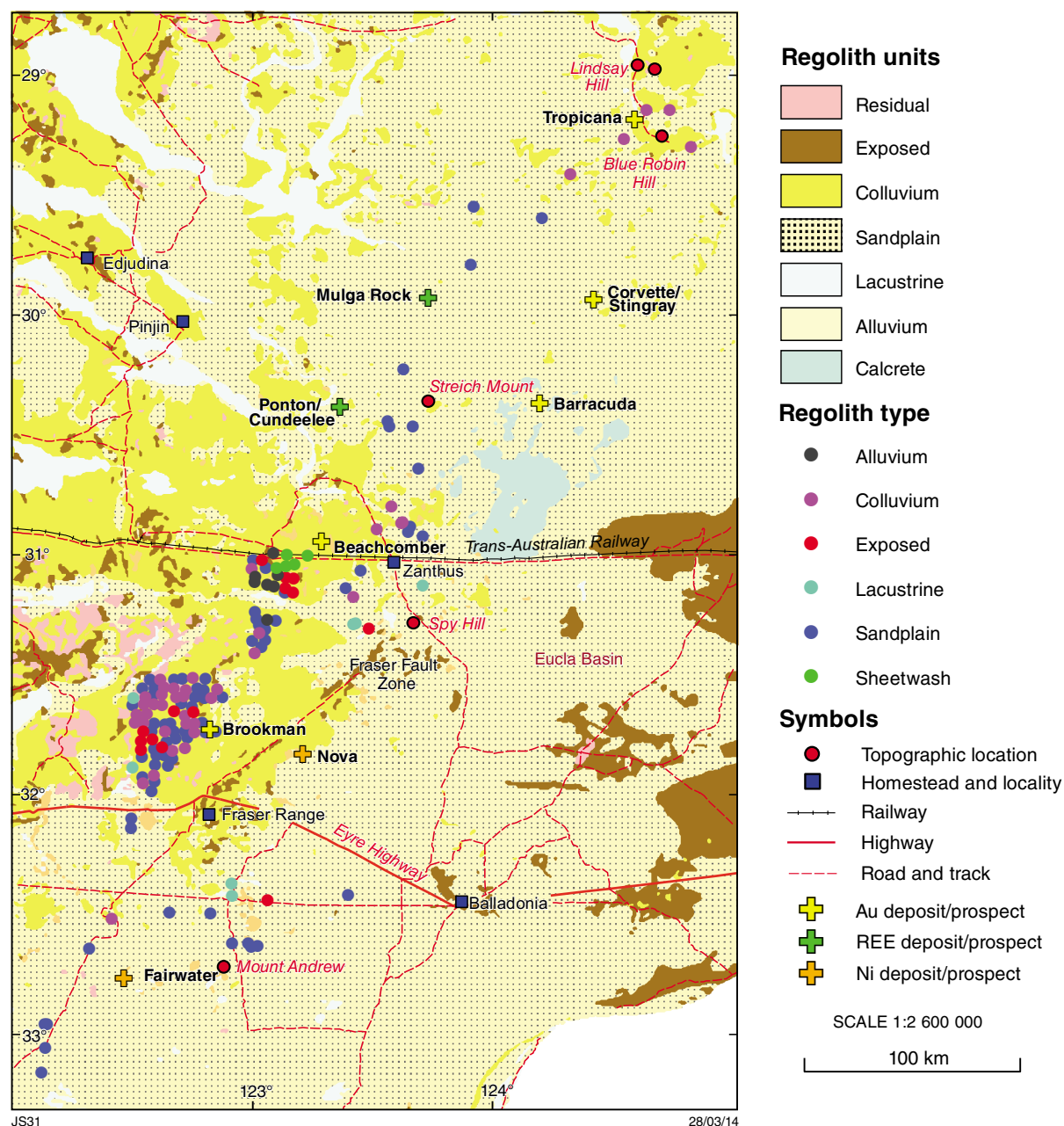


Figure 3. Regolith map of the study area derived from the 1:500 000 scale regolith cover map of Western Australia (Marnham et al., 2002); map also shows the recorded regolith type at GSWA sample site locations and a selection of mineral deposits and prospects

Table 2. Regolith types and associated number of samples based on the 1:250 000 scale Fraser Range Regolith map (Morris et al., 2000) and the 1:500 000 scale State regolith map (Marnham et al., 2002)

Regolith type	Number of samples	Description
Alluvium	7	Cobbles, gravel, sand, and silt in active alluvial channels
Colluvium	41	Predominantly transported residual and eolian sand, silt, and clay
Exposed	15	Outcrop of bedrock, saprock or subrock derived predominantly from granite and granitic gneiss
Lacustrine	7	Predominantly sand silt and evaporitic material in mixed playa and dune terrain
Sandplain	75	Residual and eolian sand, silt, and clay in variable proportions
Sheetwash	5	Sand- and clay-dominated colluvium or sheetwash with indistinct alluvial channels

near Lake Minigwal, this regolith and bedrock succession is >400 m thick (Perincek, 1998). In this area, an extensive assessment of data for more than 1100 drillholes indicates average depths to the regolith–basement interface of between 55 and 58 m. However, the thicknesses in each dataset ranged from 5 to 121 and 5 to 210 m, respectively (Morris, 2013a).

Figure 4a,b displays photographs from the Zanthus area showing a typical sampling site and Figure 4c shows a cross section through an Fe-rich (lateritic) transported regolith. Figure 4d depicts typical scenery at Mulga Rock of sandplain and small (5–10 m) dunes in the background.

Formation of regolith carbonate

Calcrete, which is indurated secondary carbonate composed predominately of calcite, covers approximately 21% of Australia's land surface, although it is predominantly found south of 30°S (Chen et al., 2002). Chen et al. (2002) list three main sources for the formation and accumulation of regolith carbonate: weathering of bedrock, eolian dust, rainwater, and groundwater. This finding is consistent with the observations of McQueen (2006), who also stated that the ultimate source of the cations (Ca, Mg, etc.) concentrated in calcrete are either bedrock or transported material such as eolian dust, aerosols, and rainwater. A detailed account on the origin, formation, and classification of regolith carbonate in Australia, in particular calcrete, is given by Chen et al. (2002).

Regolith carbonate, as described by Hill et al. (1999), is a collective term, and the preferred term for this study. It includes indurated deposits such as calcrete or dolocrete, and all pedogenic (authigenic) carbonate deposits that consist of numerous carbonate minerals and vary in content and degree of cementation (Hill et al., 1999; Chen et al., 2002). The most commonly described mechanism for the formation of regolith carbonate accumulations involves concentration by evaporation and subsequent precipitation from vadose (soil) and shallow phreatic (ground) waters that are saturated with carbonate minerals (Hill et al., 1999).

Regolith carbonate and Au

Across the southern part of Australia, calcretes and soil carbonates have been particularly targeted for Au, resulting in many mineral deposit discoveries. Across the Yilgarn Craton, the association of Au with pedogenic carbonate is thought to be due to the cycling of Au from depth to the surface by vegetation, mobilization of the Au as organo-complexes, and reprecipitation with carbonate under evaporative conditions. However, the precise processes and mechanisms for the accumulation of Au with regolith carbonates are currently not fully understood (McQueen, 2006).

Based on several case studies, Chen et al. (2002) and Lintern (2002) suggested that where transported regolith exceeds 10 m in thickness, it is unlikely that

any geochemical response in the calcrete (or supergene carbonate) can be directly attributed to underlying mineralization. These authors concluded that the thicker the transported regolith, the less effective calcrete (or supergene carbonate) is as an exploration sample medium for Au, while indurated and pedogenic carbonate in residual and in situ weathered regolith are less problematic. In the study area, most regolith samples are sourced from transported regolith, some of which exceeds 10 m thickness. This should be kept in mind when evaluating the relationship between Au and Ca.

Mineral deposits and prospects

The GSWA's MINEDEX database provides information on locations of known mineralization, deposits and mines for a range of commodities throughout the State. In the study area, the dominant commodities are precious and speciality metals such as Au, Ni–Cu, rare earth elements, and uranium (U). The most abundant commodity is Au from deposits associated with greenstones of the Kurnalpi Terrane along the southeastern margin of the Yilgarn Craton. Of the selected deposits (Figs 1 and 2), only Tropicana, Mulga Rock, and more recently, Nova, have demonstrated economic resources.

The Tropicana (–Havana) deposit lies just to the east of the northeast-trending Cundeelee Fault, which marks the edge of the Yilgarn Craton (Fig. 2). The deposit lies within an area of northwest-trending magnetic highs and moderate gravity anomalies, which are cut by northeast- to east-trending shear zones and mafic dykes (Spaggiari et al. 2010). Doyle et al. (2009) reported that the Au mineralization is hosted by Archean garnetiferous gneiss and K-feldspar-rich quartzofeldspathic gneiss, which in turn are concentrated in ore shoots within the saprolite (Lintern and Anand, 2011). Spaggiari et al. (2010), however, highlighted that the regional geology is dominated by metagranitic rocks of the Biranup Zone, and listed several possible scenarios for this margin setting.

The initial discovery was made after following up a regional soil geochemical dataset that highlighted several low-order (+4 µg/kg), northeast-trending Au soil anomalies across the Tropicana tenements; the largest was approximately 6 × 1 km in size (Tropicana Joint Venture, 2010; Perkins, 2004). The above dataset originated from open-file company reports by WMC Resources Ltd (e.g. McKinnon-Mathews, 1998), which explored the Pleiades Lakes during the 1990s targeting for Voisey's Bay-style mafic-hosted nickel sulfide deposits.

Other Au prospects within the east Albany–Fraser Orogen stretch over several hundred kilometres from the Tropicana to the Beachcomber deposits and beyond, subparallel to the Cundeelee Fault, at the margin with the Yilgarn Craton.

Exploration at Mulga Rock by Energy and Minerals Australia Ltd focused on three separate U-bearing polymetallic mineral deposits: Ambassador, Emperor, and Shogun.

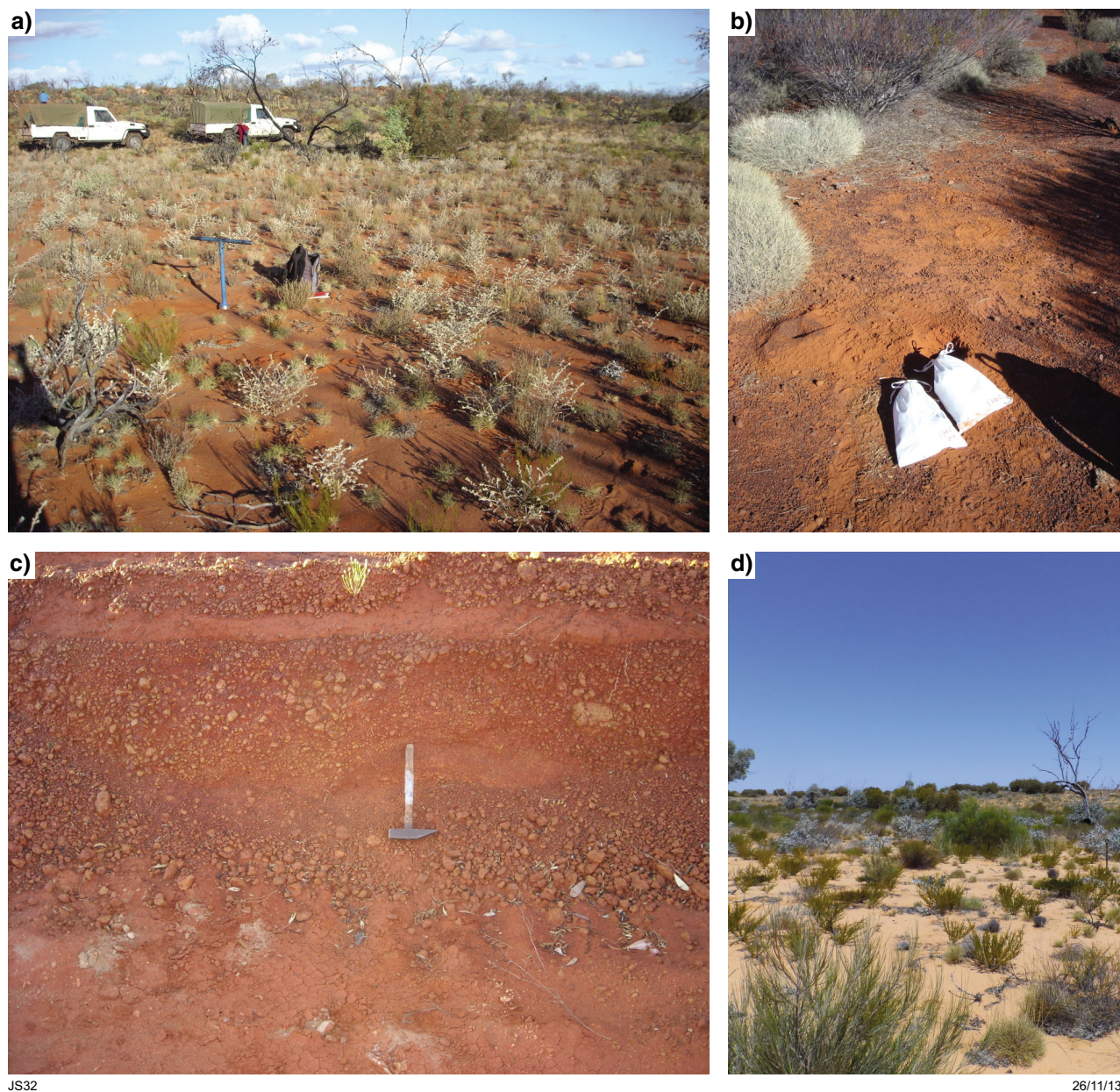


Figure 4. a) View of soil sample location GSWA 194036 (MGA 567577E 6577531N), a sandy colluvium near outcrop; b) photo of sample location GSWA 194031 (MGA 549667E 6580929N), a sandy soil with abundant ferruginous lag; c) cross section through approximately 1 m of transported laterite near Zanthus; and d) typical scenery at Mulga Rock showing sandplain with a sand dune in the background (5–10 m high).

The Ni (–Cu) sulfide deposit at Nova is the most recent discovery in this area and is hosted by mafic granulite (metagabbro) within the Fraser Zone (Fig. 2). Its location coincides with anomalous Ni and Cu concentration in a sheetwash sample east of Symons Hill reported by Morris et al. (2000) following the geochemical mapping of the Fraser Range region. Additionally to Sirius Resources NL's discovery, Enterprise Metals Ltd (2012a,b) announced several soil anomalies across their Fraser Range project area, including Au, Cu, Zn, As, Bi, Sb, and a 'Nova-style' Ni–Cu anomaly, all of which are located within the Fraser Zone and on similar northeast–southwest-trending tectonic structures.

Methods — sampling and analyses

Of the 151 regolith samples discussed here, 109 are from the Fraser Range region (YARDILLA and COONANA 1:100 000 sheets; Fig. 1), collected as part of the Fraser Range regolith geochemistry mapping project (Morris et al., 2000; Fig. 1). A further 42 samples were collected during 2006 and 2007 over about 500 km, broadly parallel to the Yilgarn Craton margin (Fig. 2), using the same sampling approach as the Fraser Range regolith geochemistry program. Appendix 1 lists all samples with their corresponding GSWA numbers and MGA grid references. Table 1 gives the names of the 1:250 000 and 1:100 000 map sheets and corresponding numbers of samples for the study area.

Regolith sampling

For GSWA's regional regolith geochemistry program, such as that carried out in the Fraser Range region (Morris et al., 2000), sheetwash, colluvium, soil, sandplain, and lake sediments are sampled where drainage is absent or only weakly developed. At each site, the top 5–10 cm of regolith is removed, and approximately 5 kg of regolith is collected from pits or trenches to a depth of 30 cm. For the remaining samples, approximately 4–5 kg of regolith was collected from a depth of about 30 cm using either a hand auger or a spade.

Analytical methods

Eight analytical methods have been used for a variety of size fractions, and pH is given for bulk samples, as summarized in Table 3. A list of methods applied to each sample is given in Appendix 2. Figure 5 shows the distribution of sample locations categorized according to analytical method.

The data can be divided into two groups: those resulting from a 'total' analytical approach (either X-ray fluorescence [XRF] spectrometry or inductively coupled plasma ICP-based methods) following a total digest, and those resulting from analysis of samples after partial digestion, also using ICP-based methods. The latter methods include a combination of ICP-mass spectrometry

(ICP-MS) and ICP-optical emission spectrometry (ICP-OES), depending on the analyte. For the total data, different grain size fractions were used for XRF (<2 mm; $n = 42$) than for ICP analysis (<2 mm to >45 μm ; $n = 109$). The grain size effects are assessed using data for eight samples that were analysed by both methods (Fig. 5, Category 3; Appendix 2). As part of the total ICP analysis, Au was also determined by fire assay (FA) of the <2 mm to >45 μm fraction of 109 samples.

A mixture of the bulk sample and deionized water (1:5) was analysed using a portable Jenway pH meter calibrated using solutions of pH 4 and pH 7. Loss on ignition (LOI) is the weight percent loss of the sample following ignition at 1000°C.

Partial digestion methods were applied to the fine fraction (<50 μm) using four digests: aqua regia (AR), TerraLeach9 (TL9; sodium pyrophosphate for the recovery of elements in humic acid), TerraLeach7 (TL7; 4M hydrochloric acid to remove amorphous iron and manganese oxide and/or hydroxides that host metals), and TerraLeach0 (TL0; deionized water). Total analysis by XRF, and partial digestion chemistry, were carried out by Intertek–Genalysis, and total analysis for the <2 mm to >45 μm fraction was carried out by ICP by Amdel Laboratories.

Quality control

Quality control involves assessing the precision and accuracy of chemical analysis. Monitoring chemical analysis is achieved by inserting a series of reference materials, sample duplicates, and blanks. In GSWA's regolith geochemistry program, approximately 10% of all samples are related to quality control (Morris et al., 2000).

Quality control of total data of the 109 samples analysed by ICP-MS and ICP-OES (Table 3) are summarized in Morris et al. (2000) as these form part of the Fraser Range regolith geochemistry program. For this program, which involved the analysis of 994 regolith samples, 50 analytical blanks and 93 sample duplicates were analysed following fusion and acid digestion and ICP analysis. Similarly, 25 analyses each of three reference materials (OREAS-42P, OREAS-43P, and OREAS-44P) were carried out. For the fire assay procedure, used to determine the concentrations of Au, Pd, and Pt, 26 blank analyses were carried out, along with 50 sample duplicates and 28 analyses each of the reference materials PM7 and PM8. Thirteen samples were analysed by a second laboratory.

Precision was assessed using the covariance or percent relative standard deviation ($\text{RSD}\% = 100 \times [\text{SD}/\text{mean}]$). A value of <20 when the analyte concentration was at least $10\times$ the lower limit of detection (LLD) was deemed satisfactory. Duplicates and reference materials were assessed using the half relative deviation (HRD):

$$\text{HRD} = 100 \times ([\text{assay1} - \text{assay2}]/[\text{assay1} + \text{assay2}])$$

Values of <10% were taken as satisfactory if the analyte concentration was at least $10 \times \text{LLD}$.

Table 3. List of analytical methods, sample number, size fraction, and determinants used in the study

Analytical method	Description	Number of samples	Size fraction	Analyte (element or oxide) or measured property
AR	ICP-MS and ICP-OES following aqua regia (nitro-hydrochloric acid) digestion	151	<50 µm	Ag, Al, As, Au, Ba, Be, Bi, Ca, Cd, Ce, Co, Cr, Cs, Cu, Dy, Er, Eu, Fe, Ga, Gd, Ge, Hf, Hg, Ho, In, K, La, Li, Lu, Mn, Mo, Nb, Nd, Ni, Pb, Pd, Pr, Pt, Rb, Re, Sb, Sc, Se, Sm, Sn, Sr, Ta, Tb, Te, Th, Tl, Tm, U, V, W, Y, Yb, Zn, Zr
TL9	TerraLeach9; ICP-MS and OES following sodium pyrophosphate digestion	146	<50 µm	Ag, As, Au, Ba, Be, Bi, Ca, Cd, Ce, Co, Cr, Cu, Dy, Er, Eu, Fe, Ga, Gd, Ge, Hf, Hg, Ho, In, La, Li, Lu, Mn, Mo, Nb, Nd, Ni, Pb, Pd, Pr, Pt, Sb, Sc, Se, Sm, Sn, Ta, Tb, Te, Th, Tl, Tm, U, V, W, Y, Yb, Zn, Zr
TL7	TerraLeach7; ICP-MS and OES following 4M hydrochloric acid (HCl) digestion	146	<50 µm	
TL0	TerraLeach0; ICP-MS and ICP-OES following deionized water digestion	22	<50 µm	
Total analysis	XRF	50 (42 ^(a))	<2 mm	SiO ₂ , TiO ₂ , Al ₂ O ₃ , Fe ₂ O ₃ , MnO, MgO, CaO, Na ₂ O, K ₂ O, P ₂ O ₅ , and some trace elements
	ICP-MS and ICP-OES following a total digest in hydrofluoric acid (HF)	109	<2 mm to >45 µm	
FA	Common analytical method to obtain Au	109	<2 mm to >45 µm	Au
pH	1:5 slurry of sample and deionized water	151	Bulk sample	pH
LOI	Weight loss after ignition at 1000°C	151	<2 mm	LOI

NOTES: (a) samples located outside the Fraser Range region
 AR aqua regia digest
 FA fire assay
 ICP-MS inductively coupled plasma–mass spectrometry
 ICP-OES inductively coupled plasma–optical emission spectrometry
 LOI loss on ignition
 XRF X-ray fluorescence spectrometry

Sample duplicates produced acceptable results, apart from Nb in several samples and Bi in one sample. Both precision and accuracy were acceptable for Au and Pt, although the accuracy of Pd in reference materials PM7 and PM8 was poor, possibly caused by unreliable Pd values provided for the reference materials. Analysis of three GSWA in-house reference materials (Morris, 2000) produced acceptable results, apart from Cr and W. The relatively poor data for elements such as Cr and Nb may reflect difficulty in releasing these elements into solution, as they are commonly found in resistate minerals. For the 13 samples analysed by two laboratories, there is good agreement for major elements, although some between-laboratory variation was observed for several trace elements, including Ce, Co, Cr, La, Nb, Sc, Zn, and Zr. Again, it is possible that these discrepancies reflect different digestion conditions at the two laboratories, as these elements are commonly found in resistate phases.

For XRF analysis of 42 samples, six samples were analysed in duplicate, producing acceptable agreement for all analytes. However, the LLD values for most trace elements were 50 to 100 mg/kg (ppm), making these data of limited use. Results for five reference materials produce acceptable agreement, and blank analyses were acceptably low. The main use of these data is for the major element oxides.

For AR analysis, samples were analysed in two batches. In one batch (duplicates, $n = 5$), elements that showed >10% disagreement in more than one pair included Hf, Sn, and Zr. In the second batch (duplicates, $n = 6$), a more diverse group of elements showing disagreement included Au, Cu, Ga, Hf, La, Li, Nb, Nd, Pr, Rb, Sn, Sr, U, Zn, and Zr; however, for several of these elements, the poor disagreement is restricted to one duplicate pair. For the first batch, three reference materials were analysed for a variety of trace elements, and Au was analysed in two reference materials. Elements that showed RSD > 20% in two or more reference materials included Ag and Nb. For the second batch, five reference materials were analysed, with RSD > 20% for Ge, Nb, W, and Zr. Blanks are acceptably low in this second batch.

The fine fraction of 146 samples was digested with 4M HCl and analysed by ICP-MS and OES (TL7) in three batches. All elements showed good agreement for duplicates, apart from Ag, Li, and Ni (two or more duplicates); Ag, Th, and Li showed RSD > 20% for two or more reference material determinations.

The fine fraction of 146 samples was analysed by ICP-MS and OES after digestion with sodium pyrophosphate (TL9), a digest used to release elements bound in organic compounds (Hall, 1998). Samples were analysed in three batches.

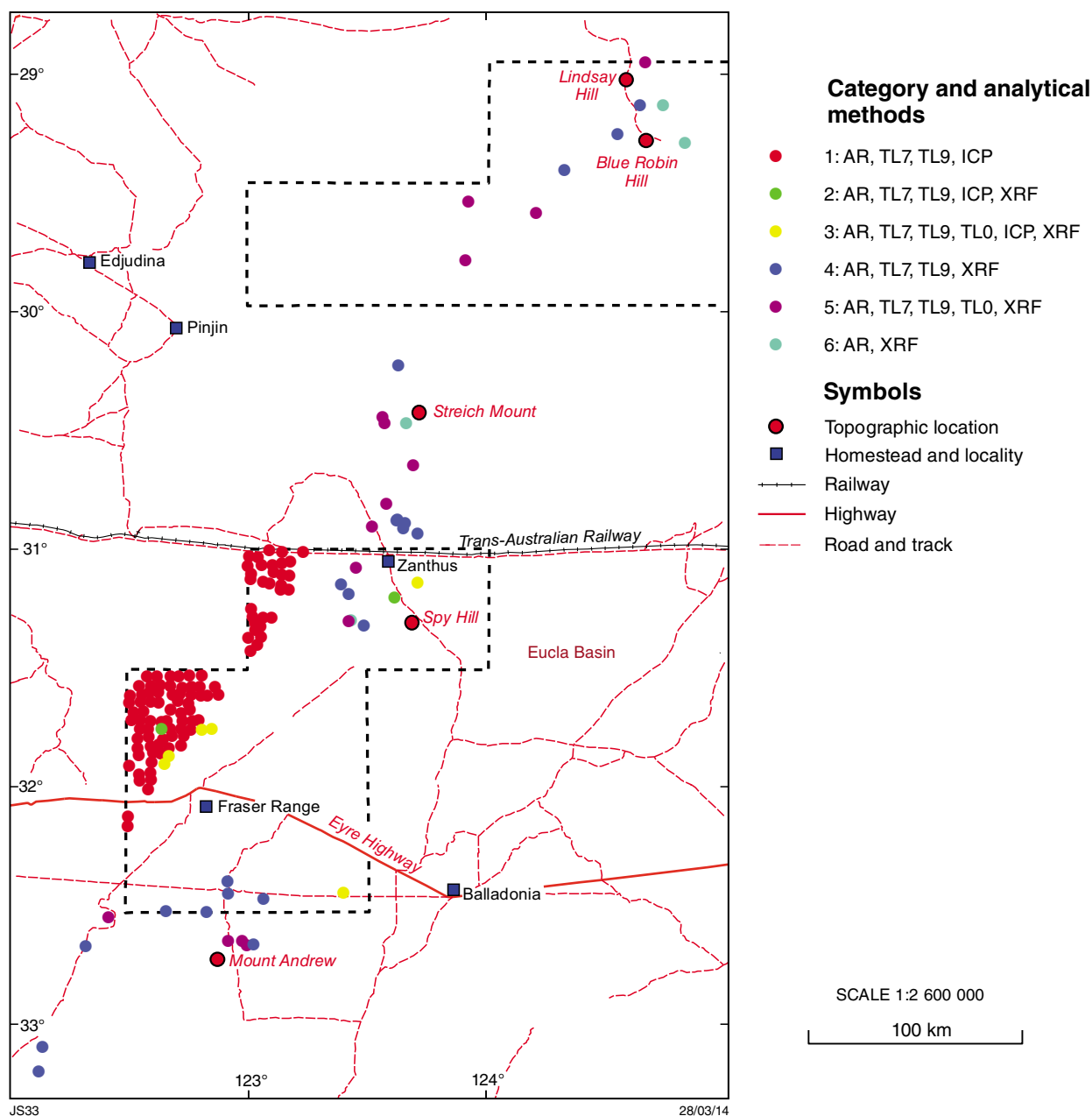


Figure 5. Distribution of GSWA sample sites indicating the method and digestion applied as part of the analytical program; see Table 3 for list of analytical methods and abbreviations

For Al, Be, Fe, and Lu, two to three duplicate pairs showed HRD > 10 in batch 3, although there was no consistent pattern of elements showing poor agreement; in the occasional duplicate, several elements showed HRD > 10, particularly rare earth elements. Reference material analyses were typically acceptable in terms of RSD, with only Ca and V showing RSD > 20% in one reference material in one batch. Blank analyses were acceptably low.

Deionized water is the weakest digest, and 22 samples have been analysed for a variety of elements following deionized water digestion. One duplicate was analysed, providing good agreement for most elements apart from

several rare earth elements (including Ce, Dy, Er, Gd, La, Nd, and Yb) and U. Although two reference materials were analysed, there are no consensus values available to assess accuracy.

Eight samples were analysed by both XRF and ICP. The ratios of XRF (<2 mm fraction) to ICP-MS (<2 mm to >45 µm fraction) for major elements show that there is little difference for Si, Fe, Mg, and Ca. However, concentrations determined by ICP-MS are 20 to 35% lower than XRF for Ti, Al, K, and Na. As several of these elements are found in clay minerals, it is likely that this variation reflects removal of the <45 µm fraction for samples analysed by

ICP-MS. Data for P and Mn are difficult to interpret, as several samples returned concentrations less than the LLD.

Statistical and spatial data analysis

In this study, element concentrations are termed anomalous if they are above the 95th percentile. For several elements, concentrations are less than the LLD, so in order to statistically evaluate these data, they are replaced with values equal to one-half the LLD. Both Reimann et al. (2010) and Stanford et al. (1993) recommend a maximum of 10 to 20% of such data be replaced in order to maintain statistical integrity. Issues relating to the amount of such censored data for specific elements are discussed below.

Spearman rank correlation matrices are used in preference to the Pearson correlation approach because the former uses ranked data, and is therefore less influenced by outliers, thus removing the need to log-transform the original data. In the following analysis, the degree of significance of the correlation for each pair is expressed as ***very high ($p < 0.001$), **high ($0.001 < p < 0.01$), and *significant ($0.01 < p < 0.05$); no symbol indicates weak or no significance. Some data are also displayed as box-and-whisker plots, generated in the software R (R Development Core Team, 2008). These plots show the interquartile range (IQR, i.e. the 25th and 75th percentile, shown as the box on a box-and-whisker plot), the median (horizontal line), the lower and upper whiskers ($\pm 1.5 \times \text{IQR}$) and the anomalous outliers and extremes (black circles for values greater or less than $\pm 1.5 \times \text{IQR}$). The spatial distribution of geochemical data is expressed as coloured, graduated dots (bubble plots). Symbol sizes correspond to the 25th, 50th, 75th, and 95th percentile classes.

Results — regolith geochemistry

Regolith matrix

Major element chemistry, LOI and pH

Major element concentrations for the 151 regolith samples (Table 4) are based on the combined XRF and ICP-MS data. Major element ICP-MS data were determined on the <2 mm to >45 μm fraction, but XRF major element data were determined on the <2 mm fraction. Omission of the fine fraction for ICP-MS analysis is reflected in the typically lower K_2O , Al_2O_3 , and TiO_2 values obtained from ICP-MS analysis.

The median SiO_2 content of regolith is 70.7%, with Al_2O_3 , Fe_2O_3 , and CaO making up most of the remaining oxide fraction, and Na_2O , K_2O , and P_2O_5 commonly $<1\%$ (Table 5). All median values for regolith samples are lower

than an upper continental crust average (UCC; Rudnick and Gao, 2003), with the exception of SiO_2 . Most oxide distributions, with the exception of SiO_2 , Al_2O_3 , and CaO, are positively skewed due to high concentrations in some samples.

LOI ranges from 0.8 to 23.7%, with a median value of 8.5%. Samples with LOI greater than the median are largely from the Fraser Range region (Fig. 6a), in particular in areas of greenstones of the Kurnalpi Terrane. A more detailed map of this area (Fig. 6b) shows that samples with higher LOI values ($>12\%$) are mainly found near exposed bedrock (especially greenstones); some of the lowest LOI values ($<4\%$) are found in areas of colluvium. Elsewhere, several individual sites of elevated LOI values are found near Zanthus, and to the east and west of Mount Andrew. Samples from the northern part of the study area typically have low LOI values.

Regolith samples are predominantly alkaline. More than one-half of the samples show $\text{pH} > 8.5$, and only about 20% show $\text{pH} < 7$. Samples with low pH (i.e. <7 ; Fig. 7a,b) also have low LOI ($<4\%$); these are located in the Gunbarrel Basin, northwest of Fraser Range and around Coonaanna Hill, and in the south of the study area. Furthermore, samples with low pH and LOI have high SiO_2 content, commonly $>70\%$ (Fig. 8a,b). In contrast, regolith samples with $<60\%$ SiO_2 are found mainly around Archean greenstones of the Kurnalpi Terrane northwest of Fraser Range homestead. These regolith samples have higher LOI and pH. Samples with the highest SiO_2 concentrations ($>88.6\%$; 95th percentile) are found entirely to the east of the Cundeelee Fault and relate predominantly to sandplain deposits over rocks of the Biranup Zone (Figs 2 and 8). Figure 8b shows that most of the lowest SiO_2 concentrations are found in regolith overlying Archean greenstones west of the Cundeelee Fault.

Samples with elevated CaO (Fig. 9a,b) are found west of the Cundeelee Fault near the Brookman deposit and within the Cherternerlynyer Lagoon (Fig. 2), and also correspond to high LOI. The lowest CaO concentrations ($<2.2\%$) correspond to sandplain-dominated areas over the southeastern Yilgarn Craton and the Gunbarrel Basin in northern part of the study area and areas of alluvium and sheetwash near Coonaanna Hill (Fig. 9a,b).

Samples with high iron contents ($>6.8\%$ Fe_2O_3 ; 75th percentile; Table 5) are almost entirely found over the southeastern Yilgarn Craton west of the Cundeelee Fault and spatially related to greenstones. Their distribution mirrors that of the lowest SiO_2 and highest CaO concentrations (Figs 8 and 9). One sample (GWSA 163132; Appendix 1), located just to the west of the Cundeelee Fault, has 38.4% Fe_2O_3 and 39.1% SiO_2 .

Assessing carbonate contents in regolith samples

Apart from using CaO as a proxy, the relative amount of carbonate in regolith can be further assessed by the ratio of SiO_2 to CaO and its relationship to LOI (Fig. 11a).

Table 4. Major element total concentrations of eight regolith samples analysed by both ICP-MS and XRF, including element ratios

	GSWA number	SiO ₂ (%)	TiO ₂ (%)	Al ₂ O ₃ (%)	Fe ₂ O ₃ (%)	MnO (%)	MgO (%)	CaO (%)	Na ₂ O (%)	K ₂ O (%)	P ₂ O ₅ (%)	LOI (%)
XRF	161753	62.14	0.78	12.14	7.39	0.064	2.07	3.4	0.29	1.78	0.04	9.43
	163136	57.51	0.72	11.38	4.99	0.041	2.14	8.53	0.86	1.62	0.04	12.07
	163350	59.11	0.77	9.29	5.07	0.078	2.47	9.12	0.73	1.37	0.05	12.2
	163617	30.91	0.48	8.16	3.99	0.102	2.8	17.83	2.07	1.3	0.09	11.28
	163718	60.29	0.72	5.31	2.29	0.037	5.55	9.69	0.53	1.06	0.03	15.05
	163842	57.69	0.59	19.63	5.61	0.013	0.65	0.28	0.5	2.09	0.07	14.55
	163932	63.79	0.8	8.84	4.66	0.054	2.22	7.25	0.47	1.21	0.04	10.51
	163934	62.41	0.67	9.66	4.59	0.05	2.43	7.19	0.39	1.62	0.03	11.21
ICP-MS	161753	56.7	0.58	8.7	15.8	0.1	1.6	3	0.2	1.1	(a)0.025	11.3
	163136	59	0.5	9.3	8.2	0.05	1.8	7	0.7	1.2	(a)0.025	12
	163350	57.7	0.5	6.9	7.2	0.1	2.3	9.7	0.5	0.9	(a)0.025	13.3
	163617	23.5	0.31	5.4	2.6	0.05	2	21.3	1.5	0.8	0.06	13.5
	163718	54.5	0.33	3.4	1.6	(a)0.025	6.2	13.1	0.4	0.7	(a)0.025	20.1
	163842	50.5	0.43	18.3	5.2	(a)0.025	0.6	0.2	0.7	3	0.06	21.4
	163932	66.8	0.56	6.9	4.8	0.05	2	6.8	0.4	0.9	(a)0.025	11.3
	163934	60.6	0.51	7.8	7.9	0.05	2.5	6.6	0.3	1.2	(a)0.025	12
Ratios	161753	1.10	1.34	1.40	0.47	0.64	1.29	1.13	1.45	1.62	1.60	0.83
	163136	0.97	1.44	1.22	0.61	0.82	1.19	1.22	1.23	1.35	1.60	1.01
	163350	1.02	1.54	1.35	0.70	0.78	1.07	0.94	1.46	1.52	2.00	0.92
	163617	1.32	1.55	1.51	1.53	2.04	1.40	0.84	1.38	1.63	1.50	0.84
	163718	1.11	2.18	1.56	1.43	1.48	0.90	0.74	1.33	1.51	1.20	0.75
	163842	1.14	1.37	1.07	1.08	0.52	1.08	1.40	0.71	0.70	1.17	0.68
	163932	0.95	1.43	1.28	0.97	1.08	1.11	1.07	1.18	1.34	1.60	0.93
	163934	1.03	1.31	1.24	0.58	1.00	0.97	1.09	1.30	1.35	1.20	0.93
Average		1.08	1.52	1.33	0.92	0.67	1.13	1.05	1.25	1.38	1.48	0.86

NOTES: (a) set to one-half the lower limit of detection
 ICP-MS inductively coupled plasma-mass spectrometry
 LOI loss on ignition
 XRF X-ray fluorescence spectrometry

Table 5. Summary statistics of the total major element chemistry and values for LOI, pH, and chemical index of alteration (CIA) for the coarse fraction (<2 mm to >45 µm) of 151 regolith samples

	SiO ₂ (%)	TiO ₂ (%)	Al ₂ O ₃ (%)	Fe ₂ O ₃ (%)	MnO (%)	MgO (%)	CaO (%)	Na ₂ O (%)	K ₂ O (%)	P ₂ O ₅ (%)	LOI (%)	pH	CIA (%)
Min	31.2	0.11	2.06	0.75	^(a) 0.0025	^(a) 0.05	0.02	^(a) 0.01	0.19	^(a) 0.005	0.81	4.20	15.4
Mean	69.8	0.52	8.27	5.73	0.05	1.45	3.69	0.56	1.12	0.027	8.49	7.98	63.6
Median	70.7	0.50	7.81	3.73	0.03	1.07	2.23	0.40	0.91	0.025	8.45	8.50	66.9
75th	79.9	0.63	10.4	6.78	0.06	1.90	6.08	0.70	1.30	0.025	12.0	8.70	77.6
95th	88.5	0.92	14.0	16.2	0.11	3.37	11.3	1.67	2.70	0.05	17.2	9.00	92.0
Max	96.7	2.53	18.3	38.4	0.26	15.9	16.2	4.20	4.20	0.09	23.7	9.70	96.9
SD	12.6	0.30	3.20	5.41	0.03	1.74	3.83	0.56	0.69	0.01	4.88	1.14	18.9
Skew	-0.26	2.92	0.50	3.07	2.29	4.69	1.11	3.08	1.98	2.32	0.54	-1.42	-0.33
UCC	66.6	0.64	15.4	^(b) 5.04	0.10	2.48	3.59	3.27	2.80	0.15	—	—	—

NOTES: (a) data are reported below the lower limit detection (LLD) and replaced by values of half the LLD
 (b) total FeO
 CIA = chemical index of alteration = $\text{Al}_2\text{O}_3 / (\text{Al}_2\text{O}_3 + \text{Na}_2\text{O} + \text{CaO} \# + \text{K}_2\text{O}) \times 100$ (oxides in molar proportions) (Nesbitt and Young, 1982)
 UCC = upper continental crust average (Rudnick and Gao 2003)
 — not applicable

Here, samples with lower SiO₂/CaO ratios and higher LOI values correspond to relatively high carbonate and low silicate material. In relation to pH, more carbonate-rich samples (i.e. lower ratios) have higher pH (Fig. 11b).

The chemical index of alteration (CIA; Nesbitt and Young, 1982) provides an indication of the combined effects of weathering of the bedrock source of regolith, and the weathering of the regolith:

$\text{CIA} = \text{Al}_2\text{O}_3 / (\text{Al}_2\text{O}_3 + \text{Na}_2\text{O} + \text{CaO} \# + \text{K}_2\text{O}) \times 100$ (oxides in molar proportions)

In this equation, CaO# is the amount of CaO in the silicate fraction, so samples containing non-silicate phases such as calcite or gypsum can result in low CIA values (Reimann et al., 2012). The index reflects the breakdown of feldspar and mica to clay minerals such as kaolinite, although for regolith it reflects the total chemical weathering history of the material (McQueen and Scott, 2008). In regolith-related studies, the CIA is commonly applied to establish alteration and weathering trends within a regolith profile from the pedolith to the saprolite (McQueen and Scott, 2008).

CIA values for the 151 regolith samples discussed here range from 15.4 to 96.9% with a median of 66.9% (Table 5), with higher values indicating more chemical weathering. In comparison, the median CIA value is 72% for overbank sediments from the whole of Australia (De Caritat et al., 2012) and 60% for European soils (Reimann et al., 2012). Values for unweathered felsic and mafic igneous rocks are around 40% (Nesbitt and Young, 1982), with upper parts of regolith profiles corresponding to CIA values in excess of 90% (Nesbitt et al., 1997). The influence of carbonate on the CIA index (Fig. 11c) is shown by the strong positive correlation of Si/Ca ratios and the CIA (Fig. 11c).

Samples with the highest CIA values ($\geq 92\%$; Table 5) are found in areas of sandplain over the Gunbarrel Basin and northern Albany–Fraser Orogen (Fig. 10a). Samples with lower CIA values (indicating less alteration and/or the influence of non-silicate CaO) are commonly found across the Kurnalpi Terrane and the Northern Foreland of the densely sampled part of the Fraser Range region (Fig. 10b).

Variation across regolith types

In terms of regolith type, samples with the highest CaO concentrations are from lacustrine areas (Fig. 12a; black horizontal line; median of 7%), although samples with the lowest CaO concentrations (<1%) are found in regolith near exposed bedrock and alluvium. Samples from colluvium, sandplain, and sheetwash have lower median values than lacustrine areas. The wider range of CaO for colluvium and sandplain may reflect the greater number of samples.

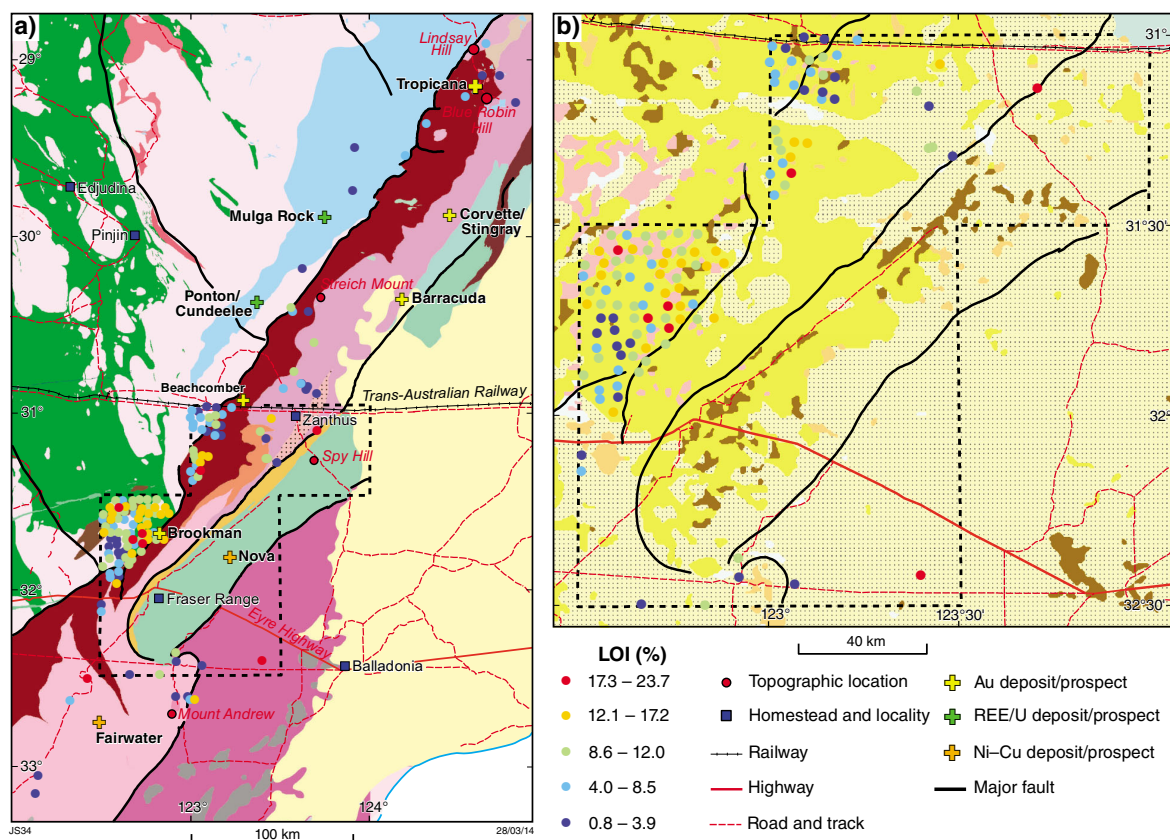


Figure 6. Graduated colour dot map of loss on ignition (LOI) data for 151 regolith samples: a) the study area; b) a detailed view of the Fraser Range region; for geology and regolith backdrop refer to Figures 2 and 3

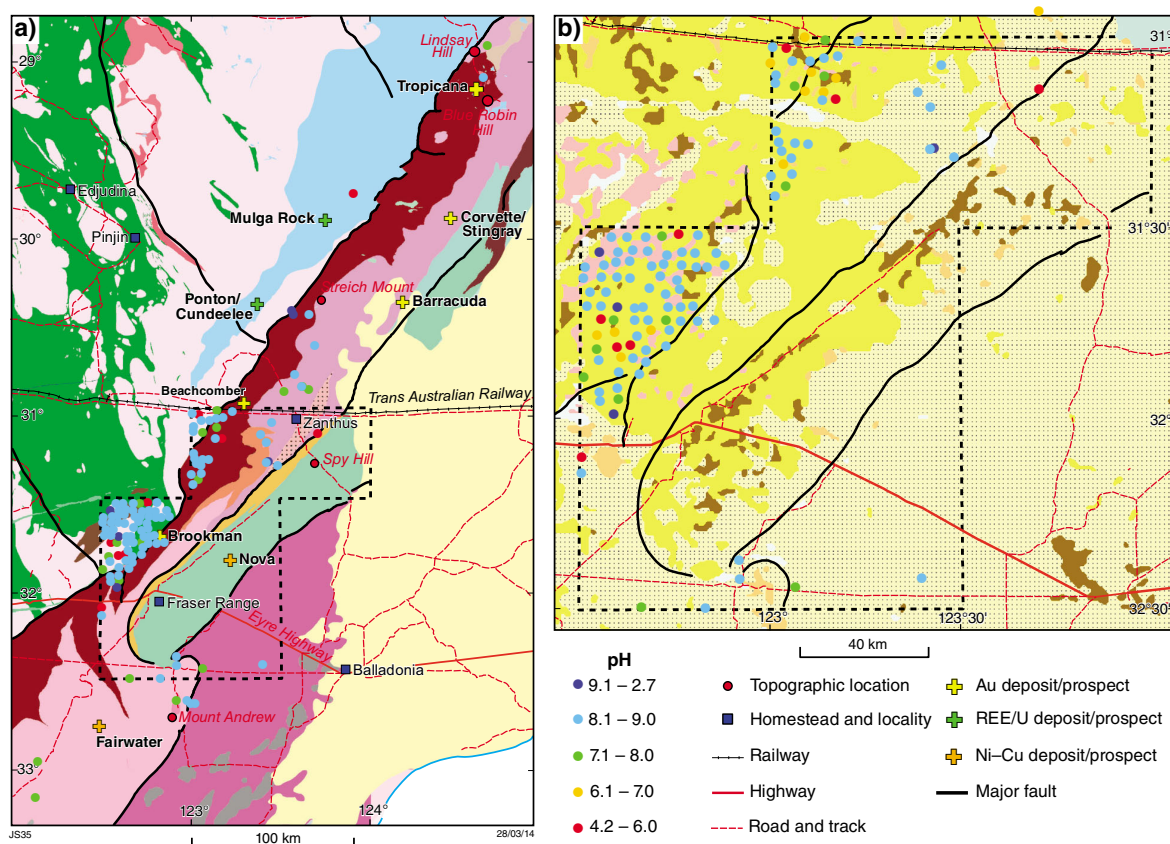


Figure 7. Graduated colour dot map of pH data for 151 regolith samples: a) the study area; b) a detailed view of the Fraser Range region; for geology and regolith backdrop refer to Figures 2 and 3

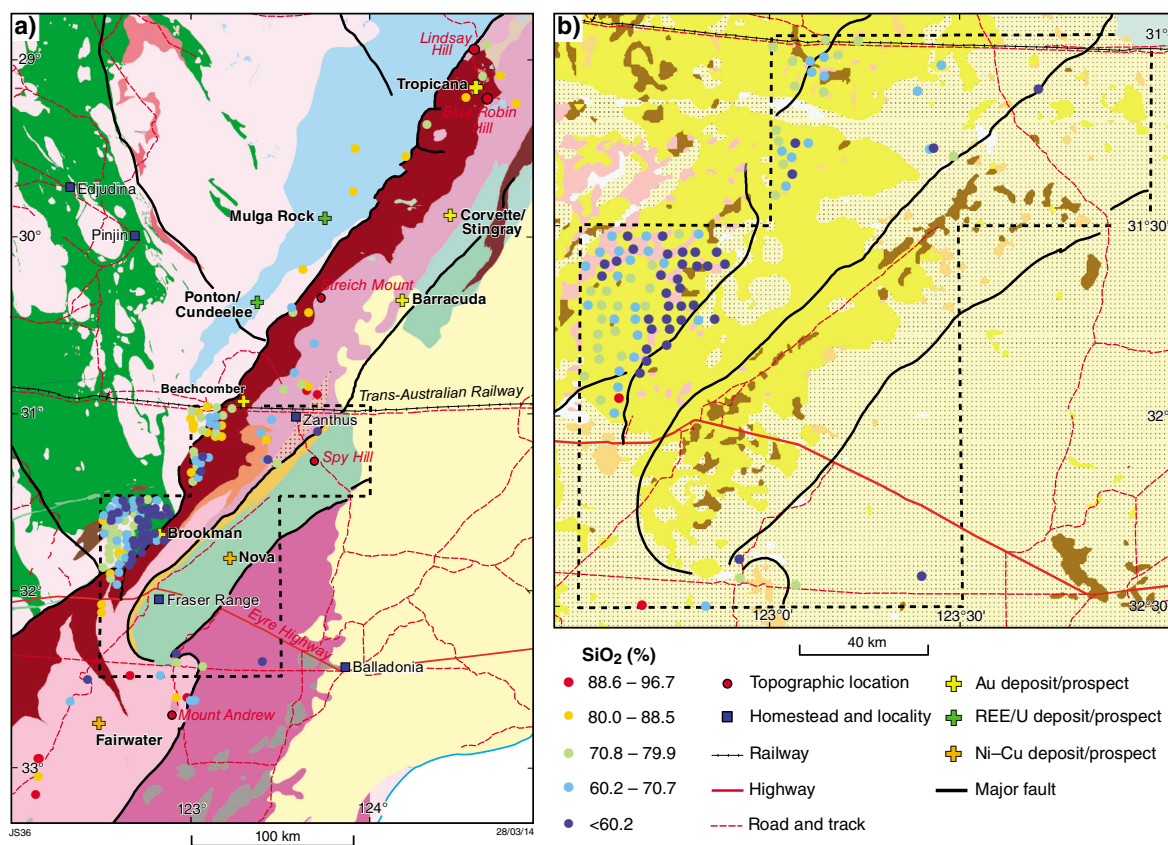


Figure 8. Graduated colour dot map of the SiO₂ concentration in 151 regolith samples: a) the study area; b) a detailed view of the Fraser Range region; for geology and regolith backdrop refer to Figures 2 and 3

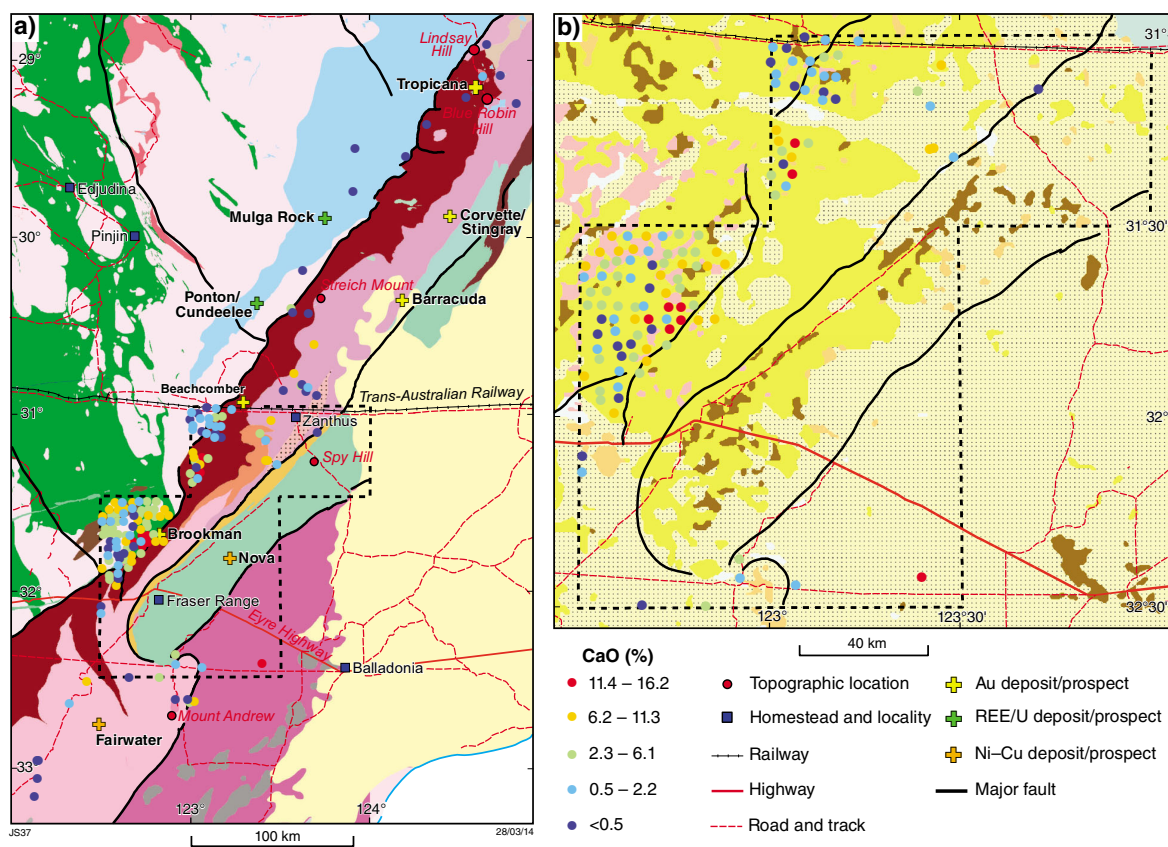


Figure 9. Graduated colour dot map of the CaO concentration in 151 regolith samples: a) the study area; b) a detailed view of the Fraser Range region; for geology and regolith backdrop refer to Figures 2 and 3

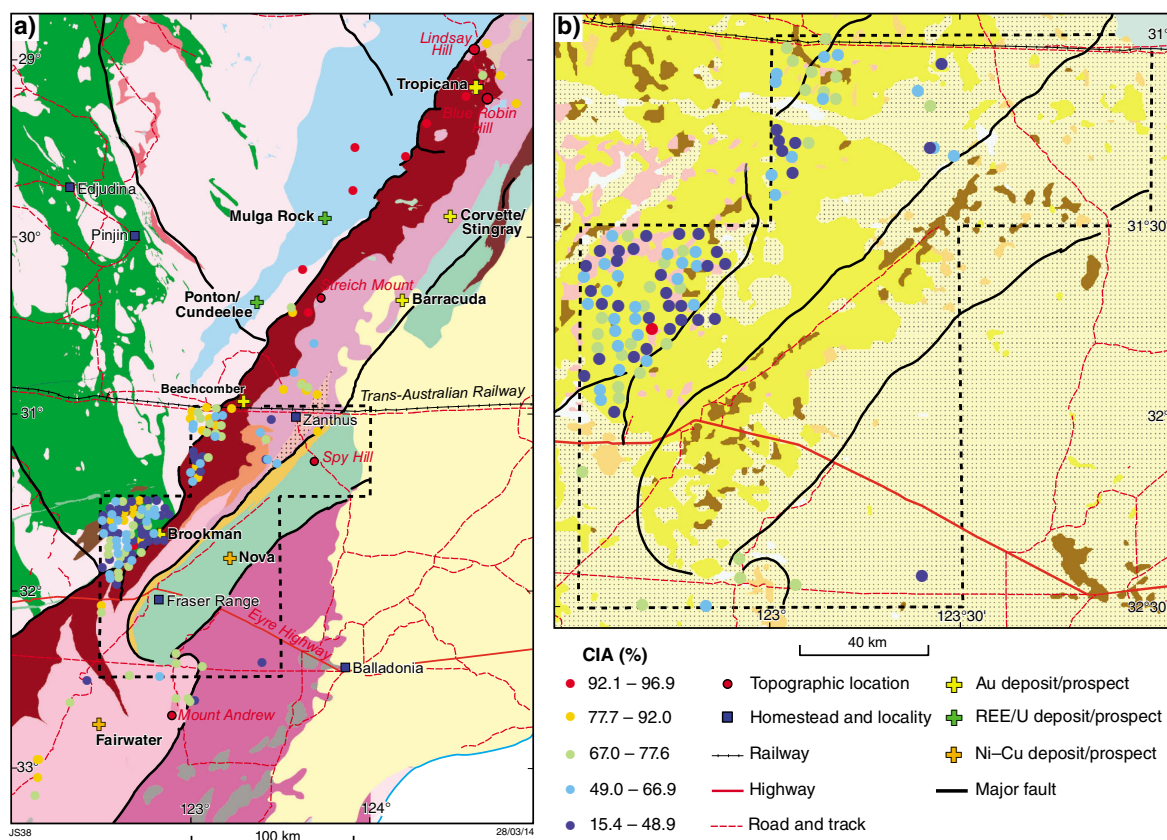


Figure 10. Graduated colour dot map of the chemical index of alteration (CIA) for 151 regolith samples of: a) the study area; b) a detailed view of the Fraser Range region. For geology and regolith backdrop refer to Figures 2 and 3

The SiO_2 concentrations (Fig. 12b) display the opposite distribution to CaO . Samples with the highest SiO_2 contents ($\sim 80\%$) are found in areas of alluvium and near exposed bedrock. Lowest median values for SiO_2 ($<66\%$) correspond to colluvium and lacustrine deposits. Surprisingly, samples from areas of sandplain have a median of 69%, but have the widest concentration range, including some of the highest SiO_2 values.

The distribution of LOI data in relation to the regolith types (Fig. 12c) is similar to that shown by CaO . The highest LOI values (median of 11%) correspond to samples from lacustrine deposits, closely followed by samples in areas of colluvium. Sandplain deposits again display the widest data range with the third-highest median of 9%. The lowest LOI measurements are found in samples from exposed areas of bedrock and alluvium, with these areas also accounting for some of the lowest pH values (Fig. 12d). The median pH for samples from colluvium near to exposed bedrock is <7 , whereas the highest pH median values (>8.5) relate to lacustrine, colluvium, and sheetwash. These three sample types show the narrowest concentration range and indicate highly alkaline conditions.

Relating the regolith matrix to the fine-fraction chemistry

The data presented to describe the regolith matrix correspond to the coarse fraction of the samples. Major element concentrations such as SiO_2 and CaO , and pH and LOI data are not available for the fine fraction ($<50 \mu\text{m}$) of regolith samples, which have been analysed for approximately 49 trace elements using four partial digests. Thus, in order to assess the regolith matrix and the effects of the carbonate content on the trace element chemistry of the fine fraction, it is important to find a trace element proxy that can be used instead of the Si/Ca ratio or LOI.

Summary statistics of Table 6 show that 'total' CaO concentrations in the $<2 \text{ mm}$ sample fraction and Ca concentrations determined by AR and hydrochloric acid (TL7) in the $<50 \mu\text{m}$ fraction are almost identical. This is also expressed by a positive correlation between total CaO with extractable Ca in the $<50 \mu\text{m}$ fraction of AR and TL7 data (Fig. 13). Calcium concentrations from TL9 and TL0 digestion are less than 2% of the total CaO values (Table 6); there is also a weak linear relationship between total CaO values and TL0 data ($r^2 = 0.37$; Fig. 13) and no linear relationship for TL9 data.

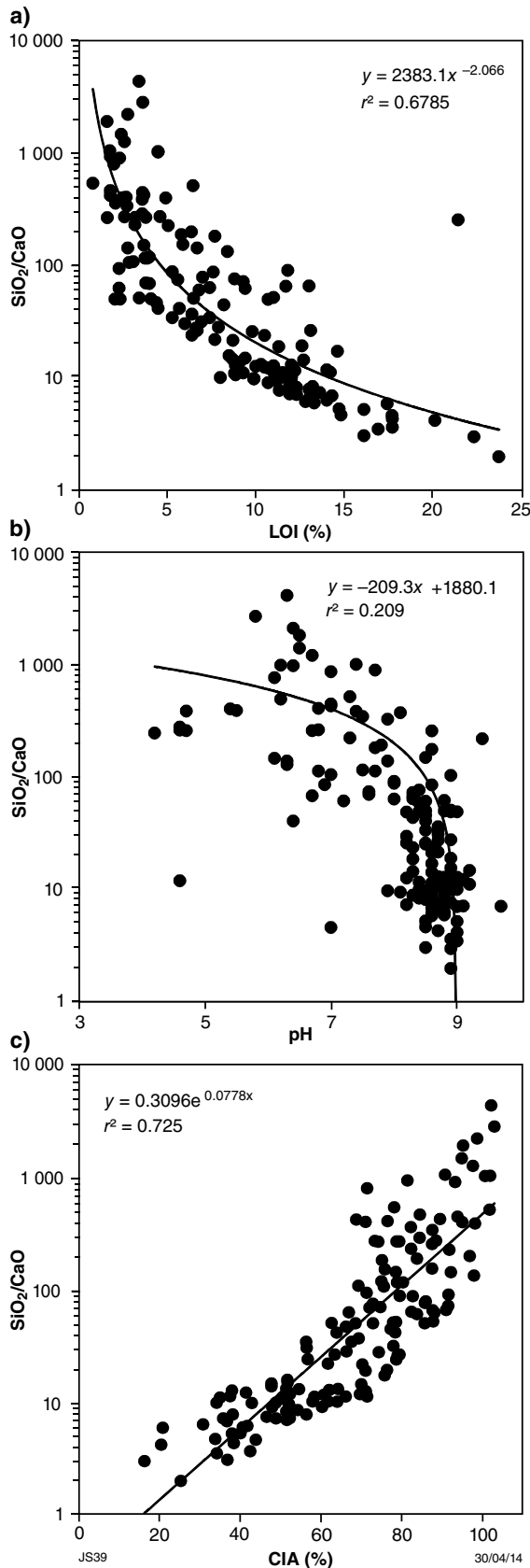


Figure 11. Bivariate plots of the SiO_2 to CaO ratio against: a) LOI; b) pH; and c) chemical index of alteration (CIA) for the coarse sample fraction (<2 mm to >45 μm) of 151 regolith samples (<2 mm for XRF data)

Figure 14a,b shows that increasing Ca from AR and TL7 digestions is accompanied by an increase in LOI and a decrease in SiO_2 . The relationship with pH (Fig. 14c) is not as clear, although samples with $\text{pH} < 8$ typically show low Ca concentrations (<2%). A good relationship is displayed in Figure 14d where increasing extractable Ca concentrations relate to decreasing CIA values. Partial digest TL9 data show indistinct relationships with SiO_2 concentration, pH, LOI, and CIA (Fig. 14).

The similar ionic radii and same charge of Ca and Sr ions mean that they readily substitute for each other in the carbonate matrix. Figure 15a shows that an increase in concentration of Sr extractable by AR is accompanied by a gradual decrease in Si/Ca ratio. Thus, AR-extractable Sr in the <50 μm fraction is also a measure of the carbonate content of regolith. Although no clear relationship exists between a Si/Ca ratio of the <2 mm fraction and the AR-extractable Rb concentrations (Fig. 15b), the ratios of Rb to Sr and Rb to Ca from the AR dataset seem to indicate a strong relationship with the Si/Ca ratio (Fig. 15c,d). Thus, either of the latter two ratios can be used as a proxy for the regolith matrix, where high ratios indicate a silicate-dominated and low ratios a carbonate-dominated matrix.

Discussion of the regolith matrix

The total major element, LOI, pH, and CIA data in the coarse fraction of regolith samples are closely related. In general, samples with low pH and LOI correspond to elevated SiO_2 contents and CIA values, but regolith samples with high pH values have elevated LOI, high CaO concentration, low SiO_2 concentration, and low CIA. Across the study area, the regolith is alkaline and silica-dominated with a median SiO_2 concentration of 71%. However, there is a wide range in SiO_2 content, especially in samples from areas of sandplain and colluvium (Fig. 12), indicating heterogeneous regolith composition. Those regolith samples with low pH (<7) are also high in SiO_2 and reflect close proximity to Ca-poor granitic bedrock of the Yilgarn Craton. Regolith samples with high CaO, pH, and LOI are mainly found in colluvium and lacustrine deposits. Colluvium samples are mostly spatially related to Ca-rich mafic rocks of Archean greenstone belts. This finding is consistent with Anand and Smith (2005) and Anand et al. (1997), who established a close genetic relationship between calcrete and greenstones in the Mt Gibson area of the Youanmi Terrane. In lacustrine deposits, elevated CaO concentrations reflect evaporate-rich successions, with carbonates and sulfates (e.g. gypsum, alunite), which are commonly associated with such saline environments. Elevated CaO contents in some sandplain samples are likely related to either the presence of carbonate clasts as discussed by Morris et al. (2000), or the influx of Ca-rich eolian dust. Of the carbonate in the fine fraction, less than 0.13% is soluble. Calcium concentrations produced by sodium pyrophosphate (TL9) digestion show a negative correlation with LOI, pH, and total CaO and a positive relationship with SiO_2 , indicating that this Ca content is not released from carbonate, but is possibly bound within organic parts of the sample.

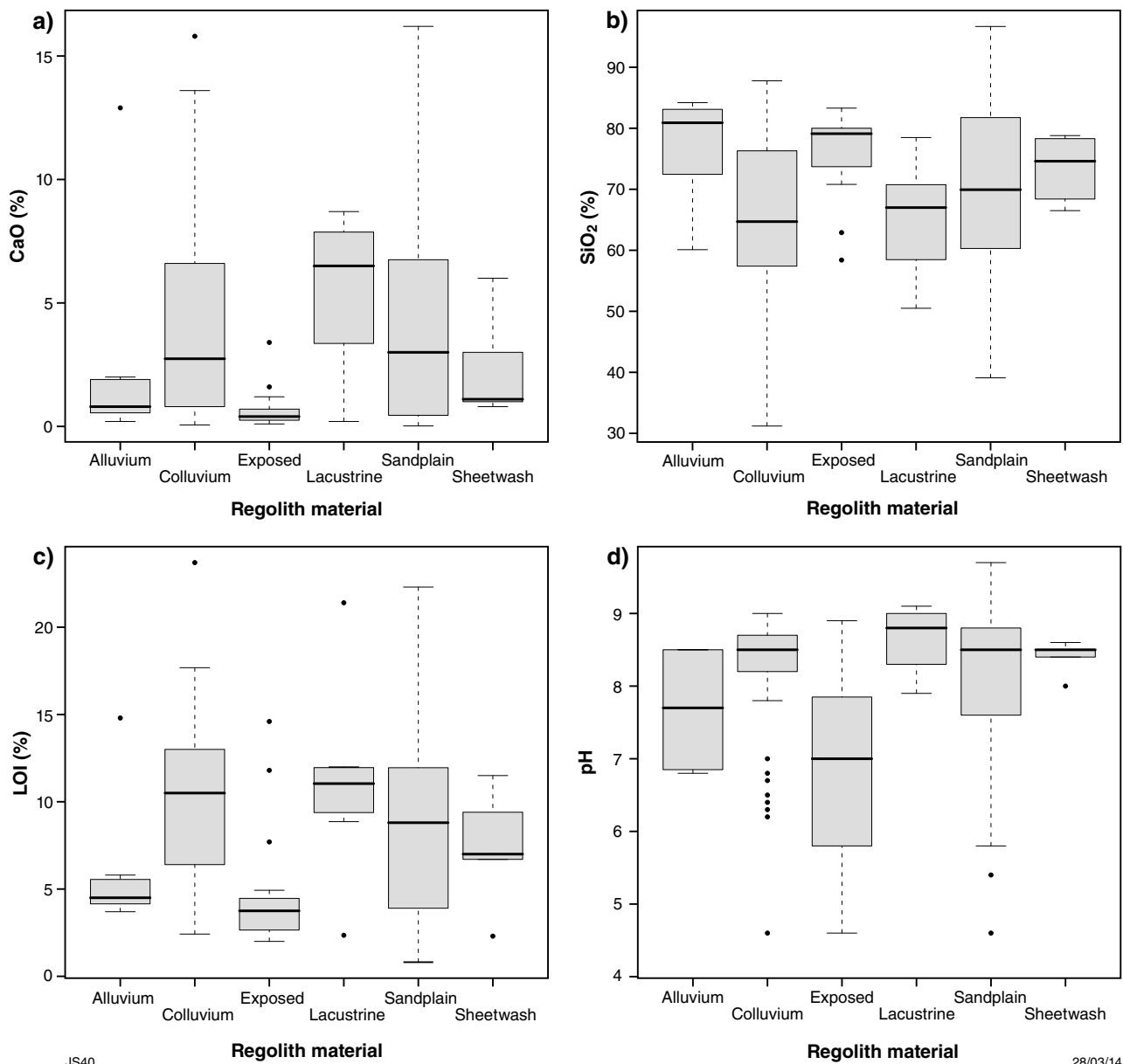


Figure 12. Box-and-whisker plots: a) CaO concentrations; b) SiO₂ concentrations; c) loss on ignition (LOI) values; d) pH values in the coarse fraction (<2 mm to >45 μ m for ICP and <2 mm for XRF analyses) for the six regolith types present in the study area: alluvium $n = 7$, colluvium $n = 41$, (near) exposed bedrock $n = 15$, lacustrine $n = 7$, sandplain $n = 75$, and sheetwash $n = 5$; black horizontal line within each box indicates the median, whiskers represent values of $1.5 \times$ the interquartile range (IQR) and outliers (black dots) are greater or less than $IQR \pm (1.5 \times IQR)$.

The influence of grain size on chemistry is shown by the lower Al, Na, and K contents (i.e. sequestered in silt and clay) of the <2 mm to >45 μ m fraction than the <2 mm fraction (Table 5).

When assessing the weathering state of regolith, CIA data should be viewed with caution as they include both the weathering state of the bedrock source and the weathering of the regolith itself. Furthermore, the presence of carbonate results in an artificially low CIA value. Thus, CIA values <60% are most likely affected by the presence

of carbonate, and CIA values do not reflect silicate weathering, as discussed by Scheib (2013).

As the total CaO concentrations in the coarse fraction are almost identical to those extracted from the fine fraction by aqua regia, carbonate is present in both grain size fractions. This result means that AR-extracted Ca can be used as a proxy for the carbonate content. The silicate content is best reflected by the AR-extracted Rb/Ca ratio of the fine fraction, where elevated Rb/Ca ratios indicate silicate-rich regolith.

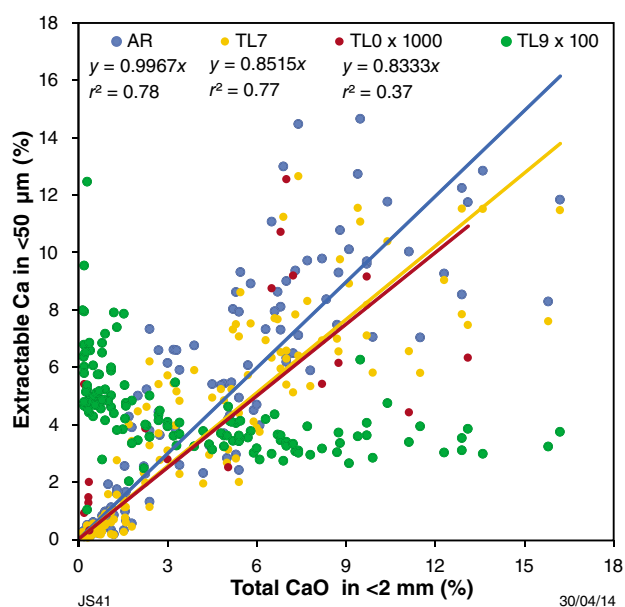


Figure 13. (left) Bivariate plot of extractable Ca concentrations (converted to %) following aqua regia (AR), TerraLeach (TL)9, and TL7 digestion of the <50 µm fraction against total CaO concentrations of the <2 mm to >45 µm fraction (<2 mm for XRF analyses); linear regression equations and correlation coefficient (r^2) displayed for AR, TL0, and TL7 data

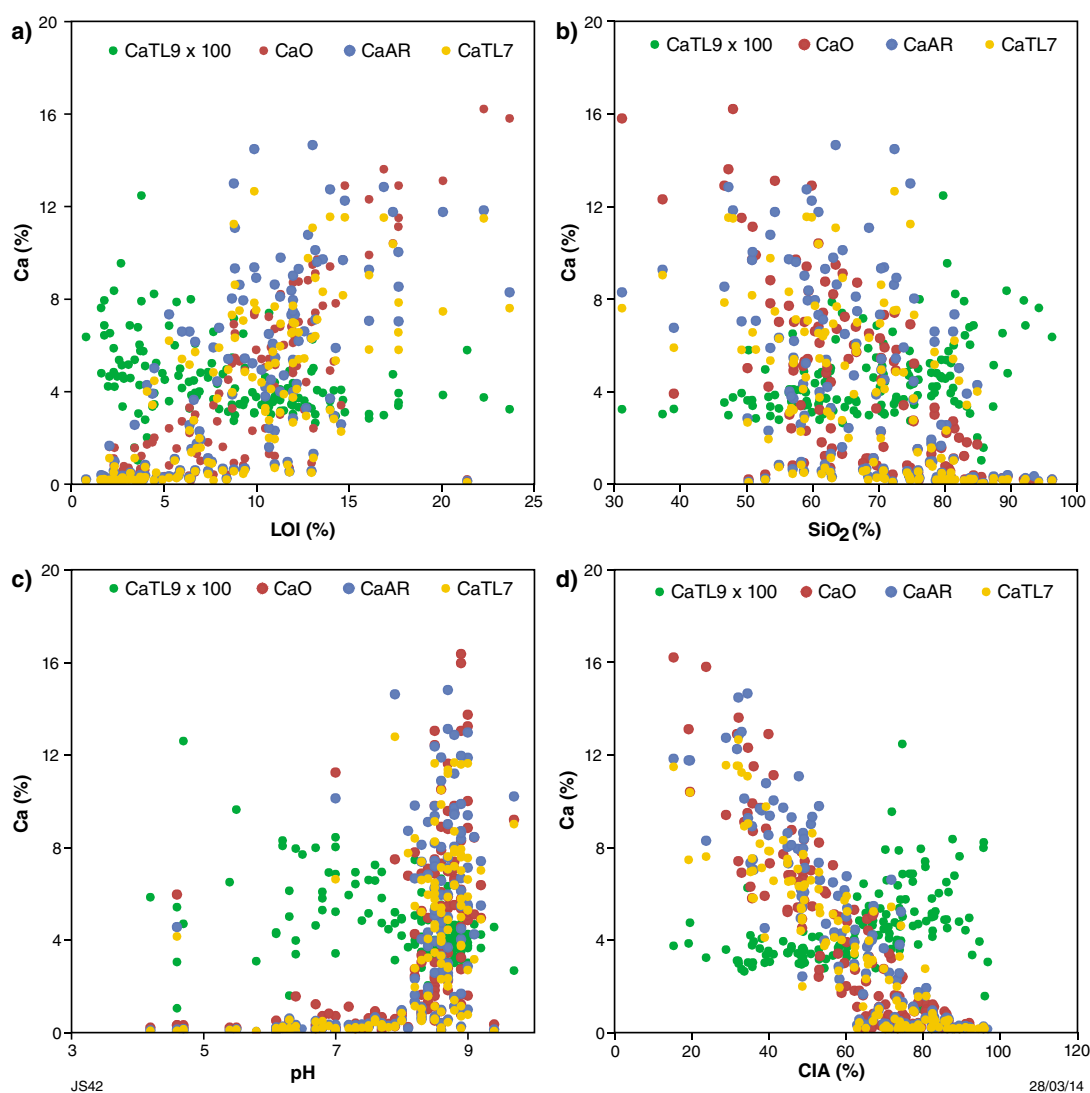
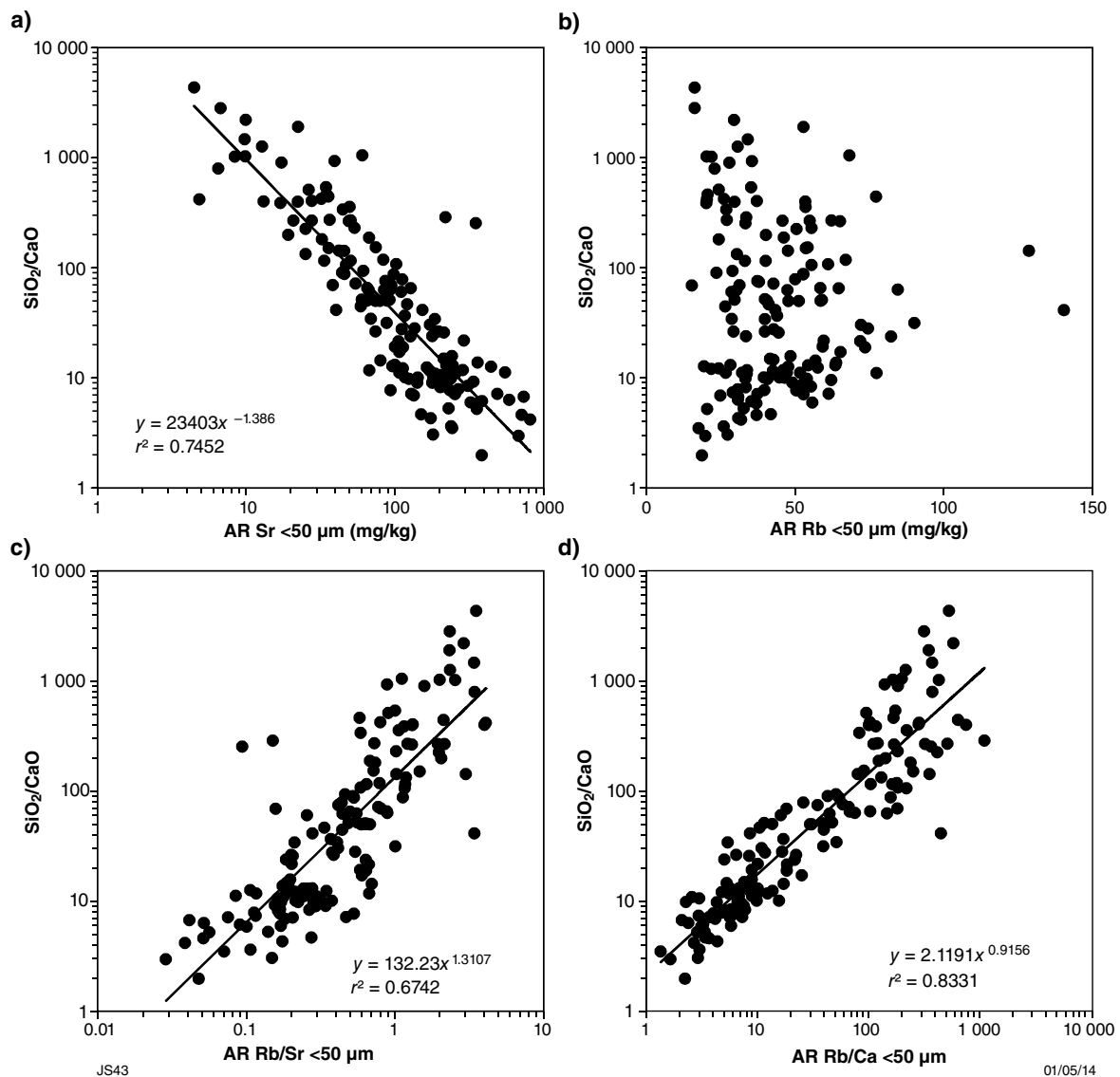


Figure 14. Bivariate plots of aqua regia (AR), TerraLeach (TL)7, and TL9-extractable Ca concentrations (of the <50 µm fraction) and the total CaO concentration (of the <2 mm to >45 µm fraction and <2 mm for XRF analyses) against: a) loss on ignition (LOI); b) SiO₂ concentration; c) pH; d) chemical index of alteration (CIA)

Table 6. Summary statistics of total CaO and extractable Ca concentrations determined by aqua regia (AR), sodium pyrophosphate (TL9), hydrochloric acid (TL7), and deionized water (TL0) digestions

	CaO (<2 mm)	Ca (<50 µm)			
	Total (%)	AR ^(a) (%)	TL9 (%)	TL7 (%)	TL0 (%)
Min	0.02	0.03	0.01	0.01	0.0003
Mean	3.69	3.94	0.04	3.43	0.0044
Median	2.23	2.55	0.04	2.66	0.0033
75th	6.08	7.05	0.05	5.95	0.0063
95th	11.3	11.8	0.08	10.1	0.0106
Max	16.2	14.7	0.12	12.7	0.0125
SD	3.83	4.02	0.02	3.43	0.0037
Skew	1.11	0.76	1.53	0.76	0.75

NOTE: (a) AR, TL9, TL7, TL0 are described in Table 3.

**Figure 15. Bivariate plots of the ratio of SiO₂ to CaO concentrations in the coarse fraction (<2 mm to >45 µm and <2 mm for XRF analyses) against aqua regia (AR)-extractable concentrations of: a) Sr; b) Rb; c) Rb/Sr ratio; d) Rb/Ca ratio in the fine fraction (<50 µm)**

Trace element chemistry in the fine fraction

Gold

Mineral exploration in areas of thick, transported regolith has focused locally on the most carbonate-rich fraction of regolith; thus the process of carbonate formation has been linked to the presence of gold (Lintern, 1997, 2002). However, other studies have shown that elevated concentrations of gold in regolith are found in the fine fraction, yet there is no clear relationship with the carbonate content of the sample (Morris, 2013a). In this study, Au data from the fine fraction are assessed in relation to digestion methods and regolith matrix, i.e. the carbonate and silicate contents.

Summary statistics for Au according to partial digest of the <50 µm fraction (Table 7; Fig. 16) show that measured Au concentrations decrease in the following order AR >> FA > TL9 > TL7 > TL0, with AR concentrations notably higher than for other digests. Fire assay results from the coarser, <2 mm to >45 µm, fraction are lower than AR concentration, indicating that a substantial amount of gold is sequestered in the fine fraction (Table 7). Compared with AR data, TL9 and TL7 digestions can only extract 20 and 14% of Au, respectively. Furthermore, only 4% of the AR-extracted Au is released following deionized water digestion. Results for TL9 and TL0 digestions produced censored data for >20% of samples (Table 7).

Bivariate plots (Fig. 17) show positive correlations in AR-extracted Au concentration for FA, TL9, and TL0 data (Fig. 17a,c,d), although there is poor correlation with TL7 data (Fig. 17b). The three most anomalously high samples in terms of AR digestion (>26.1 µg/kg; GSWA 161753, 163932, and 163136; labels 1, 2 and 3, respectively) also have the highest Au values of other approaches (Fig. 17), with the exception of TL0 for GSWA 163136 (Fig. 17d, label 3).

Most anomalously high Au concentrations (>13.7 µg/kg; 95th percentile; red stars in Fig. 18) are found in regolith samples over rocks of the Northern Foreland and close to the Cundeelee and Jerdacuttup Faults northwest of Fraser Range homestead (GSWA 161738, 161753, 163136, 163350, and 163932; Appendix 1). A more detailed coverage (Fig. 18b) shows that latter five anomalous samples are commonly found close to exposed bedrock, and to known Au occurrences (e.g. Brookman in Fig. 18b). In the remainder of the study area, two samples with anomalous Au concentrations are located south of Zanthus (Fig. 18b; GSWA 194030 and 163842) with one further sample of elevated Au concentration (>11 µg/kg) north of Zanthus. These three sites correspond to regolith samples from within the Biranup Zone, where sample GSWA 163842 is located right on the Fraser Fault Zone (Figs 2 and 18).

The relationship between the regolith matrix and the extractable Au concentrations by various analytical approaches is expressed in Figure 19, where AR-extractable Ca concentrations are proxy for the carbonate content and Rb/Ca ratios obtained by AR digestion provide a

measure of the silicate content. Figure 19a,b shows no clear relationships between Au and carbonate, although there is weak positive correlation between AR and TL9 Au data. Although the graphical correlation between Au datasets and the extractable Ca concentrations is not particularly convincing, Spearman ranked correlation coefficients listed in Table 8 support a close relationship between Ca and Au in the fine fraction of the regolith samples.

Plots of extractable Au by various analytical approaches vs Rb/Ca ratio (Fig. 19c,d) show no clear relationships either, with the exception of a suggested weak negative correlation between AR and TL9 Au data. Here, the higher anomalous Au concentrations (e.g. >13.7 µg/kg AR-extractable Au) relate to overall low Rb/Ca ratios, which indicate high carbonate and low silicate content. Ranked Spearman correlation calculated for AR-extractable Au data and Rb/Ca ratio returns a coefficient of -0.49, indicating a significant negative relationship between them.

By regolith type, concentrations of AR-extractable Au are highest in alluvial samples (>75% above the median of 6 µg/kg), followed by colluvium and lacustrine deposits, with the lowest measured in regolith samples collected near exposed bedrock (Fig. 20a). However, alluvium samples yield the lowest Au concentrations by FA analysis (Fig. 20b), which is based on the coarse grain size fraction. The highest FA Au values are found in samples from lacustrine areas, then colluvium and sandplain. These three regolith types also correspond to the highest extractable Au concentrations using TL7 and TL9 (Fig. 20c,d, respectively). Although the highest median values (solid black lines; Fig. 20a,d) correspond to samples from lacustrine regolith and colluvium, most samples with anomalous Au concentrations are found in sandplain samples. For all four analytical approaches (Fig. 20), the overall lowest Au concentrations relate to regolith samples near exposed, commonly granitic, bedrock.

Assessment of digestion methods for the fine fraction

Some partial digests, such as AR, can provide near-total concentrations for many trace elements. They are therefore commonly applied in exploration geochemical mapping programs. AR targets oxides and sulfides, but is largely ineffective for dissolving silicates (Chao, 1984; Leybourne and Rice, 2013). This effect can be shown by the behaviour of Ba and Zr (commonly found in silicates) compared with Zn (associated with sulfides). For Zn, there is good agreement between AR-extractable and total (XRF) data (Fig. 21a). However, AR-extractable concentrations for Ba and Zr are underestimated (Fig. 21b,c); in the case of Zr, by more than an order of magnitude.

The median concentrations for 52 elements determined by four digests in the fine fraction of regolith samples are shown in Appendix 3. TerraLeach data for some elements (e.g. Hg, In, Te, Ta, Pt, and Pd) are not tabulated due to the high proportion of censored data, especially for TL0 digestion.

Table 7. Summary statistics of extractable Au concentrations from digestions using aqua regia (AR), sodium pyrophosphate (TL9), hydrochloric acid (TL7), and deionized water (TL0) in the fine fraction (<50 µm), and Au concentration determined by fire assay (FA) in the coarse fraction (<2 mm to >45 µm)

Au	Unit	AR	TL9	TL7	TL0	FA
LLD	µg/kg	1.00	0.50	0.10	0.05	1.00
Min	µg/kg	1.40	^(a) 0.25	^(a) 0.05	^(a) 0.025	^(a) 0.50
Mean	µg/kg	7.35	1.33	1.02	1.20	2.70
Median	µg/kg	6.00	1.20	0.86	0.22	2.00
75th	µg/kg	9.00	2.00	1.38	1.12	4.00
95th	µg/kg	13.7	3.40	2.30	5.30	8.65
Max	µg/kg	33.5	11.3	4.15	8.42	26.0
SD	—	4.80	1.85	0.79	2.14	3.82
Skew	—	2.61	2.39	1.26	2.47	3.08
n	—	148	146	146	22	109
Censored ^(b)	%	0	28	7	25	21

NOTES: (a) statistics used values of one-half the lower limit of detection (LLD), where data reported below the LLD.

(b) censored data in percentage of values reported below LLD
— not applicable

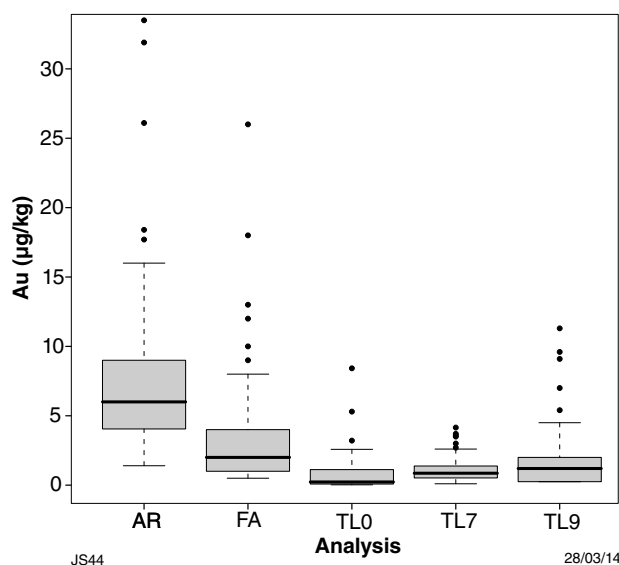
Table 8. Summary of Spearman ranked correlation coefficients between all extractable Au and Ca concentrations in the fine fraction (<50 µm) and total CaO concentrations and loss on ignition (LOI) in the coarse fraction (<2 mm) of 151 regolith samples

	Au AR	Au FA ^(a)	Au TL9	Au TL7	CaO ^(b)	Ca AR	Ca TL9	Ca TL7	LOI ^(b)
Au AR	1	*** ^(c)	***	***	***	***	***	***	***
Au FA ^(a)	0.43	1	***	***	***	***	***	***	***
Au TL9	0.67	0.58	1	***	***	***	***	***	***
Au TL7	0.5	0.33	0.62	1	*	*	***	**	**
CaO ^(b)	0.45	0.67	0.4	0.21	1	***	***	***	***
Ca AR	0.48	0.63	0.47	0.21	0.94	1	***	***	***
Ca TL9	-0.34	-0.37	-0.45	-0.32	-0.6	-0.59	1	***	***
Ca TL7	0.48	0.62	0.46	0.23	0.94	0.99	-0.59	1	***
LOI ^(b)	0.44	0.75	0.41	0.27	0.82	0.73	-0.45	0.74	1

NOTES: (a) coefficients are calculated for 109 samples only

(b) based on coarse fraction data (<2 mm to >45 µm and <2 mm for X-ray fluorescence (XRF) spectrometry)

(c) degree of significance of the correlation for each pair: ***very high ($p < 0.001$), **high ($0.001 < p < 0.01$), *significant ($0.01 < p < 0.05$)

**Figure 16. Box-and-whisker plot of Au concentrations determined by aqua regia (AR), TerraLeach (TL)7, TL9, and TL0 digestions, and fire assay (FA); black horizontal line within each box indicates the median, whiskers represent values of 1.5x the interquartile range (IQR) and outliers (black dots) are greater or less than $IQR \pm (1.5 \times IQR)$**

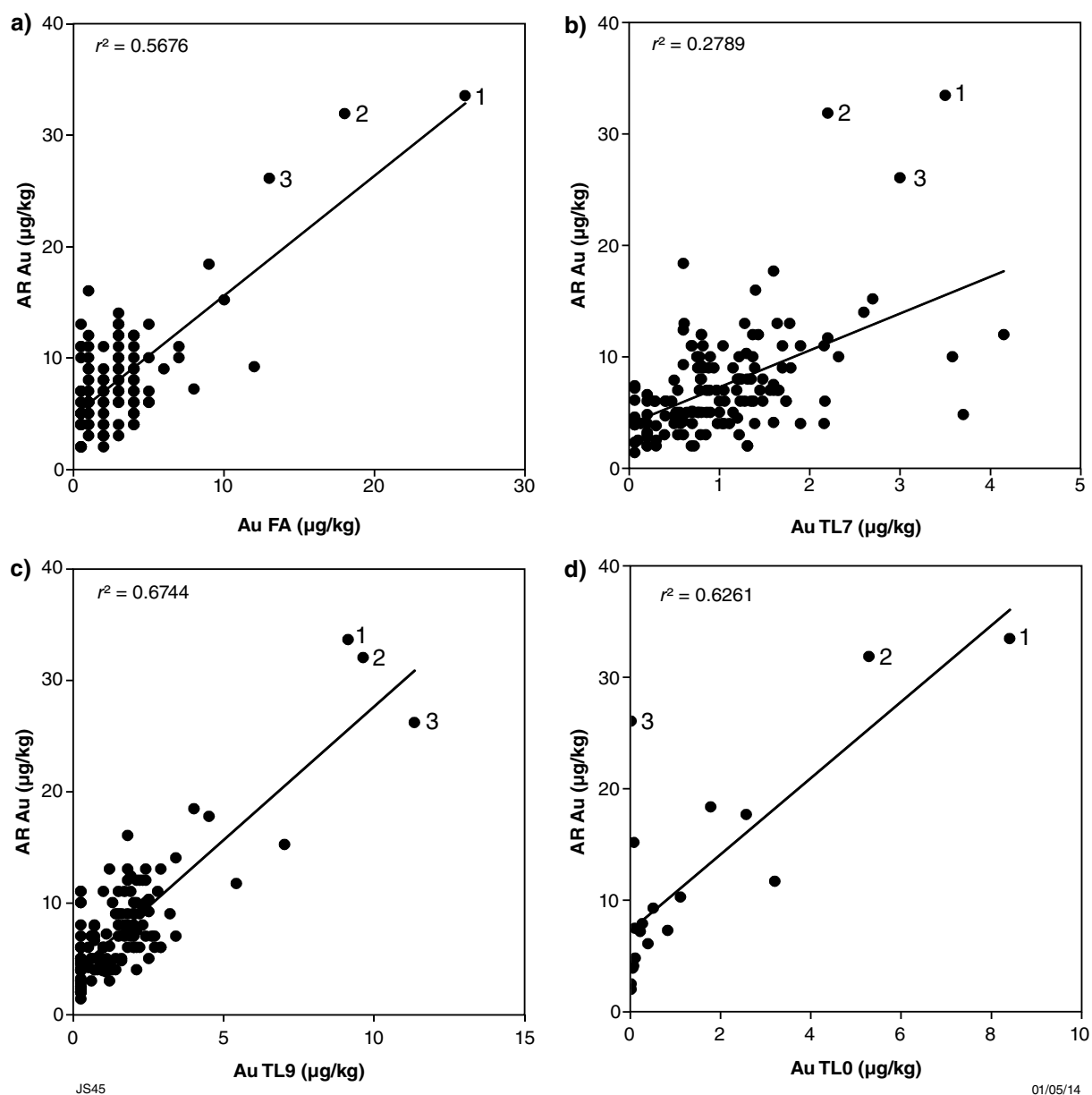


Figure 17. Bivariate plots of aqua regia (AR)-extractable Au concentrations against Au concentrations determined by: a) fire assay (FA); b) TerraLeach (TL)7; c) TL9; d) TL0 digestions; most anomalous Au concentrations are labelled, 1 = GSWA 161753, 2 = GSWA 163932, and 3 = GSWA 163136; values below the lower limit of detection (LLD) were replaced with values one-half of the LLD

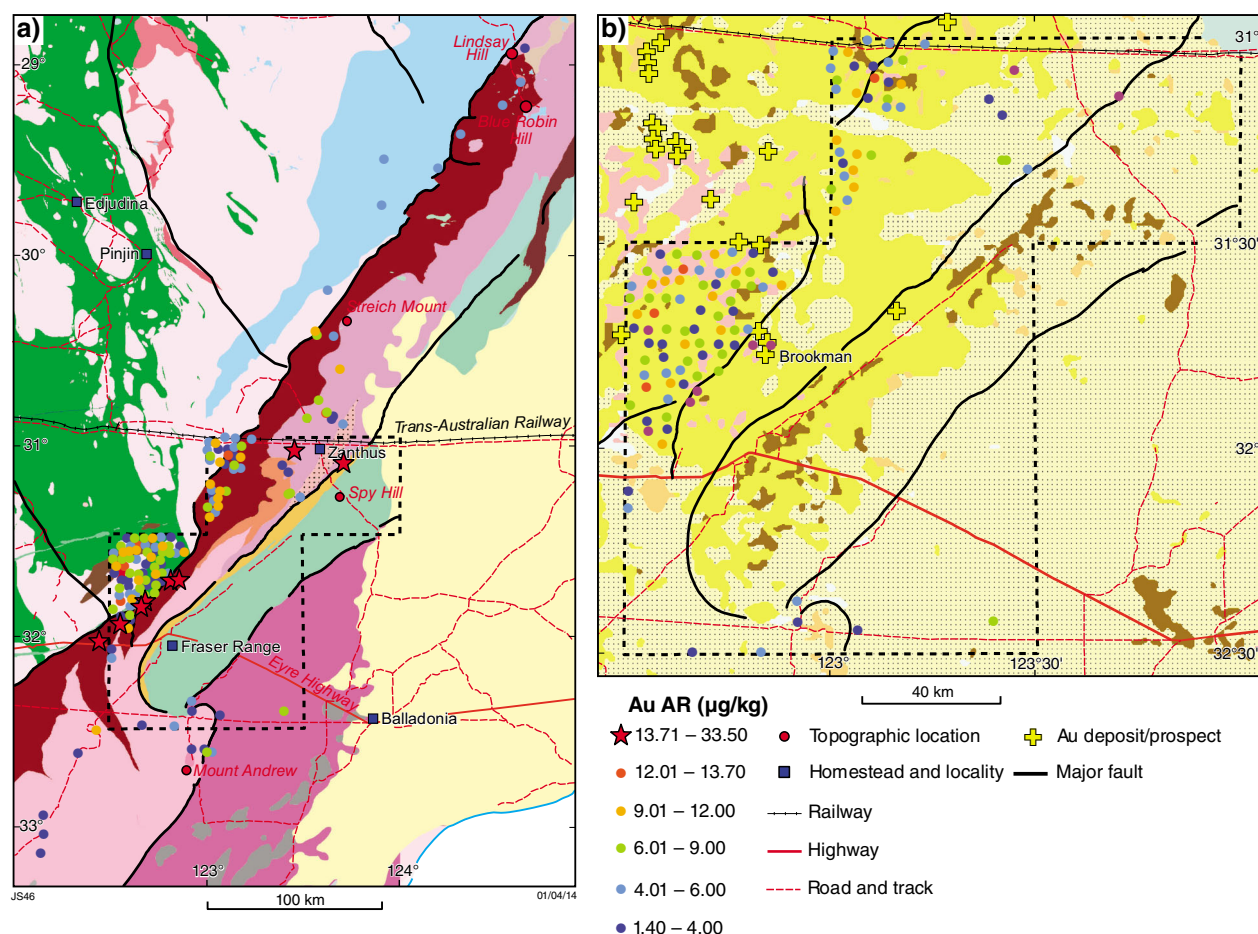


Figure 18. Graduated colour dot map of the aqua regia (AR)-extractable Au concentrations in 151 regolith samples: a) the study area; b) a detailed view of the Fraser Range region; locations marked with a red star correspond to concentrations above the 95th percentile; for geology and regolith backdrop refer to Figures 2 and 3

Median element concentrations typically decrease in the order $AR > TL9 \gg TL7 \gg TL0$, except for Au, As, and Sb where TL9 digestion yields the second-highest median values. Median element concentrations following deionized water digestion (TL0) are at least two, and in some cases more than three, orders of magnitude lower than those following AR (and occasionally TL7) digestion. Deionized water digestion is largely ineffective on the samples, as it provides much lower concentrations than other extraction methods. Median values for all rare earth elements, and Y, Ag, and Cd determined by TL7 are similar to AR results.

Bivariate plots for a selection of elements (Appendix 4) illustrate the behaviour of various TerraLeach digests in relation to AR-extractable data. Nickel, Co, Ce, and Ba clearly indicate much stronger linear relationships between AR and TL7 results, compared with TL9 data. Gallium, Zr, and Sb display the weakest relationships between the

TL and AR methods. All TL0 data show poor agreement with AR data.

A means of graphically illustrating anomalous element behaviour according to digest method is to use the contrast ratio (i.e. 90th percentile value divided by the median). High ratios indicate skewed data caused by anomalously high concentrations. Censored data have been replaced by a value of one-half of the LLD, which can result in a slightly lower contrast ratio. Data for elements where >50% of values are censored have not been considered. Contrast ratio data show two main features (Fig. 22). First, the lowest and most consistent ratios correspond to AR and TL7 data, particularly for the rare earth elements and base metals (e.g. Cr, Ni, Cu, Pb, Zn), which have ratios commonly between 1 and 2. Second, high contrast ratios are more common for TL9 and TL0 data, especially for rare earth elements and high field strength elements (HFSE) such as Hf, Zr, and Nb.

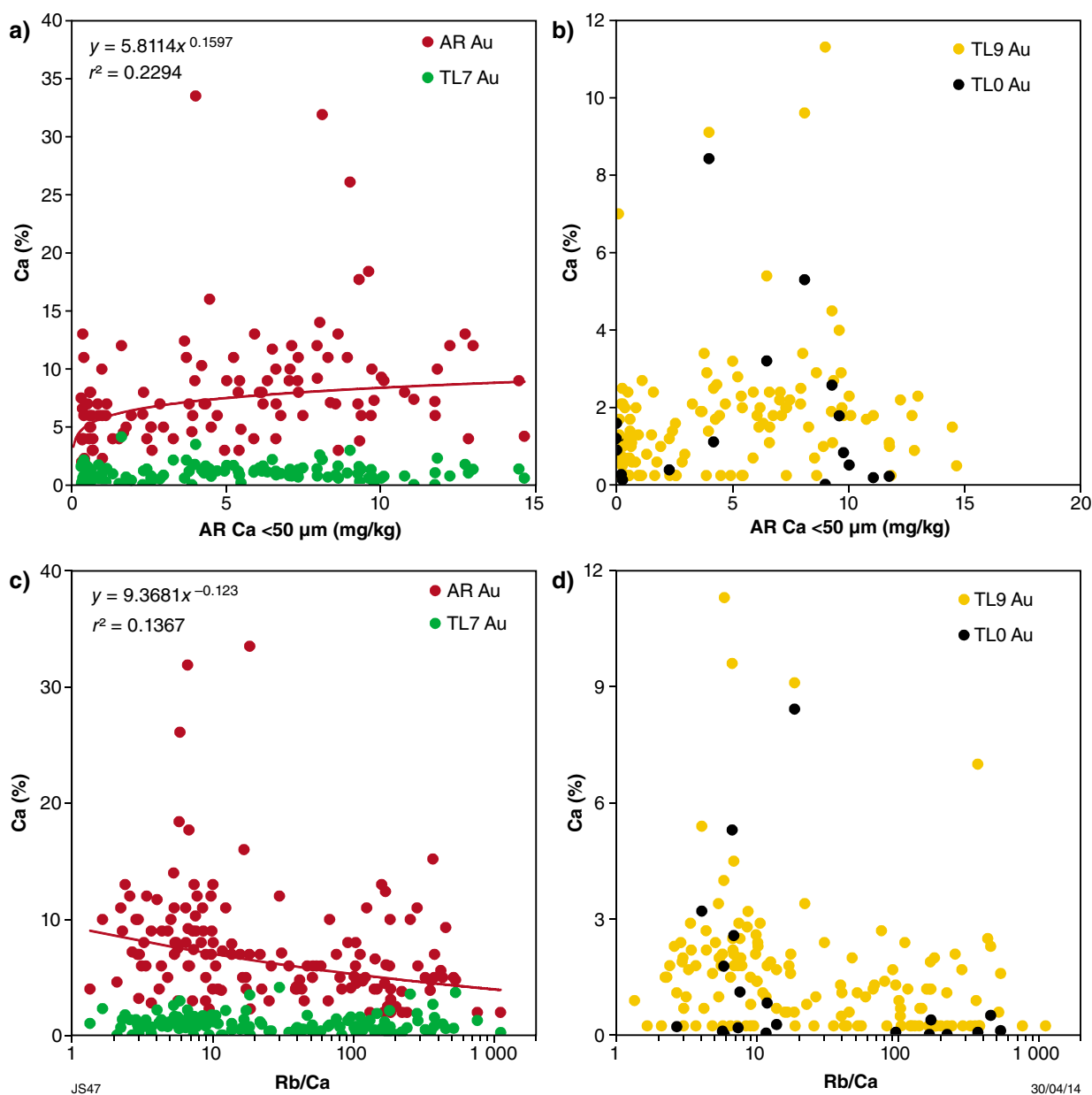


Figure 19. Bivariate plots of: a) aqua regia (AR) and TerraLeach (TL) 7-extractable Au concentrations; b) TL9 and TL0-extractable Au concentrations against the AR-extractable Ca concentrations; and bivariate plots of c) AR and TL7-extractable Au concentrations; d) TL9 and TL0-extractable Au concentrations against the Rb/Ca ratio (both AR-extractable concentrations); all data relate to the fine grain size fraction (<50 µm)

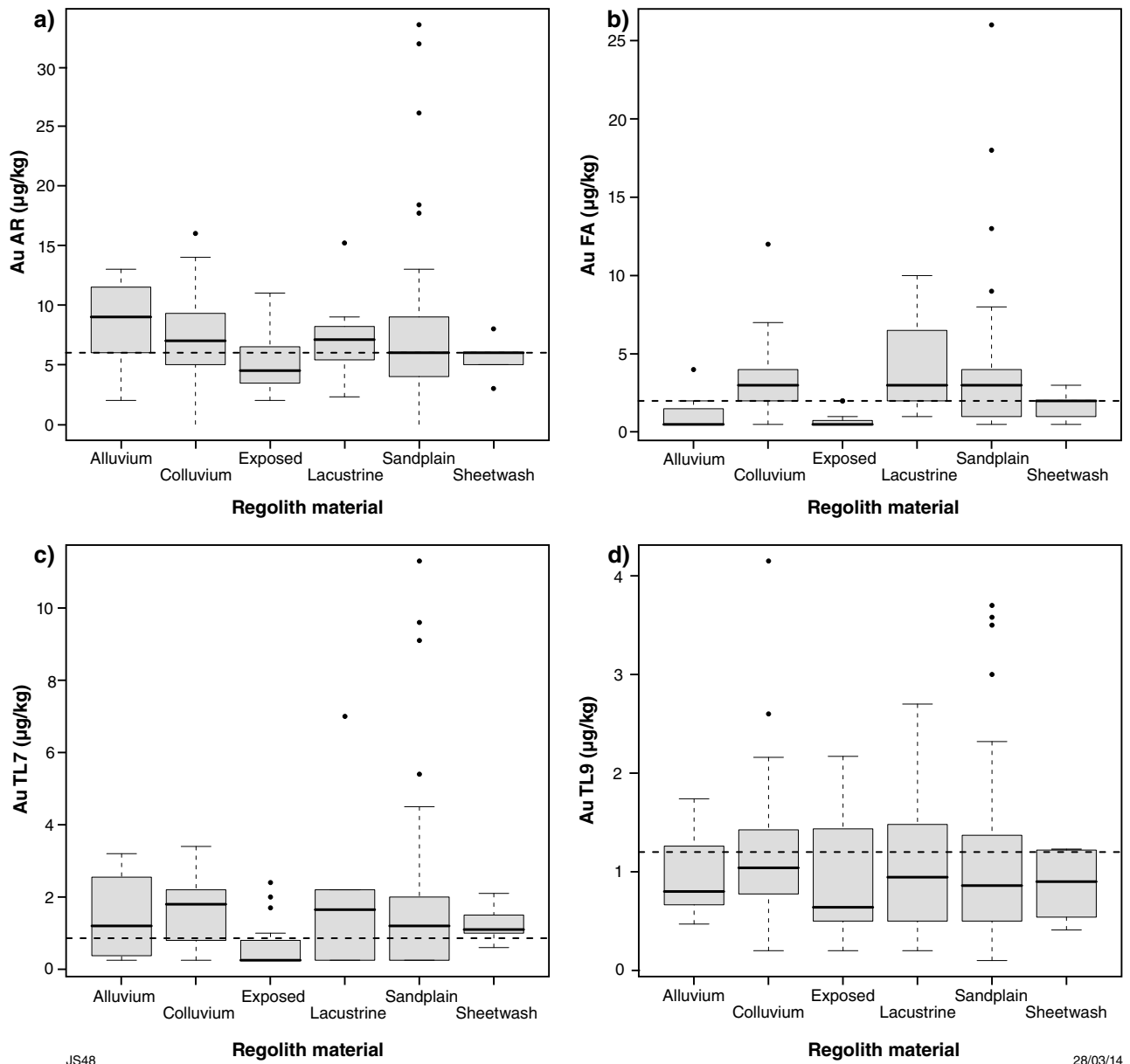


Figure 20. Box-and-whisker plots of Au concentrations obtained by a) aqua regia (AR) extraction; b) fire assay (FA); c) TerraLeach (TL) 7 extraction; (d) TL9 extraction grouped by six regolith types in the study area; dotted line indicates the overall median of the respective analytical method (Table 7); alluvium sample number $n = 7/7$ (first number relates to AR and second to FA data), colluvium $n = 41/30$, exposed $n = 15/12$, lacustrine $n = 7/3$, sandplain $n = 75/52$, and sheetwash $n = 5/5$; black horizontal line within the box indicates the median, the whiskers represent values of $1.5 \times$ interquartile range (IQR) and outliers (black dots) are greater or less than the $IQR \pm (1.5 \times IQR)$

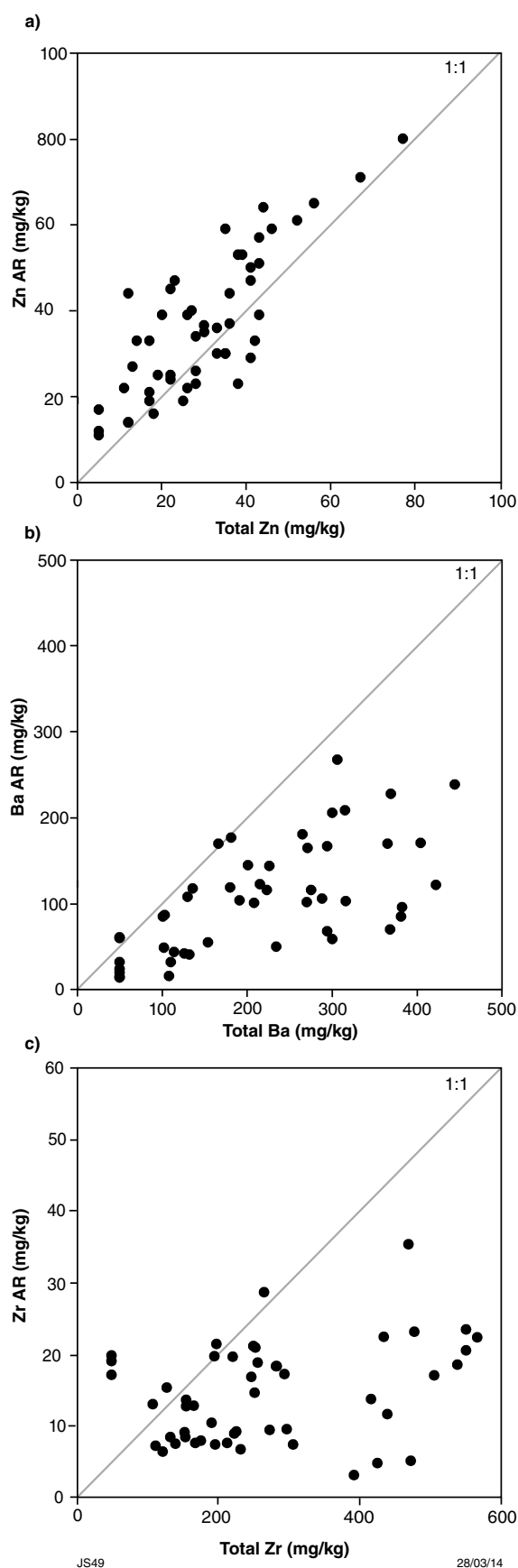


Figure 21. Bivariate plot of total (XRF) vs aqua regia (AR)-extractable concentrations of: a) Zn; b) Ba; c) Zr in the fine fraction of 50 regolith samples (refer to Table 3 for description of analytical methods)

Multi-element associations and groupings in the fine fraction

To further assess the multi-element dataset spatially and in context with the regolith types, AR-extractable data of the fine fraction (<50 μm) are summarized by using an additive index approach for four common element associations. These are the chalcophile (As–Ag–Bi–Cd–Sb–Mo), ferro-alloy (Ni–Cr–Mo–Co–V), rare earth element (Ce–Dy–Er–Eu–Gd–Ho–La–Nd–Pr–Sm–Tb–Tm–Yb), and base metal (As–Bi–Cu–Pb–Sb–Sn–Zn) associations. These indices have been widely used by GSWA's regional geochemistry program to highlight areas of potential mineralization (Morris et al., 1998, 2000; Pye et al., 1998; Morris and Verren, 2001).

The additive indices are based on the sum of standard scores, which are calculated by subtracting the mean from the raw value and dividing the product by the standard deviation. Prior to this, however, the log was calculated for each raw value to reduce the effect of extremely high or low values. At this point, any censored data were replaced with values equal to one-half of their respective LLD.

Index maps for the four element associations are displayed in Figures 23 to 26. Sample locations with index values above the 95th percentile are indicated by red stars. Bivariate plots (Fig. 27a,b) display index values in relation to AR-extractable Ca concentrations and the Rb/Ca ratio to assess possible relationships to the carbonate and silicate content. A detailed discussion on the index distribution for the whole Fraser Range region (Fig. 1) can be found in Morris et al. (2000).

Chalcophile index

The assessment of the chalcophile (CP) index should be carried out with care as some of the chalcophile group elements have a high percentage of censored data (e.g. Ag and Cd each at 66%). Samples with CP index values >4.37 (95th percentile) are found north of Zanthus (GSWA 194031 and 194033; Appendix 1), near the Cundeelee and Jerdacuttup Faults northwest of Fraser Range homestead (GSWA 161753 and 163553) and from the Cherternerlynyer Lagoon (GSWA 161747, 163757, 163817, and 164037; Fig. 1). All these areas correspond to colluvium or sandplain, apart from GSWA 163817, which comes from an area of alluvium within the Cherternerlynyer Lagoon. The two samples north of Zanthus correspond to the maximum and third-highest index values, close to a further two samples (GSWA 194034 and 194039) with a chalcophile signature (>2.0; Fig. 23). All of these samples, which are near Ponton Creek, were collected from colluvium and described as sandy with abundant ferruginous lag (Fig. 4).

A series of samples with negative CP index values form a north–south trend along the edge of greenstones of the Kurnalpi Terrane, similar to that shown for samples with low SiO_2 (Fig. 8). Regolith samples from the northern part of the study area, largely the Gunbarrel Basin and northern Albany–Fraser Orogen, have low positive to negative indices. Bivariate plots (Fig. 27a,b) display no

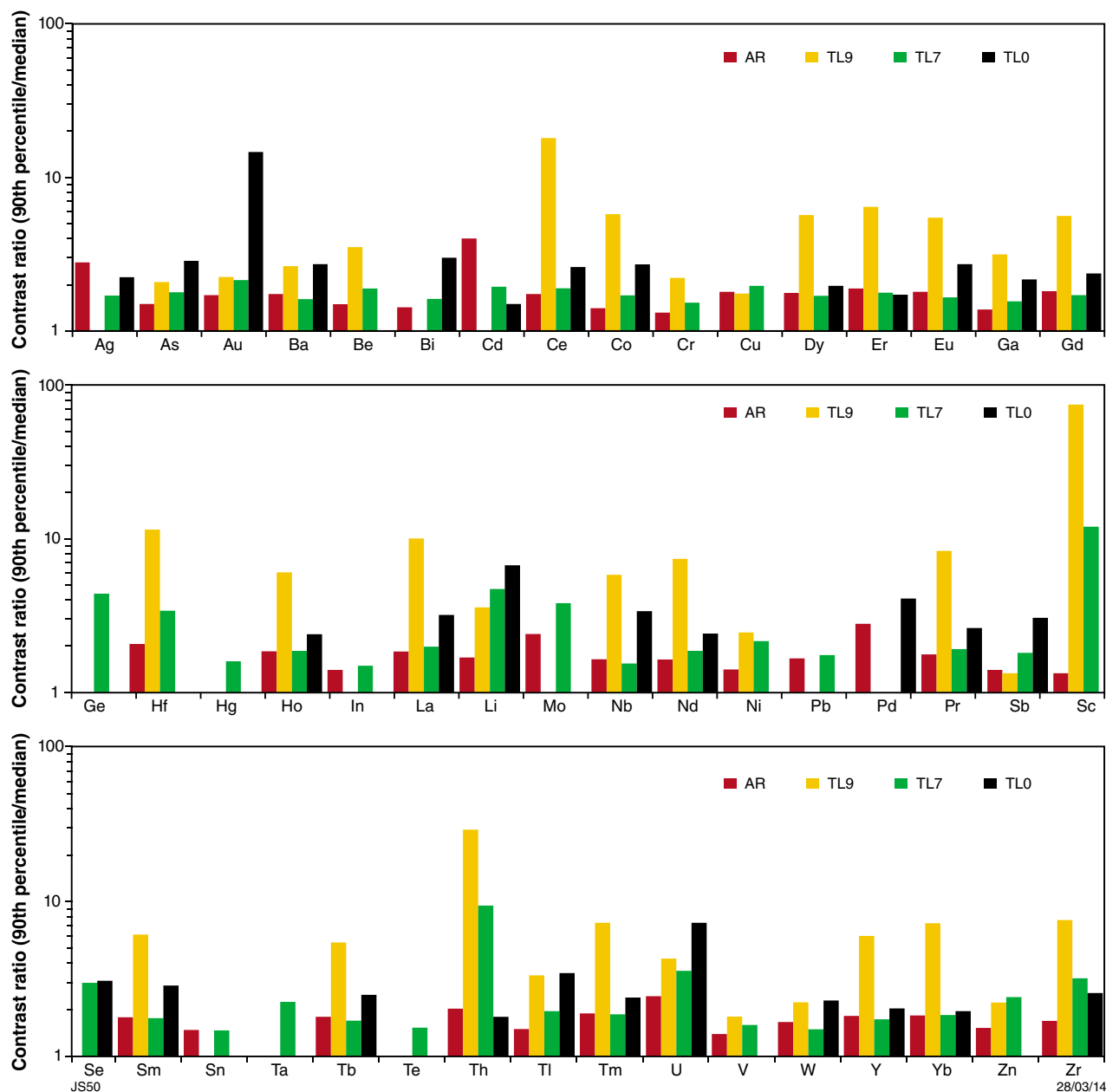


Figure 22. Bar chart of contrast ratios (90th percentile/median) for 48 elements calculated for aqua regia (AR), TerraLeach (TL) 9, TL7, and TL0 data of the fine fraction (<50 μm)

clear relationships between the CP index values and the carbonate (AR-extractable Ca) or silicate (based on Rb/Ca ratio) content in the regolith matrix.

Ferro-alloy index

The highest FA indices (>4.57; 95th percentile) are found in areas of either sandplain or colluvium in two broad areas. Three samples are located to the northwest (Fig. 24; GSWA 194031, 194033, and 194034; Appendix 1) and one sample is to the southwest (GSWA 194027) of Zanthus. Here, regolith samples are over migmatitic, monzogranitic,

and syenogranitic gneiss of the Biranup Zone, although the latter sample may be related to rocks of the Eddy Suite.

A further three samples (GSWA 163941, 161753, and 163553) form a cluster northwest of Fraser Range homestead and are related to regolith over rocks of the Northern Foreland just east of the Cundeelee and Jerdacuttup Faults. The only sample with a high FA index not located within the Albany–Fraser Orogen is GSWA 163753, which is located in the Kurnalpi Terrane close to greenstone.

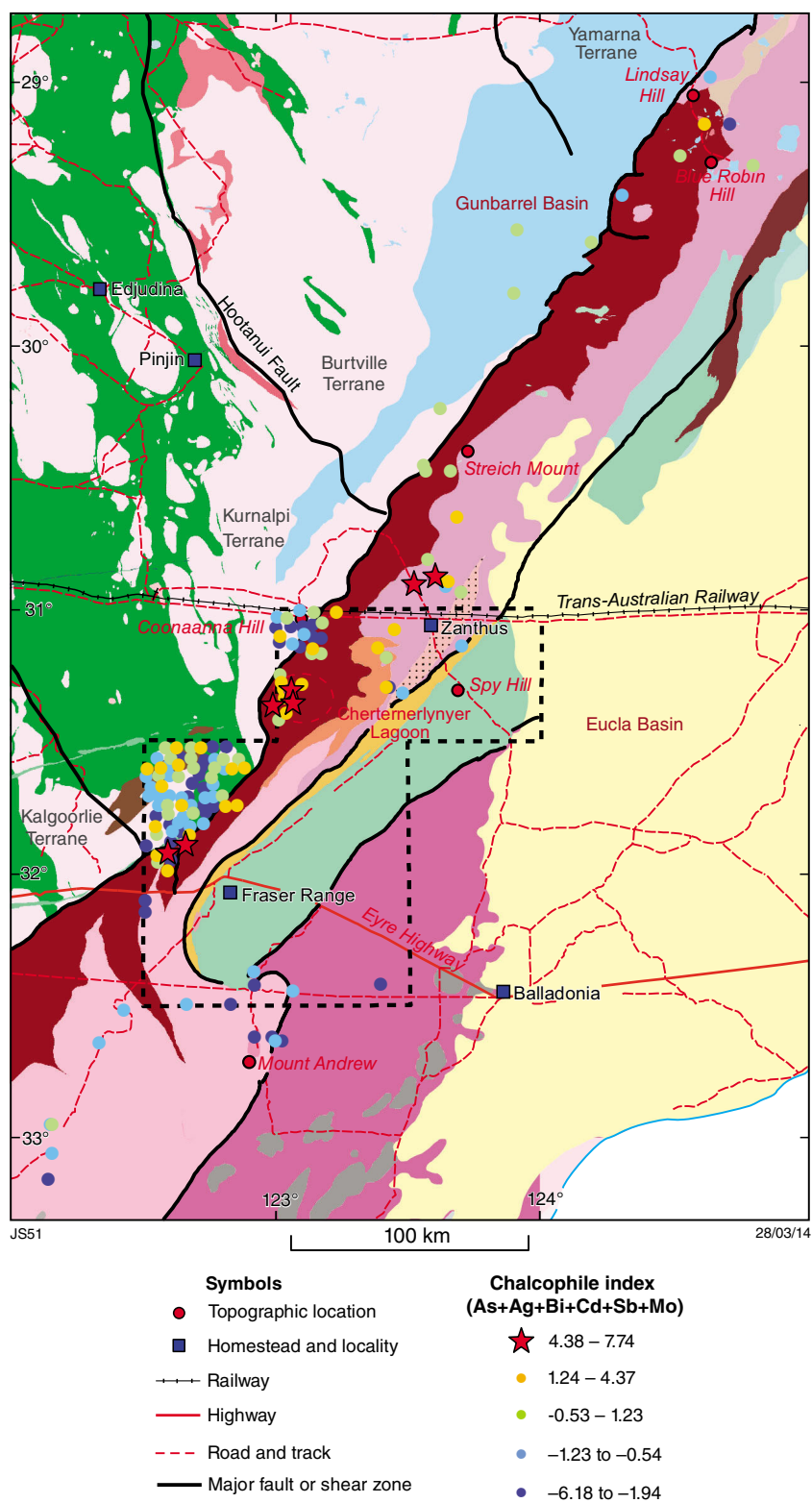


Figure 23. Distribution of the chalcophile index (As+Ag+Bi+Cd+Sb+Mo) calculated for 151 regolith samples across the study area; sites marked with red stars correspond to values above the 95th percentile; for geology backdrop refer to Figure 2

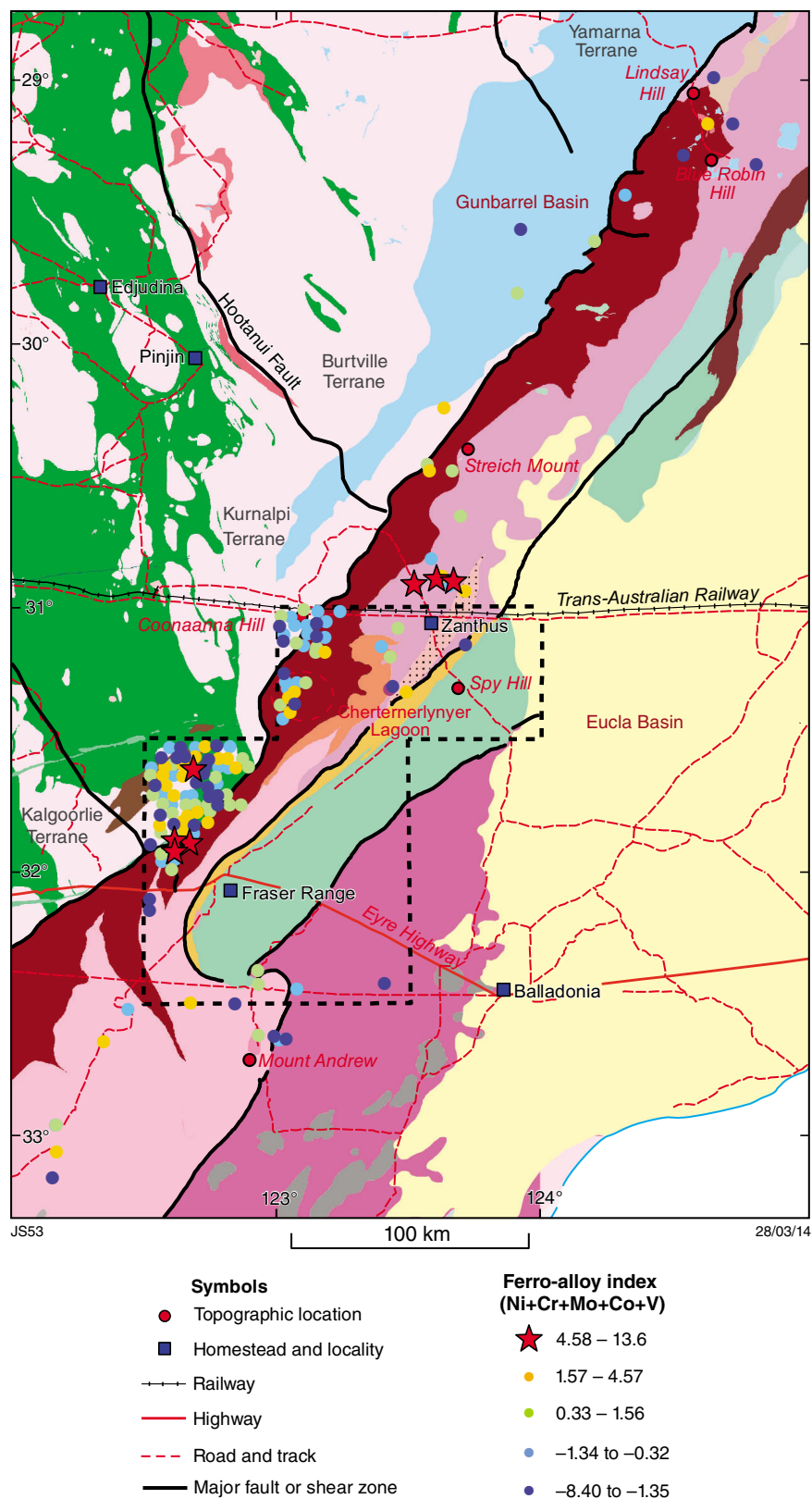


Figure 24. Distribution of the ferro-alloy index (Ni+Cr+Mo+Co+V) calculated for 151 regolith samples across the study area; sites marked with red stars correspond to values above the 95th percentile; for geology backdrop refer to Figure 2

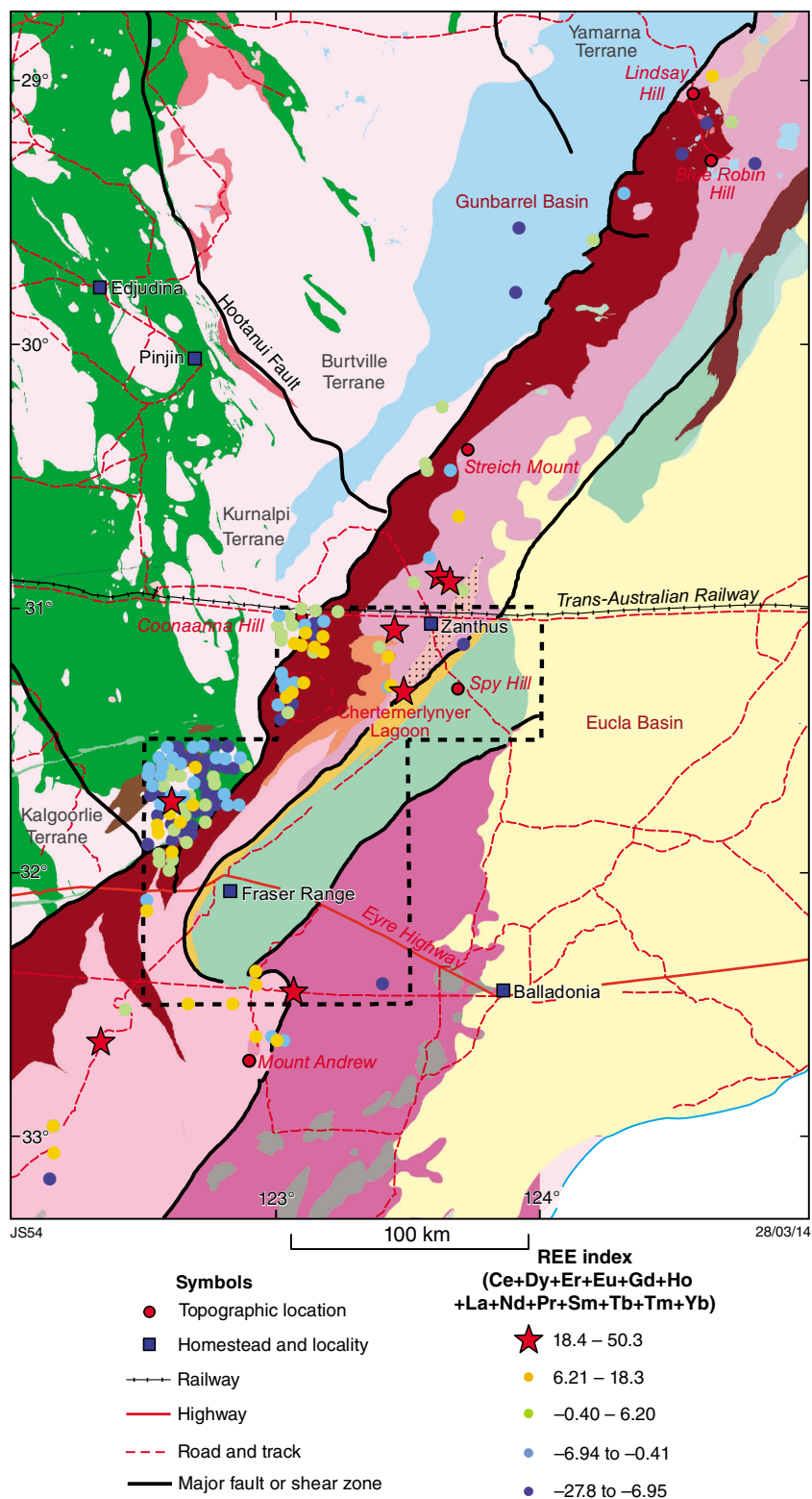


Figure 25. Distribution of the rare earth element (REE) index (Ce+Dy+Er+Eu+Gd+Ho+La+Nd+Pr+Sm+Tb+Tm+Yb) calculated for 151 regolith samples across the study area; sites marked with red stars correspond to values above the 95th percentile; for geology backdrop refer to Figure 2

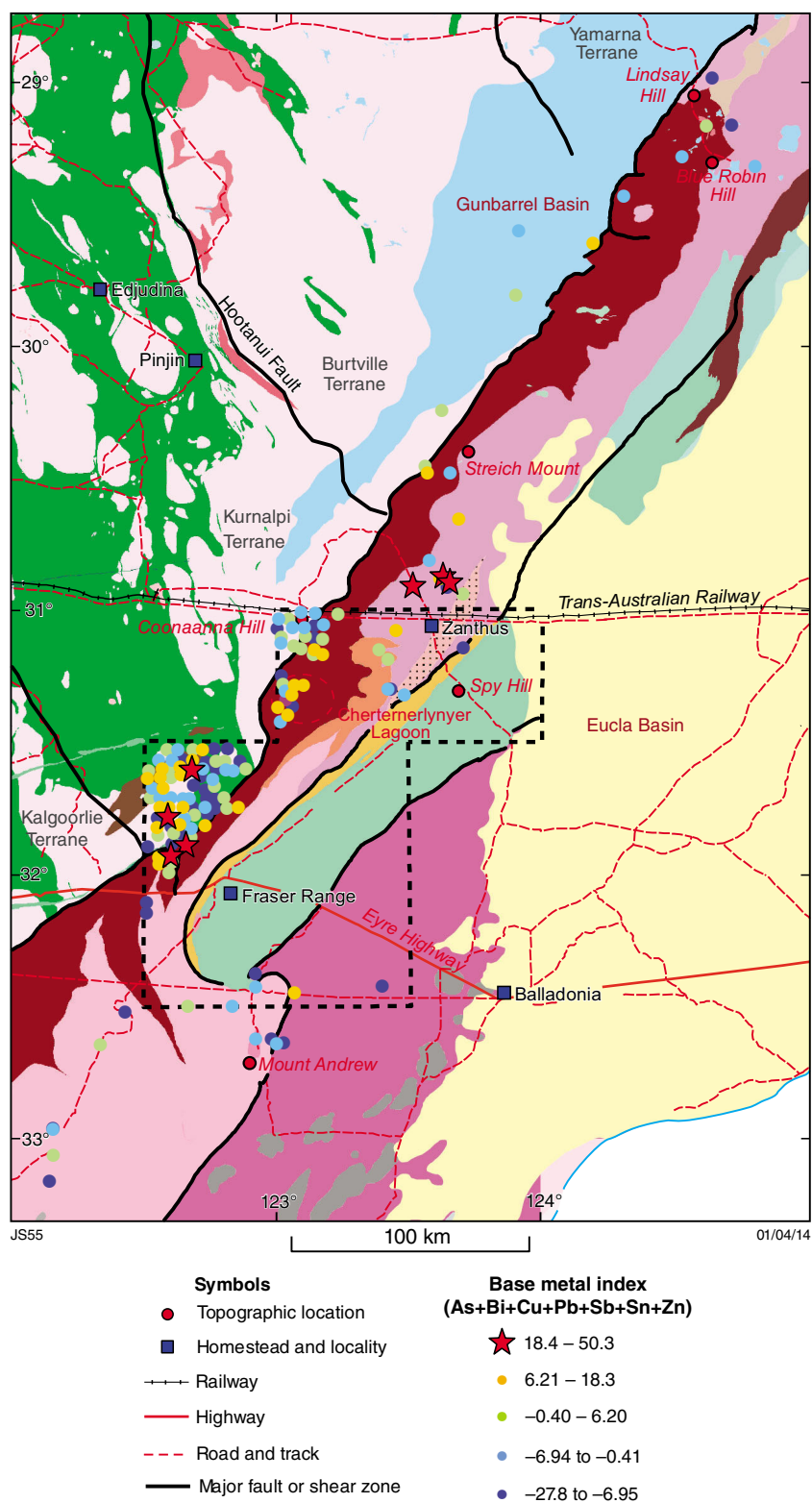


Figure 26. Distribution of the base metal (BM) index (As+Bi+Cu+Pb+Sb+Sn+Zn) calculated for 151 regolith samples across the study area; sites marked with red stars correspond to values above the 95th percentile; for geology backdrop refer to Figure 2

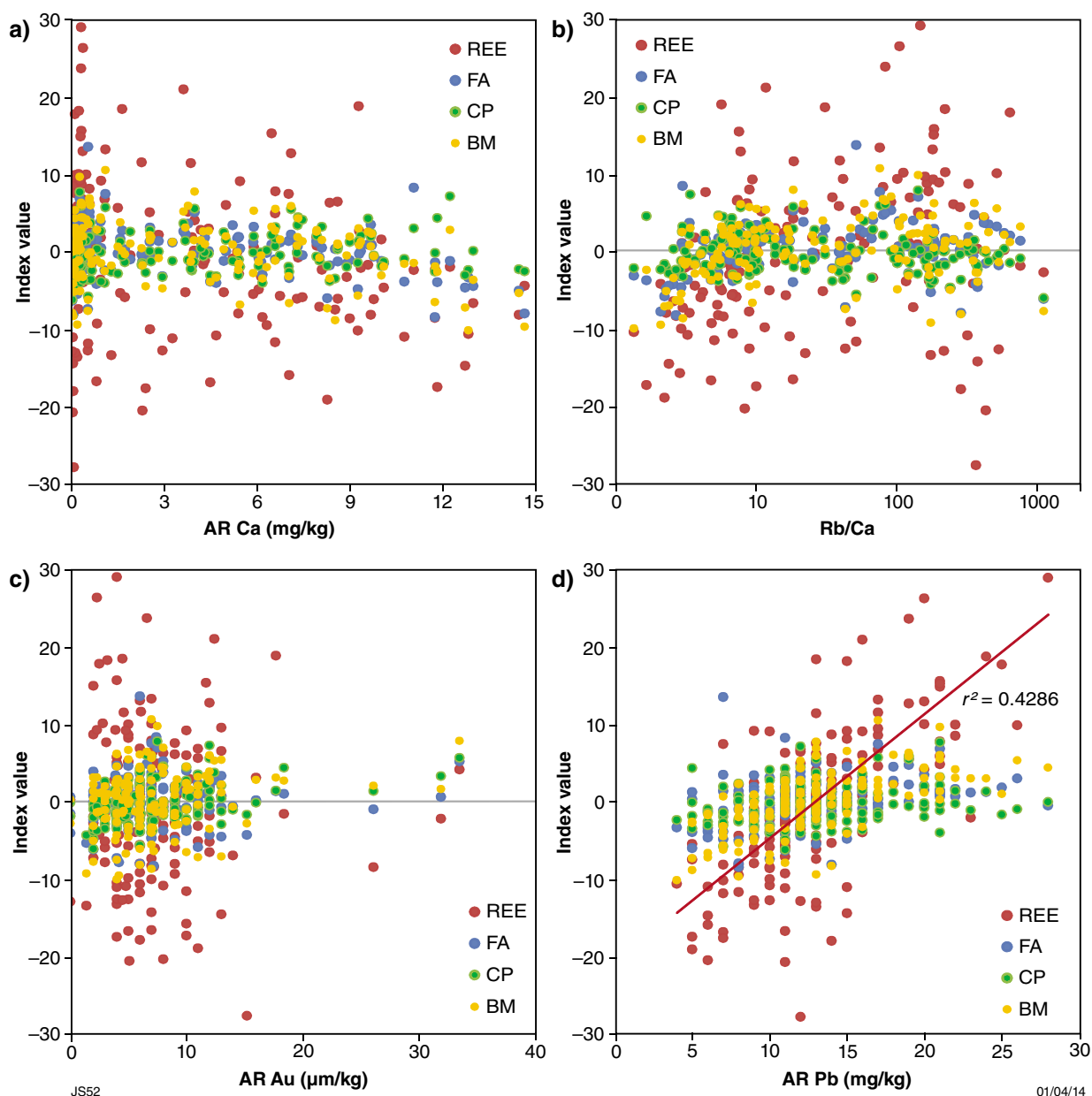


Figure 27. Bivariate plots of the chalcophile (CP), ferro-alloy (FA), rare earth element (REE), and base metal (BM) indices against the aqua regia (AR)-extractable concentrations of a) calcium (Ca); b) Rb/Ca ratio; c) gold (Au); and d) lead (Pb); all data relate to the fine fraction (<50 μm); note y-axis has been truncated and rare earth element indices >30 are omitted

Similar to the distribution of CP indices, samples with FA indices <1.56 are found across the Gunbarrel Basin and in the southernmost part of the Kurnalpi Terrane. Similarly, samples with negative FA values also have low CP index values (Fig. 23), especially for regolith samples that correspond to greenstones in the southern part of the Kurnalpi Terrane. Bivariate plots (Fig. 27a,b) display no clear relationships between the FA index values and the carbonate (AR-extractable Ca) or silicate (Rb/Ca) contents.

Rare earth element index

Samples with anomalous (>18.3) rare earth element indices are found almost entirely in regolith from within the Albany–Fraser Orogen (Fig. 25), except for GSWA 161747 (Appendix 1), which is located over granitic rocks within the Kurnalpi Terrane northwest of Fraser Range homestead.

The Zanthus area has four anomalous samples (GSWA 194030, 194033, 194034, and 194039), which are predominantly from areas of sandplain over granitic gneiss of the Biranup Zone. A further sample (GSWA 194022) collected near an area of exposed bedrock of the Eddy Suite south of Zanthus is also anomalous.

Two further samples with a rare earth element index >18.3 are found to the southwest (GSWA 194006) and southeast (GSWA 194016) of Fraser Range homestead. The former sample corresponds to the highest index (50.3), and comes from an area of sandplain overlying granitic gneiss of the Biranup Zone. Sample GSWA 194016 was collected near an area of exposed rocks of the Recherche Supersuite. Additionally, it is located near the Newman Shear Zone, a major structure that separates the Biranup and Nornalup Zones. The area south of Fraser Range homestead provided about six samples with high rare earth element indices (>6.2), which may indicate a regional pattern.

Bivariate plots of the rare earth element index distribution (Figure 27a,b) show the widest range of index values of the four datasets. However, the rare earth element index does not indicate any relationship with either the carbonate (AR-extractable Ca) or silicate (Rb/Ca) contents.

Base metal index

The distribution of base metal (BM) index values is similar to that of the CP and FA indices. Four of the highest BM index values (>6.06 ; 95th percentile; Fig. 26) correspond to samples northeast of Fraser Range homestead from areas of colluvium and sandplain. Two samples are located over Archean granitic rocks of the Kurnalpi Terrane (GSWA 163753 and 163935; Appendix 1), and two over metagranitic rocks of the Northern Foreland (GSWA 161753 and 163553; Appendix 1). GSWA 163935 was collected near exposed granitic bedrock. Overall, regolith samples collected over granitic lithologies of the Kurnalpi Terrane (Woodline Formation) correspond to moderate to strong BM indices, although samples collected

over greenstones of the same terrane correspond to predominantly negative indices, as shown by north–south-trending dark blue dots north of Fraser Range homestead (Fig. 26).

Indices for samples from the Cherternerlynyer Lagoon are overall high, with one sample index >6.06 . The remaining three highest BM indices (GSWA 194031, 194033, and 194034) were collected north of Zanthus at the same locations discussed in previous sections. The latter two samples are located close to Ponton Creek and outcrops of strongly foliated garnetiferous granitic gneiss, quartzofeldspathic gneiss, migmatitic metamonzogranite, and psammitic gneiss (Kirkland et al., 2010, 2011a) of the Biranup Zone. Bivariate plots (Fig. 27a,b) are similar to previous indices and do not indicate a relationship between the BM index and the carbonate (AR-extractable Ca) or silicate (Rb/Ca) contents.

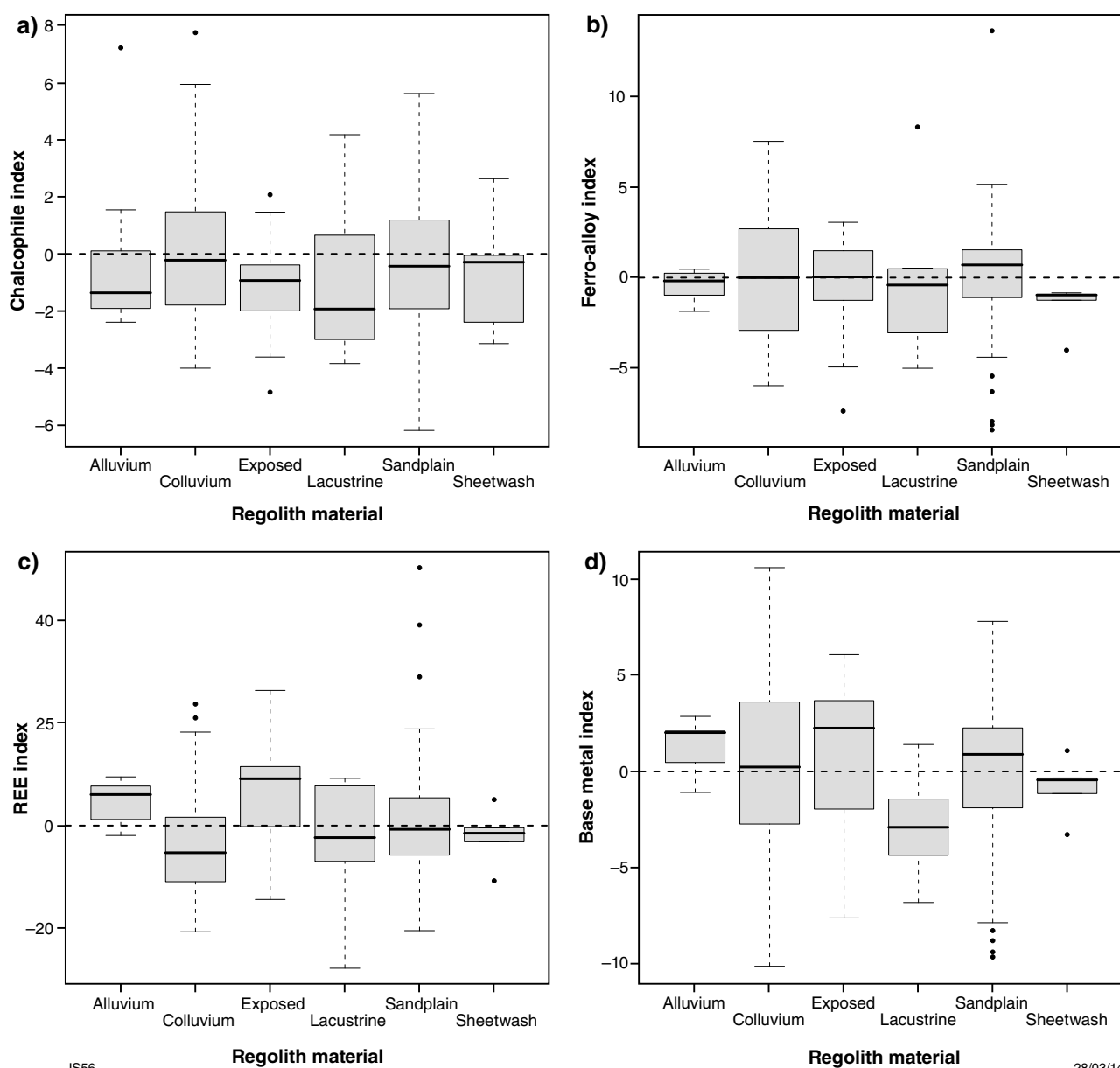
Relationship of indices to regolith type

In relation to regolith type, the highest and widest range of CP index values are found in samples from areas of colluvium and sandplain; many of the lowest indices are from areas of alluvium and sheetwash, with lacustrine samples having the lowest index median of -1.9 (Fig. 28a). In all diagrams, the median (solid black line) is below the dotted line, indicating that more than one-half of the samples have negative CP index values regardless of regolith type.

Ferro-alloy index values (Fig. 28b) for regolith samples near exposed bedrock, sandplain, and colluvium are almost identical, with positive values for at least one-half of the samples. Data for sandplain and colluvium again display the widest range and some of the highest indices, although alluvium, lacustrine, and sheetwash samples are similar to CP results, which are among the lowest with almost entirely negative values.

The distribution of rare earth element indices across the six regolith types (Fig. 28c) contrasts with distributions for CP and FA. The highest rare earth element indices correspond to samples collected near exposed bedrock with samples from alluvial deposits providing the second highest median (2.1). Samples from colluvium have the lowest index median (-4.9), closely followed by lacustrine, sheetwash, and sandplain deposits, which also have negative medians. Colluvium and sandplain deposits, however, correspond to some of the highest rare earth element indices.

The two highest BM index median values correspond to samples collected near exposed bedrock and alluvium (Fig. 28d). Positive medians also correspond to colluvium and sandplain samples, which similar to data shown on Fig. 28a–c, display the widest data ranges. The lowest (negative) BM index values are for samples from sheetwash and lacustrine deposits; the sheetwash deposits are located just to the north of the alluvial samples (Figs 3 and 26).



JS56

28/03/14

Figure 28. Box-and-whisker plots of: a) chalcophile; b) ferro-alloy; c) rare earth element (REE); d) base metal indices grouped by the six regolith types found in the study area; horizontal lines indicate zero; sample numbers for alluvium $n = 7$, colluvium $n = 41$, exposed $n = 15$, lacustrine $n = 7$, sandplain $n = 75$, and sheetwash $n = 5$; black horizontal line within each box indicates the median, whiskers represent values of $1.5 \times$ the interquartile range (IQR) and outliers (black dots) are greater or less than the $IQR \pm (1.5 \times IQR)$.

Discussion of trace element data

Gold in the fine fraction of the regolith

The assessment of Au data following five different analytical methods shows that the highest Au concentrations in the fine fraction are achieved using AR digestion. Fire assay determination (<2 mm to >0.45 µm fraction) recovers only around one-third of the AR-extracted Au concentrations, which suggests that substantial Au is present in the fine grain size fraction (<50 µm). This effect is particularly evident for samples from areas of alluvium, which contain some of the highest AR-extractable Au concentrations in the fine fraction, although the lowest FA-determined Au concentrations relate to the coarser sample fraction. Weaker digestions are only capable of releasing <20% of the Au from the fine fraction compared with AR analysis, although the FA data show a positive correlation with AR data.

Regolith samples with the lowest Au concentrations, regardless of analytical method, were collected near exposed bedrock, with the highest concentrations associated with transported regolith. A comparison of Au data with carbonate and silicate proxies such as AR-extracted Ca data and the Rb/Ca ratio show only a weak relationship, although ranked correlation coefficients indicate that Au data from all analytical methods express statistically significant positive correlations with the carbonate content in the fine fraction. Samples with the highest anomalous AR-extracted Au concentrations (17.7 – 33.5 µg/kg) are from sandplain, although these samples also show a strong carbonate signature. These results relate to the southern part of the study area and are contrary to the observations of Morris (2013a), who noted that regolith samples from the East Wongatha area (Fig. 1) show no consistent relationship between the carbonate content of regolith and Au content. This result may be because the East Wongatha area is slightly further north and therefore there is potentially less chance of regolith carbonate developing, or is related to an increase in cover.

The samples with the highest anomalous AR-extractable Au concentrations (>13.7 µg/kg, 95th percentile) are located over the Northern Foreland and follow the northeast–southwest-trending Cundeelee and Jerdacuttup Faults, highlighting the prospectivity of this area. Two of the five anomalous regolith samples are located very close to the Brookman Au prospect and former fault (Fig. 18b). Elevated Au concentrations (>11.0 µg/kg AR, 90th percentile) are also found in a series of regolith samples over metagranitic and metamafic rocks of the Northern Foreland (Cherternerlynyer Lagoon), and in regolith samples over the Yilgarn Craton close to exposed greenstone or known Au mineralization (Fig. 18b). A relationship between elevated Au concentrations and primary sulfides might be evident for sandplain samples from the Cherternerlynyer Lagoon, where samples correspond to strong CP indices. Furthermore, across the densely sampled area of the Fraser Range region most regolith samples have Au concentrations <9 µg/kg, which suggests that the surface expressions of anomalous Au is restricted to local rather than distal dispersion of Au.

In the remaining, more sparsely sampled, part of the study area, two samples with AR-extracted Au concentrations >13.7 µg/kg and two with Au >11.0 µg/kg are located within the Biranup Zone, south and north of Zanthus, respectively. These sample locations also fall within areas of ongoing exploration activity between the Beachcomber prospect and Tropicana deposit. For example, across several tenements northeast of Zanthus, partly covering Ponton Creek, surface geochemistry has indicated a broad low-level Au anomaly in calcrete nodules within the sand cover (da Silva, 2007a,b). Reconnaissance drilling has since been carried out to test potential bedrock mineralization. Work across tenements to the east of Streich Mount has also returned anomalous data for elements such as Ag, As, Ba, Cr, and Pd (da Silva, 2007b).

The Tropicana gold deposit (Fig. 2) was discovered by following up an unexplained Au soil anomaly in a public, regional dataset from the 1990s (Tropicana Joint Venture, 2010). However, sandplain and colluvium samples collected around Tropicana yield overall low AR-extractable Au concentrations (<6 µg/kg), failing to indicate any further anomalies at the surface. Thus, if other buried Au mineralization exists in this area, then the occurrence of surface expression must be very localized. Chen et al. (2002) argued that Au anomalies might stay undetected if the transported regolith were deeper than 10 m. This might be the case in the northeastern part of the study area including the Gunbarrel Basin, which is covered by at least 5 to 10 m of recent eolian sands and in turn overlies partly indurated Cenozoic eolian sediments several tens of metres thick. Additionally, samples for this study were collected 30 cm below the surface and reflect largely recent transported material into which potential migration of Au had not yet taken place. This effect was shown by a recent project in the Gunbarrel Basin (northeast of Mulga Rock) that saw Au concentrations below background (9 µg/kg) at the surface (<30 cm) steadily increase to 30.9 µg/kg Au at a depth of 1.8 m (Morris, 2013b). This recently transported cover may also explain why no anomalous Au concentrations were detected in samples from the prospective Tropicana area.

Element extractability

The evaluation of fine-fraction, multi-element data shows that the highest element concentrations are achieved by AR digestion, closely followed by TL7. For some trace elements, AR digestion provides near-total concentration data (e.g. Zn; Fig. 21a). However, AR is not effective in the determination of other elements, such as the HFSE (Hf, Nb, and Zr; Fig. 21c), which are associated with accessory minerals that are more resistant to chemical attack.

The difference between AR and TL7 concentrations varies according to element. Data for rare earth elements obtained by the two digests are similar; however, concentrations of metals such as As, Ni, Sb, Mo, and Zn are an order of magnitude lower using TL7. The TL7 method was especially developed to digest amorphous iron and manganese oxide and hydroxides, which may suggest that rare earth elements are partly hosted by

these secondary minerals, yet the TL7 digest is relatively ineffective for releasing chalcophile elements in sulfides. Concentrations following TL9 digestion are typically lower than those obtained by AR, although TL9 data show some of the highest contrast ratios (7 to 18). Similar to TL9 digestion, concentrations of elements following deionized water digestion (TL0) are much lower. Although some anomalous values are also determined by those methods, TL9 and TL0 suffer from a high proportion of censored data. Nevertheless, TL0 produces usable data for elements such as Ba and W, although TL0 extracts less Au than does AR from the fine fraction (Table 7), which suggests that Au in the fine fraction is not water-soluble (compare Morris, 2013a). Lintern (1997), however, showed that the application of deionized water as digest could extract Au (and possibly many other elements) from the sample matrix, particularly if used over a long period. The difference between AR and TL0 results indicates the importance of a relatively strong partial digest such as AR to extract Au.

Element associations

The spatial distribution of the multi-element chemistry through a series of index maps reveals that almost all positive anomalous indices correspond to transported (allochthonous) regolith (colluvium or sandplain), although most samples with elevated indices are located close to outcrops of bedrock. Of interest is that most regolith samples collected over Archean greenstones of the Kurnalpi Terrane have low or negative CP, FA, BM, and rare earth element indices, producing a north–south trend of negative values.

Samples indicating a strong chalcophile signature appear as clusters in the Cherternerlynyer Lagoon area and northwest of Fraser Range homestead. Both areas relate to colluvium and sandplain over metamafic and metagranitic rocks of the Northern Foreland. A third area of high positive CP values corresponds to Ponton Creek (10 km north of Zanthus), where regolith samples are located close to rocks of the Biranup Zone, comprising strongly foliated garnetiferous granitic gneiss, quartzofeldspathic gneiss, migmatitic metamonzogranite, and psammitic gneiss (Kirkland et al., 2010, 2011a). The same three areas also have the highest BM and FA indices, thus indicating a close spatial relationship with elevated values found predominantly in transported regolith over rocks of the Northern Foreland (Albany–Fraser Orogen). Samples with elevated indices near Cherternerlynyer Lagoon (Fig. 1) and northwest of Fraser Range homestead all lie within 7 km of the Cundeelee and Jerdacuttup Faults, which mark the boundary of the Yilgarn Craton with the Northern Foreland. If elevated element indices are indicative of mineralization, the proximity to the Cundeelee Fault may indicate some structurally controlled mineralization. In other areas (e.g. over granitic rocks of the Yilgarn Craton), samples have both high and low element indices, indicating that there is no simple explanation for the index values.

Some of the highest rare earth element indices are found mainly in regolith samples over the migmatitic and granitic gneisses of the Biranup Zone (Albany–Fraser

Orogen) and correspond in most areas to high CP, BM, and FA indices, except for sites to the south of the Fraser Range homestead. Colluvium and sandplain samples from the Zanthus area show some of the highest rare earth element indices. Minerals such as garnet are a likely source of rare earth elements found in the regolith, particularly heavy rare earth elements. The extraction of elevated concentrations of rare earth elements from regolith using TL7 indicates that rare earth elements may also be hosted in (secondary) amorphous iron and manganese oxide or hydroxides. Strong BM and rare earth element indices in alluvial samples may reflect the proximity of the regolith to exposed Archean granites of the Yilgarn Craton in the Coonaanna Hill area.

Regolith samples from an area south of Fraser Range homestead indicate a strong rare earth element signature in the fine fraction, which may relate to garnet-rich rocks of the area, although equally, the samples could indicate a surface expression of supergene rare earth element enrichment in the silt to clay matrix of the regolith.

None of the four indices indicates a relationship with carbonate or silicate content in the regolith. Similarly, the four indices fail to highlight any substantial relationship to AR-extractable Au (Fig. 27c), consistent with the poor agreement between Au and index data reported from the East Wongatha area (Morris, 2013a). Compared with other AR data of the fine fraction, positive correlations are observed between the AR-extractable Fe concentrations and the CP, BM, and FA indices (not shown) and for Pb and the rare earth element index (Fig. 27d). The latter relationship may indicate two shared sources for rare earth elements and Pb: primary accessory minerals, such as garnets, and secondary oxides and hydroxides that capture and release rare earth elements and Pb.

Summary and conclusions

The regolith geochemistry data from the southeast Yilgarn Craton and east Albany–Fraser Orogen show that in areas of extensive, commonly transported regolith typical of parts of southeast Western Australia, geochemical sampling and analysis should focus on the fine fraction of regolith, using aqua regia (AR), at least as a first pass, as the preferred digest. Most other digestion methods resulted in much lower element concentrations, with the exception of digestion using hydrochloric acid, which worked well for extracting rare earth elements from the sample matrix. The regolith geochemical data indicated several surface anomalies that may be an indication of buried mineralized zones across this largely greenfields area of the southeast Yilgarn Craton and east Albany–Fraser Orogen. These results support the prospectivity of this region, which has been highlighted by the recent discoveries of the Nova Ni–Cu and Tropicana Au deposits, warranting current and future exploration in this area.

The southeast Yilgarn Craton and east Albany–Fraser Orogen are characterized by a wide range of regolith composition that includes silica-rich, low-carbonate, acidic sandplain deposits overlying the Gunbarrel Basin and more alkaline and carbonate-rich regolith found on or near

greenstones of the Kurnalpi Terrane of the Yilgarn Craton. This variation of regolith, especially the carbonate and silicate contents, was key to unravelling the multi-element geochemical data across the area.

For Au concentration in the fine fraction and the carbonate content, Spearman correlation coefficients indicated a significant positive relationship between Au and AR-extracted Ca concentrations. Furthermore, most samples with anomalous Au had high carbonate and low silicate contents. In some respects, this finding contradicts that from the East Wongatha area where no consistent relationships between the carbonate and Au content in regolith samples were indicated (Morris, 2013a). This discrepancy can, however, be explained by the fact that the East Wongatha area has a thicker cover and is located slightly further north, therefore potentially decreasing the chance of regolith carbonate developing.

The assessment of Au data also showed that of the five analytical methods, AR provides the highest Au concentrations and most reliable results for censored data. A comparison of AR data for the fine fraction with fire assay data for the coarser sample fraction emphasized the importance of the fine fraction, which excludes the commonly barren, eolian-derived quartz-rich sand, and can act as a diluent. Furthermore, comparisons with the other, weaker, digests suggest that most of the Au is not present in labile form. This is an indication that anomalous Au accumulations are exogenic and either very old (millions of years; Cameron et al., 2004), or younger and strongly bonded in the regolith matrix.

The highest Au concentrations obtained by all digestion methods were found in samples from areas of transported regolith such as colluvium and sandplain, and are lowest in samples of regolith close to exposed bedrock. Spatially, most anomalous Au concentrations fall within a northeast to southwest-trending axis along the Cundeelee Fault and correspond to the Northern Foreland. This distribution may suggest potential for fault-related Au mineralization along this axis. Multi-element fine-fraction geochemistry also revealed strong chalcophile and base metal expressions in sandplain and colluvium samples near regional faults, including the Cundeelee Fault, which indicates potential for fault-controlled mineralization.

Elevated rare earth element signatures seem to correspond largely to transported regolith found over the migmatitic and granitic gneisses of the Biranup Zone and Barren Basin metasedimentary rocks north and south of Zanthus, and over Biranup and Nornalup Zone rocks south of the Fraser Zone. Transported regolith to the south of the Fraser Zone might relate a surface expression of supergene rare earth element enrichment. At Ponton Creek north of Zanthus, elevated rare earth element concentrations, including other element indices relating to predominantly neutral to alkaline silicate-rich and carbonate-poor colluvium, are spatially related to outcrops of strongly foliated garnetiferous granitic gneiss. This area may warrant further investigation.

Multi-element data showed that most anomalous element concentrations relate to transported regolith from within the Albany–Fraser Orogen, in particular the Northern

Foreland and Biranup Zone. The close spatial relationship of anomalous data in regolith from the Northern Foreland to the Cundeelee and Jerdacuttup Faults and in the Biranup Zone to garnetiferous granitic gneiss suggest non-distal transport and a direct relationship to fault-related and bedrock mineralization, respectively. This view is supported by Morris et al. (2000), who describe strong bedrock control on the regolith of the Fraser Range region. Morris (2013a) also showed that in the East Wongatha area, fine-fraction regolith chemistry detected both bedrock and bedrock-hosted mineralization through thick cover. In this study, however, regolith samples from the East Wongatha area, corresponding to the Gunbarrel Basin and the northeastern Albany–Fraser Orogen (Fig. 2), do not indicate anomalous element concentrations. This outcome is likely due to a shallower sampling depth and a weakened surface expression compared to Morris's (2013a) study because of a higher proportion of more recent, barren eolian material.

References

- Anand, RR and Dell, M 2005, Kanowna Bell gold deposit, WA, *in* Regolith expression of Australian ore systems *edited by* CRM Butt, IDM Robertson, KM Scott and M Cornelius: CRC LEME, Perth, Western Australia, p. 270–272.
- Anand, RR, Phang, C, Wildman, JE and Lintern, MJ 1997, Genesis of some calcretes in the southern Yilgarn Craton, Western Australia: implications for mineral exploration: *Australian Journal of Earth Sciences*, v. 44, p. 87–103.
- Anand, RR and Smith, RE 2005, Mt Gibson Gold Deposit, Western Australia, *in* Regolith expression of Australian ore systems *edited by* CRM Butt, IDM Robertson, KM Scott and M Cornelius: CRC LEME, Perth, Western Australia, p. 288–290.
- Barley, ME, Brown, SJA, Cas, RAF, Cassidy, KF, Champion, DC, Gardoll, SJ and Krapež, B 2003, An integrated geological and metallogenic framework for the eastern Yilgarn Craton: developing geodynamic models of highly mineralised Archean granite–greenstone terranes: AMIRA International Limited, AMIRA Project No P624 (unpublished report).
- Bodorkos, S and Clark, DJ 2004, Evolution of a crustal-scale transpressive shear zone in the Albany Fraser Orogen, SW Australia: 1. P–T conditions of Mesoproterozoic metamorphism in the Coramup Gneiss: *Journal of Metamorphic Geology*, v. 22, no. 8, p. 691–711.
- Butt, CRM, Horwitz, RC and Mann, AW 1977, Uranium occurrences in calcretes and associated sediments in Western Australia: CSIRO, Perth, Western Australia, 67p.
- Butt, CRM, Robertson, IDM, Scott, KM and Cornelius, M (eds.) 2005, Regolith expression of Australian ore systems: CRC LEME, Perth, Western Australia, 431p.
- Cameron, EM, Hamilton, SM, Leybourne, MI, Hall, GEM and McClenaghan, MB 2004, Finding deeply buried deposits using geochemistry: *Geochemistry: Exploration, Environment, Analysis*, v. 4, p. 7–32.
- Cassidy, KF, Champion, DF, Krapež, B, Barley, ME, Brown, SJA, Blewett, RS, Groenewald, PB and Tyler, IM 2006, A revised geological framework for the Yilgarn Craton Western Australia: Geological Survey of Western Australia, Record 2006/8, 8p.
- Chao TT, 1984, The use of partial dissolution techniques in geochemical exploration: *Journal of Geochemical Exploration*, v. 20, p. 101–135.
- Chen, XY, Lintern, MJ and Roach, IC 2002, Calcretes: characteristics, distribution and use in mineral exploration: CRC LEME, Perth, Western Australia, 160p.

- Clark, DJ, Hensen, BJ and Kinny, PD 2000, Geochronological constraints for a two-stage history of the Albany–Fraser Orogen, Western Australia: *Precambrian Research*, v. 102, no. 3, p. 155–183.
- da Silva, V 2007a, Cundeelee South (C59/2006) Group Annual Report Cundeelee E28/1344, Ponton Creek E28/1345 and Seven Sisters E28/1346, Covering the Period 1 December 2005 to 30 November 2006; Quadrio Resources Pty Ltd: Geological Survey of Western Australia, Statutory mineral exploration report, A74421 (unpublished).
- da Silva, V 2007b, Cundeelee Combined Annual Report C15/2004, Carlisle E28/1298 Yandallah E28/1299, Covering the Period 1 December 2005 to 30 November 2006; Quadrio Resources Pty Ltd: Geological Survey of Western Australia, Statutory mineral exploration report, A74453 (unpublished).
- De Caritat, P, Reimann, C, NGA project team and GEMAS project team 2012, Comparing results from two continental geochemical surveys to world soil composition and deriving Predicted Empirical Global Soil (PEGS2) reference values: *Earth and Planetary Science Letters*, v. 319–320, p. 269–276.
- Department of the Environment and Water Resources 2007, Australia's native vegetation: a summary of Australia's major vegetation groups: Australian Government, Canberra, ACT, 44p, viewed 26 March 2014, <<http://laptop.deh.gov.au/erin/nvis/publications/pubs/major-veg-summary.pdf>>.
- Douglas, GB, Butt, CRM and Gray, DJ 2003, Mulga Rock uranium and multielement deposit, Officer Basin, WA, in *Regolith expression of Australian ore systems* edited by CRM Butt, IDM Robertson, KM Scott and M Cornelius: CRC LEME, Perth, Western Australia, p. 415–417.
- Doyle, M, Gibbs, D, Savage, J and Blenkinsop, T 2009, Geology of the Tropicana Gold Project, Western Australia, in *Proceedings of the 10th Biennial SGA Meeting of the Society for Geology Applied to Mineral Deposits* edited by PJ Williams et al.: Society for Geology Applied to Mineral Deposits, Smart Science for Exploration and Mining, Townsville, Queensland, 2009, vol. 1, p. 50–52.
- Enterprise Metals Ltd 2012a, 3 km long multi-element soil geochemical anomaly at Fraser Range: ASX announcement, viewed 24 September 2013, <<http://enterprisemetals.com.au/wp-content/sharelink/20120917-new-nova-style-soil-anom-ident-at-plato-in-fraser-range-87756681365969552.pdf>>.
- Enterprise Metals Ltd 2012b, New “Nova style” soil anomaly at Plato in Fraser Range: ASX announcement, viewed 24 September 2013, <<http://enterprisemetals.com.au/wp-content/sharelink/20120917-new-nova-style-soil-anom-ident-at-plato-in-fraser-range-87756681365969552.pdf>>.
- Department of the Environment 2012, Interim Biogeographic Regionalisation for Australia, Version 7: Australian Government Department of Sustainability, Environment, Water, Population and Communities and State/Territory land management agencies, viewed 26 March 2014, <<http://www.environment.gov.au/system/files/pages/5b3d2d31-2355-4b60-820c-e370572b2520/files/bioregions-new.pdf>>.
- Geological Survey of Western Australia, 2010, East Yilgarn, 2010 update: Geological Survey of Western Australia, 1:100 000 Geological Information Series.
- Geological Survey of Western Australia 2011, East Albany–Fraser and southeast Yilgarn: Geological Survey of Western Australia, Geological Exploration Package.
- Geological Survey of Western Australia, 2013, Revised classification system for regolith in Western Australia, and the recommended approach to regolith mapping: Geological Survey of Western Australia, Record 2013/7, 26p.
- Geoscience Australia, 2013, Australia's identified mineral resources 2012: Geoscience Australia, Canberra, 162p.
- Gray, DJ, Robertson, IDM, Cornelius, M, Sergeev, NB and Porto, CG 2005, Karari and Whirling Dervish gold deposit, WA, in *Regolith expression of Australian ore systems* edited by CRM Butt, IDM Robertson, KM Scott and M Cornelius: CRC LEME, Perth, Western Australia, p. 273–275.
- Hall, GEM 1998, Analytical perspective on trace element species of interest in exploration: *Journal of Geochemical Exploration*, v. 61, p. 1–19.
- Hill, SM, McQueen, KG and Foster, KA 1999, Regolith carbonate accumulations in western and central NSW: characteristics and potential as an exploration sampling medium, in *New Approaches to an Old Continent, Proceedings of Regolith '98* edited by G Taylor and CF Pain: CRC LEME, Perth, Western Australia, p. 191–208.
- Hill, SM, Taylor, GM and McQueen, KG 1998, Discussion genesis of some calcretes in the southern Yilgarn Craton, Western Australia: implications for mineral exploration: *Australian Journal of Earth Sciences*, v. 45, p. 177–178.
- Hocking, RM 1994, Subdivisions of Western Australian Neoproterozoic and Phanerozoic sedimentary basins: Geological Survey of Western Australia, Record 1994/4, 92p.
- Joyce, K, Allen, G, Halley, S and Beeson, J 2005, Aphrodite gold deposit, Kalgoorlie, WA, in *Regolith expression of Australian ore systems* edited by CRM Butt, IDM Robertson, KM Scott and M Cornelius: CRC LEME, Perth, Western Australia, p. 213–215.
- Kirkland, CL, Spaggiari, CV, Pawley, MJ, Wingate, MTD, Smithies, RH, Howard, HM, Tyler, IM, Belousova, EA and Poujol, M 2011a, On the edge: U–Pb, Lu–Hf, and Sm–Nd data suggests reworking of the Yilgarn Craton margin during formation of the Albany–Fraser Orogen: *Precambrian Research*, v. 187, p. 223–247.
- Kirkland, CL, Spaggiari, CV, Wingate, MTD, Smithies, RH, Belousova, EA, Murphy, R and Pawley, MJ 2011b, Inferences on crust–mantle interaction from Lu–Hf isotopes: a case study from the Albany–Fraser Orogen: Geological Survey of Western Australia, Record 2011/12, 25p.
- Kirkland, CL, Wingate, MTD, Spaggiari, CV and Pawley, MJ 2010, 194731: psammitic gneiss, Ponton Creek; *Geochronology Record* 860: Geological Survey of Western Australia, 5p.
- Krapež, B, Barley, ME and Brown, SJA 2008, Late Archaean synorogenic basins of the Eastern Goldfields Superterrane, Yilgarn Craton, Western Australia. Part I. Kalgoorlie and Gindalbie Terranes: *Precambrian Research*, v. 161, p. 135–153.
- Leybourne, MI and Rice, S 2013, Determination of gold in soils and sediments by fire assay or aqua regia digestion: choosing the optimal method: *Explore*, v. 158, p. 2–10.
- Lintern, MJ 1997, Calcrete sampling for gold exploration: *MESA Journal*, v. 5, p. 5–8.
- Lintern, MJ 2001, Exploration for gold using calcrete – lessons from the Yilgarn Craton, Western Australia: *Geochemistry: Exploration, Environment, Analysis*, v. 1, p. 237–252.
- Lintern MJ 2002, Calcrete sampling for mineral exploration, in *Calcrete: characteristics, distribution and use in mineral exploration* edited by XY Chen, MJ Lintern and IDM Robertson: CRC LEME, Perth, Western Australia, p. 31–109.
- Lintern, MJ and Anand, RR 2011, Biogeochemistry and surficial geochemistry at the Tropicana Gold Deposit, Western Australia, in *Programme and abstracts, 25th International Applied Geochemistry Symposium 2011, 22–26 August 2011, Rovaniemi, Finland* edited by P Sarala, VJ Ojala and M-L Porsanger: Vuorimiesyhdistys – Finnish Association of Mining and Metallurgical Engineers, Series B 92–1, p. 162–163.
- Lintern, MJ and Butt, CRM 1993, Pedogenic carbonate: an important sampling medium for gold exploration in semi-arid areas: *Exploration Research News*, v. 7, p. 7–11.
- Lintern, MJ and Butt, CRM 1997, Calcrete sampling for gold exploration: *Australasian Institute of Mining and Metallurgy Publication Series*, v. 1/97, p. 145–149.
- Lowry, DC 1970, Geology of the western part of the Eucla Basin: Geological Survey of Western Australia, Bulletin 122, 207p.
- Marnham, J, Sanders, AJ and Morris, PA 2002, State regolith south of 26th parallel (1:500 000 scale): Geological Survey of Western Australia, GeoVIEW.WA, digital data layer, viewed 13 December 2012, <<http://www.dmp.wa.gov.au/geoview>>.

- McKinnon-Mathews, J 1998, Annual Report for the Pleiades Lakes Project for the period 19 January 1997 to 18 January 1998, Exploration Licences E38/815–818, 493–500, 849, 512–513; WMC Resources Ltd: Geological Survey of Western Australia, Statutory mineral exploration report, A53953 (unpublished).
- McQueen, KG 2006, Calcrete geochemistry in the Cobar–Girilambone region, New South Wales: CRC LEME, Open File Report 200, Perth, Western Australia, 27p.
- McQueen, KG and Scott, KM 2008, Rock weathering and structure of regolith, *in* *Regolith Science edited by* KM Scott and CF Pain: CSIRO publishing, Melbourne, 461p.
- Miller, CR 2012, Cenozoic evolution of the Nullarbor Plain paleokarst, southern Australia: Geological Survey of Western Australia, Report 119, 185p.
- Morris, PA 2013a, Fine-fraction geochemistry of regolith from the east Wongatha area, Western Australia: tracing bedrock and mineralization through cover: Geological Survey of Western Australia, Record 2012/13, 58p.
- Morris, PA 2013b, Temporal controls on gold anomaly formation in regolith, *in* GSWA 2013 extended abstracts: promoting the prospectivity of Western Australia: Geological Survey of Western Australia, Record 2013/2, p. 21–22.
- Morris, PA, Coker, J and Faulkner, JA 1998, Geochemical mapping of the Mount Egerton 1:250 000 sheet: Geological Survey of Western Australia, 1:250 000 Regolith Geochemistry Series Explanatory Notes, 63p.
- Morris, PA, Sanders, AJ, McGuinness, SA, Coker, J and King, J 2000, Geochemical mapping of the Fraser Range region: Geological Survey of Western Australia, 1:250 000 Regolith Geochemistry Series Explanatory Notes, 45p.
- Morris, PA and Verren, AL 2001, Geochemical mapping of the Byro 1:250 000 sheet: Geological Survey of Western Australia, 1:250 000 Regolith Geochemistry Series Explanatory Notes, 53p.
- Myers, JS 1995, Geology of the Esperance 1:1 000 000 sheet (2nd edition): Geological Survey of Western Australia, 1:1 000 000 Geological Series Explanatory Notes, 10p.
- Nelson, DR, Myers, JS and Nutman, AP 1995, Chronology and evolution of the Middle Proterozoic Albany–Fraser Orogen, Western Australia: *Australian Journal of Earth Sciences*, v. 42, p. 481–495.
- Nesbitt, HW, Fedo, CM and Young, GM 1997, Quartz and feldspar stability, steady and non-steady-state weathering and petrogenesis of siliclastic sands and muds: *The Journal of Geology*, v. 105, p. 173–191.
- Nesbitt, HW and Young, GM 1982, Early Proterozoic climates and plate motions inferred from major element chemistry of lutites: *Nature*, v. 299, p. 715–717.
- Newsome, D 2000, Origin of sandplains in Western Australia: a review of the debate and some recent findings: *Australian Journal of Earth Science*, v. 47, p. 695–706.
- Oorschot, CW 2011, P–T–t evolution of the Fraser Zone, Albany–Fraser Orogen, Western Australia: Geological Survey of Western Australia, Record 2011/18, 101p.
- Pawley, MJ, Wingate, MTD, Kirkland, CL, Wyche, S, Hall, CE, Romano, SS and Doublier, MP 2012, Adding pieces to the puzzle: episodic crustal growth and a new terrane in the northeast Yilgarn Craton, Western Australia: *Australian Journal of Earth Sciences*, v. 59, p. 603–623.
- Perincek, D 1998, A compilation and review of data pertaining to the hydrocarbon prospectivity of the Officer Basin: Geological Survey of Western Australia, Record 1997/6, 209p.
- Perkins, M 2004, Tropicana East JV, Annual report for the tenements: E39/951, E39/952, East JV Project, C154/2002, E39/951, E39/952, E39/954, E39/956, E39/1012, E39/1013, E39/1016 for the period 21/08/03–20/08/04, C154/2002: Anglogold Ashanti Australia Ltd: Geological Survey of Western Australia, Statutory Mineral Exploration Report, A69410 (unpublished).
- Pye, KJ, Coker, J, Faulkner, JA and Sanders, AJ 1998, Geochemical mapping of the Edmund 1:250 000 sheet: Geological Survey of Western Australia, 1:250 000 Regolith Geochemistry Series Explanatory Notes, 51p.
- R Development Core Team 2008, R: A language and environment for statistical computing, R Foundation for Statistical Computing, viewed 27 March 2014, <<http://www.R-project.org>>.
- Reimann, C, De Caritat, P, GEMAS project team and NGSa project team 2012, New soil composition data for Europe and Australia: demonstrating comparability, identifying continental-scale processes and learning lessons for global geochemical mapping: *Science of the Total Environment*, v. 416, p. 239–252.
- Reimann, C, Filzmoser, P, Garrett, RG and Dutter, R 2010, Statistical data analysis explained: John Wiley and Sons, Chichester, England, 343p.
- Rudnick, RL and Gao, S 2003, Composition of the Continental Crust: *Treatise on geochemistry*, v. 3: Elsevier, Amsterdam, The Netherlands, p. 1–64.
- Scheib, AJ 2013, The National Geochemical Survey of Australia – selected interpretations and discussion for Western Australian data: Geological Survey of Western Australia, Record 2013/4, 47p.
- Scott, KM and Howard, RW 2005, Panglo Gold District, Eastern Goldfields, WA, *in* *Regolith expression of Australian ore systems edited by* CRM Butt, IDM Robertson, KM Scott and M Cornelius: CRC LEME, Perth, Western Australia, p. 304–306.
- Sirius Resources NL 2013, Sirius Resources, Perth, viewed 18 September 2013, <<http://www.siriusresources.com.au/projects-fraserange>>.
- Smithies, RH, Spaggiari, CV, Kirkland, CL, Howard, HM and Maier, WD 2013, Petrogenesis of gabbros of the Mesoproterozoic Fraser Zone: constraints on the tectonic evolution of the Albany–Fraser Orogen: Geological Survey of Western Australia, Record 2013/5, 29p.
- Spaggiari, CV, Bodorkos, S, Barquero-Molina, M, Tyler, IM and Wingate, MTD 2009, Interpreted bedrock geology of the south Yilgarn and central Albany–Fraser Orogen, Western Australia: Geological Survey of Western Australia, Record 2009/10, 84p.
- Spaggiari, CV, Kirkland, CL, Pawley, MJ, Smithies, RH, Wingate, MTD, Doyle, MG, Blenkinsop, TG, Clarke, C, Oorschot, CW, Fox, LJ and Savage, J 2011, The geology of the east Albany–Fraser Orogen — a field guide: Geological Survey of Western Australia, Record 2011/23, 97p.
- Spaggiari, CV, Kirkland, CL, Pawley, MJ, Wingate MTD, Smithies, RH and Howard, HM 2010, Building the Proterozoic Albany–Fraser Orogen on the Yilgarn Craton margin: setting the scene for Tropicana, *in* GSWA 2013 extended abstracts: promoting the prospectivity of Western Australia: Geological Survey of Western Australia, p. 30–32.
- Spaggiari, CV and Pawley, MJ 2012, Interpreted pre-Mesozoic bedrock geology of the east Albany–Fraser Orogen and southeast Yilgarn Craton (1:500 000), *in* *The geology of the east Albany–Fraser Orogen — a field guide*: Geological Survey of Western Australia, Record 2011/23, Plate 1.
- Stanford, RF, Pierson, CT and Crovelli, RA 1993, An objective replacement method for censored geochemical data: *Mathematical Geology*, v. 25, no. 1, p. 59–80.
- Tropicana Joint Venture 2010, Tropicana gold project: Tropicana Joint Venture, viewed 24 September 2013, <<http://www.tropicana-jv.com.au/IRM/Company/ShowPage.aspx/PDFs/886-34073790/TropicanaProjectOverview>>.
- Tyler, IM and Hocking, RM 2008, 1:500 000 interpreted bedrock geology of Western Australia, 2008 update: Geological Survey of Western Australia, GeoVIEW.WA, digital data layer, viewed 13 December 2012, <<http://www.dmp.wa.gov.au/geoview>>.

Appendix 1

Site coordinates for all GSWA samples collected in the study area

GSWA number	Zone	Easting	Northing	GSWA number	Zone	Easting	Northing	GSWA number	Zone	Easting	Northing
161738	51	458187	6464124	163416	51	503560	6533217	163937	51	474493	6480447
161739	51	457757	6476064	163417	51	501538	6523950	163941	51	462748	6472752
161740	51	457382	6483345	163428	51	513689	6554030	164030	51	522350	6568960
161741	51	455577	6495770	163504	51	453668	6443285	164031	51	514168	6569320
161743	51	474402	6495400	163542	51	454835	6491927	164032	51	504457	6566825
161745	51	478082	6487563	163543	51	462361	6491705	164036	51	505640	6535030
161746	51	470067	6487930	163544	51	468823	6491676	164037	51	504228	6526730
161747	51	461486	6487826	163545	51	478106	6491546	164048	51	510670	6559825
161748	51	462373	6479828	163547	51	475302	6485009	194001	51	419807	6330606
161749	51	469567	6479165	163548	51	467290	6483160	194002	51	421218	6341750
161753	51	467887	6472079	163549	51	466320	6476824	194003	51	420957	6352780
161754	51	462695	6464839	163553	51	462512	6467871	194005	51	420980	6352755
161761	51	489048	6503850	163558	51	477230	6499458	194006	51	437595	6388128
161762	51	482024	6503396	163559	51	465493	6499929	194007	51	446321	6401771
161763	51	473778	6504031	163560	51	458389	6500242	194008	51	468594	6404424
161764	51	465408	6504930	163562	51	462560	6507622	194009	51	492797	6390700
161765	51	458973	6503924	163563	51	469936	6507787	194010	51	498319	6390688
161767	51	460786	6511970	163564	51	478406	6507514	194011	51	500176	6388966
161768	51	469361	6511962	163565	51	487008	6507389	194012	51	502647	6389175
161769	51	477555	6512670	163596	51	461589	6460493	194013	51	484412	6404211
163126	51	454023	6471122	163718	51	537735	6412785	194014	51	492805	6412405
163129	51	458278	6492005	163751	51	484694	6503209	194015	51	492621	6418059
163130	51	466645	6491288	163752	51	478330	6503941	194016	51	506528	6410253
163131	51	474999	6491499	163753	51	470906	6503657	194022	51	546206	6535184
163132	51	481208	6491977	163754	51	462003	6504706	194024	51	541259	6537629
163134	51	470800	6484837	163755	51	454278	6503270	194027	51	540271	6537501
163135	51	463386	6477146	163757	51	464702	6512071	194028	51	540330	6549828
163136	51	469561	6475511	163758	51	473413	6512175	194029	51	537271	6554186
163224	51	513825	6564055	163759	51	482460	6512521	194030	51	543157	6561952
163225	51	505916	6563108	163813	51	508988	6569965	194031	51	549667	6580929
163226	51	501842	6559196	163814	51	501031	6567209	194033	51	559618	6584128
163228	51	501854	6542882	163815	51	506494	6555759	194034	51	562725	6582154
163229	51	503228	6536942	163817	51	506546	6539230	194036	51	567577	6577531
163230	51	500586	6529847	163818	51	505811	6530309	194037	51	561910	6579944
163240	51	509821	6539109	163829	51	509060	6554521	194039	51	559287	6583645
163241	51	513455	6551894	163830	51	516819	6558325	194040	51	555461	6591237
163242	51	513870	6558772	163831	51	516709	6551980	194041	51	566107	6608788
163350	51	486456	6487895	163842	51	567493	6554791	194042	51	554122	6630916
163353	51	472988	6500787	163903	51	453721	6447781	194043	51	554857	6628196
163354	51	462257	6500346	163926	51	457978	6466943	194044	51	563308	6628069
163355	51	453870	6500038	163927	51	457291	6479219	194045	51	560403	6654463
163356	51	457826	6507477	163928	51	458310	6487974	194046	51	676139	6755527
163357	51	466169	6508054	163929	51	459535	6496057	194047	51	667638	6772853
163358	51	474747	6506895	163930	51	470299	6497007	194048	51	658368	6772853
163359	51	481593	6507257	163931	51	477793	6496804	194051	51	660746	6792496
163410	51	517277	6564716	163932	51	482370	6487604	194052	51	649143	6759923
163411	51	510288	6563185	163933	51	474455	6487893	194053	51	627668	6743611
163412	51	500428	6562690	163934	51	466650	6487827	194054	51	616168	6723937
163413	51	501624	6556711	163935	51	461746	6484336	194055	51	588892	6729273
163415	51	502425	6539689	163936	51	465608	6480571	194056	51	587557	6702621

Appendix 2

List of analytical methods carried out for each sample collected in the study area

GSWA number	XRF <2 mm	ICP-MS <2 mm to >45 µm	AR <50 µm	TL9 <50 µm	TL7 <50 µm	TL0 <50 µm	Category ^(a)	GSWA number	XRF <2 mm	ICP-MS <2 mm to >45 µm	AR <50 µm	TL9 <50 µm	TL7 <50 µm	TL0 <50 µm	Category ^(a)
194056	y	-	y	y	y	-	5	163224	-	y	y	y	y	-	1
194055	y	-	y	y	y	-	5	163225	-	y	y	y	y	-	1
194054	y	-	y	y	y	-	5	163226	-	y	y	y	y	-	1
194053	y	-	y	y	y	-	4	163228	-	y	y	y	y	-	1
194052	y	-	y	y	y	-	4	163229	-	y	y	y	y	-	1
194051	y	-	y	y	y	-	5	163230	-	y	y	y	y	-	1
194048	y	-	y	y	y	-	4	163240	-	y	y	y	y	-	1
194047	y	-	y	-	-	-	6	163241	-	y	y	y	y	-	1
194046	y	-	y	-	-	-	6	163242	-	y	y	y	y	-	1
194045	y	-	y	y	y	-	4	163353	-	y	y	y	y	-	1
194044	y	-	y	-	-	-	6	163354	-	y	y	y	y	-	1
194043	y	-	y	y	y	-	5	163355	-	y	y	y	y	-	1
194042	y	-	y	y	y	-	5	163356	-	y	y	y	y	-	1
194041	y	-	y	y	y	-	5	163357	-	y	y	y	y	-	1
194040	y	-	y	y	y	-	5	163358	-	y	y	y	y	-	1
194039	y	-	y	y	y	-	4	163359	-	y	y	y	y	-	1
194037	y	-	y	y	y	-	4	163410	-	y	y	y	y	-	1
194036	y	-	y	y	y	-	4	163411	-	y	y	y	y	-	1
194034	y	-	y	y	y	-	4	163412	-	y	y	y	y	-	1
194033	y	-	y	y	y	-	4	163413	-	y	y	y	y	-	1
194031	y	-	y	y	y	-	5	163415	-	y	y	y	y	-	1
194030	y	-	y	y	y	-	5	163416	-	y	y	y	y	-	1
194029	y	-	y	y	y	-	4	163417	-	y	y	y	y	-	1
194028	y	-	y	y	y	-	4	163428	-	y	y	y	y	-	1
194027	y	-	y	y	y	-	5	163504	-	y	y	y	y	-	1
194024	y	-	y	-	-	-	6	163542	-	y	y	y	y	-	1
194022	y	-	y	y	y	-	4	163543	-	y	y	y	y	-	1
194016	y	-	y	y	y	-	4	163544	-	y	y	y	y	-	1
194015	y	-	y	y	y	-	4	163545	-	y	y	y	y	-	1
194014	y	-	y	y	y	-	4	163547	-	y	y	y	y	-	1

GSWA number	XRF	ICP-MS	AR	TL9	TL7	TL0	Category ^(a)	GSWA number	XRF	ICP-MS	AR	TL9	TL7	TL0	Category ^(a)
	<2 mm	<2 mm to >45 µm	<50 µm	<50 µm	<50 µm	<50 µm			<2 mm	<2 mm to >45 µm	<50 µm	<50 µm	<50 µm	<50 µm	
194013	y	-	y	y	y	-	4	163548	-	y	y	y	y	-	1
194012	y	-	y	y	y	-	4	163549	-	y	y	y	y	-	1
194011	y	-	y	y	y	y	5	163553	-	y	y	y	y	-	1
194010	y	-	y	y	y	y	5	163558	-	y	y	y	y	-	1
194009	y	-	y	y	y	y	5	163559	-	y	y	y	y	-	1
194008	y	-	y	y	y	-	4	163560	-	y	y	y	y	-	1
194007	y	-	y	y	y	y	5	163562	-	y	y	y	y	-	1
194006	y	-	y	y	y	-	4	163563	-	y	y	y	y	-	1
194005	y	-	y	y	y	y	5	163564	-	y	y	y	y	-	1
194003	y	-	y	-	-	-	6	163565	-	y	y	y	y	-	1
194002	y	-	y	y	y	-	4	163596	-	y	y	y	y	-	1
194001	y	-	y	y	y	-	4	163751	-	y	y	y	y	-	1
163934	y	y	y	y	y	-	2	163752	-	y	y	y	y	-	1
163932	y	y	y	y	y	y	3	163753	-	y	y	y	y	-	1
163842	y	y	y	y	y	y	3	163754	-	y	y	y	y	-	1
163718	y	y	y	y	y	y	3	163755	-	y	y	y	y	-	1
163617	y	y	y	y	y	-	2	163757	-	y	y	y	y	-	1
163350	y	y	y	y	y	y	3	163758	-	y	y	y	y	-	1
163136	y	y	y	y	y	y	3	163759	-	y	y	y	y	-	1
161753	y	y	y	y	y	y	3	163813	-	y	y	y	y	-	1
161738	-	y	y	y	y	-	1	163814	-	y	y	y	y	-	1
161739	-	y	y	y	y	-	1	163815	-	y	y	y	y	-	1
161740	-	y	y	y	y	-	1	163817	-	y	y	y	y	-	1
161741	-	y	y	y	y	-	1	163818	-	y	y	y	y	-	1
161743	-	y	y	y	y	-	1	163829	-	y	y	y	y	-	1
161745	-	y	y	y	y	-	1	163830	-	y	y	y	y	-	1
161746	-	y	y	y	y	-	1	163831	-	y	y	y	y	-	1
161747	-	y	y	y	y	-	1	163903	-	y	y	y	y	-	1
161748	-	y	y	y	y	-	1	163926	-	y	y	y	y	-	1
161749	-	y	y	y	y	-	1	163927	-	y	y	y	y	-	1

GSWA number	XRF <2 mm	ICP-MS <2 mm to >45 µm	AR <50 µm	TL9 <50 µm	TL7 <50 µm	TL0 <50 µm	Category ^(a)	GSWA number	XRF <2 mm	ICP-MS <2 mm to >45 µm	AR <50 µm	TL9 <50 µm	TL7 <50 µm	TL0 <50 µm	Category ^(a)
161754	–	y	y	y	y	–	1	163928	–	y	y	y	y	–	1
161761	–	y	y	y	y	–	1	163929	–	y	y	y	y	–	1
161762	–	y	y	y	y	–	1	163930	–	y	y	y	y	–	1
161763	–	y	y	y	y	–	1	163931	–	y	y	y	y	–	1
161764	–	y	y	y	y	–	1	163933	–	y	y	y	y	–	1
161765	–	y	y	y	y	–	1	163935	–	y	y	y	y	–	1
161767	–	y	y	y	y	–	1	163936	–	y	y	y	y	–	1
161768	–	y	y	y	y	–	1	163937	–	y	y	y	y	–	1
161769	–	y	y	y	y	–	1	163941	–	y	y	y	y	–	1
163126	–	y	y	y	y	–	1	164030	–	y	y	y	y	–	1
163129	–	y	y	y	y	–	1	164031	–	y	y	y	y	–	1
163130	–	y	y	y	y	–	1	164032	–	y	y	y	y	–	1
163131	–	y	y	y	y	–	1	164036	–	y	y	y	y	–	1
163132	–	y	y	y	y	–	1	164037	–	y	y	y	y	–	1
163134	–	y	y	y	y	–	1	164048	–	y	y	y	y	–	1
163135	–	y	y	y	y	–	1								

NOTES: (a) 'Category' corresponds to Figure 5

– not determined
AR aqua regia digest
ICP-MS inductively coupled plasma—mass spectrometry
TL0 TerraLeach0 digest
TL7 TerraLeach7 digest
TL9 TerraLeach9 digest
XRF X-ray fluorescence spectrometry

Appendix 3

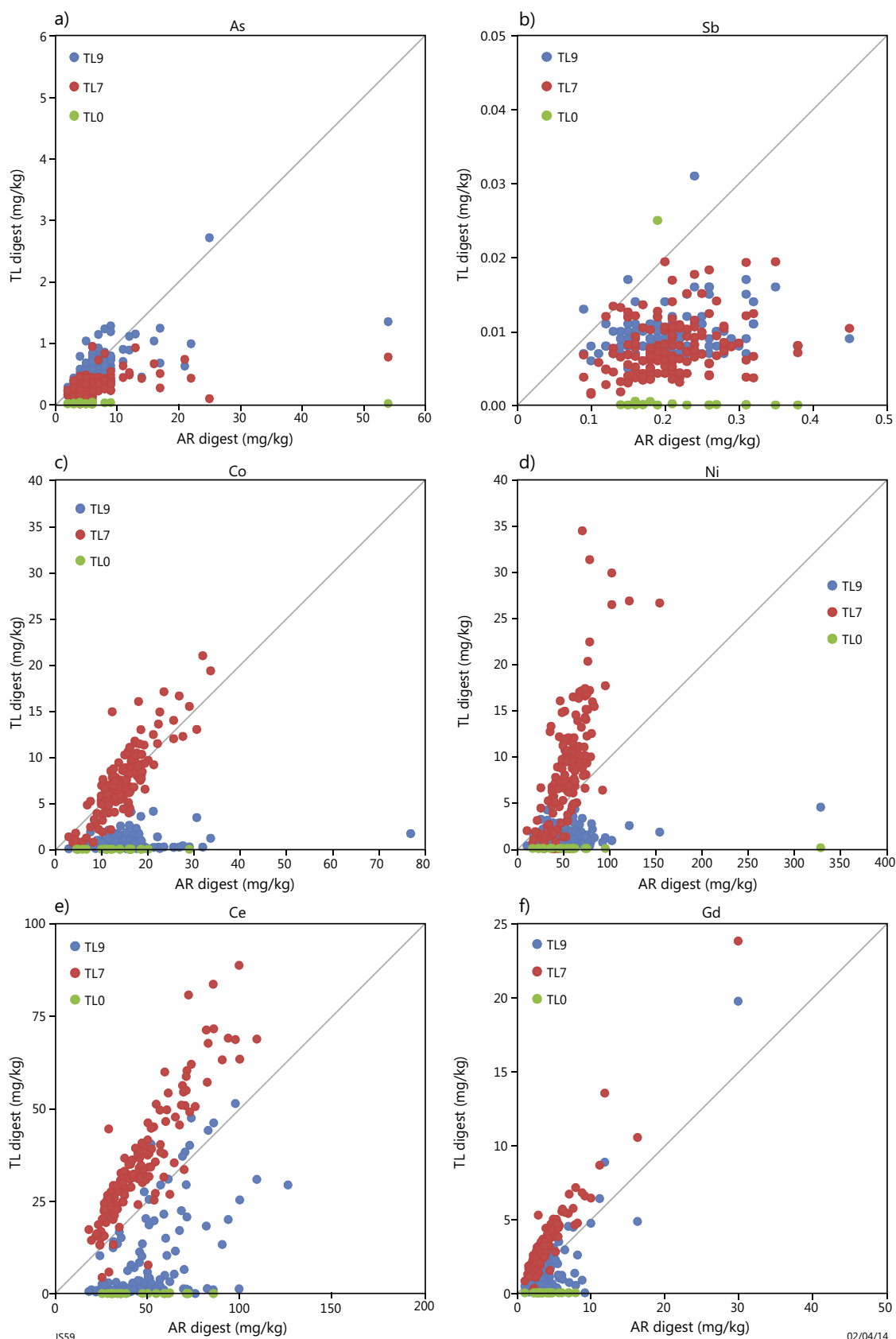
Median concentrations of 52 trace elements in the fine fraction (<50 µm) following various digestions, and the reported lower limit of detection

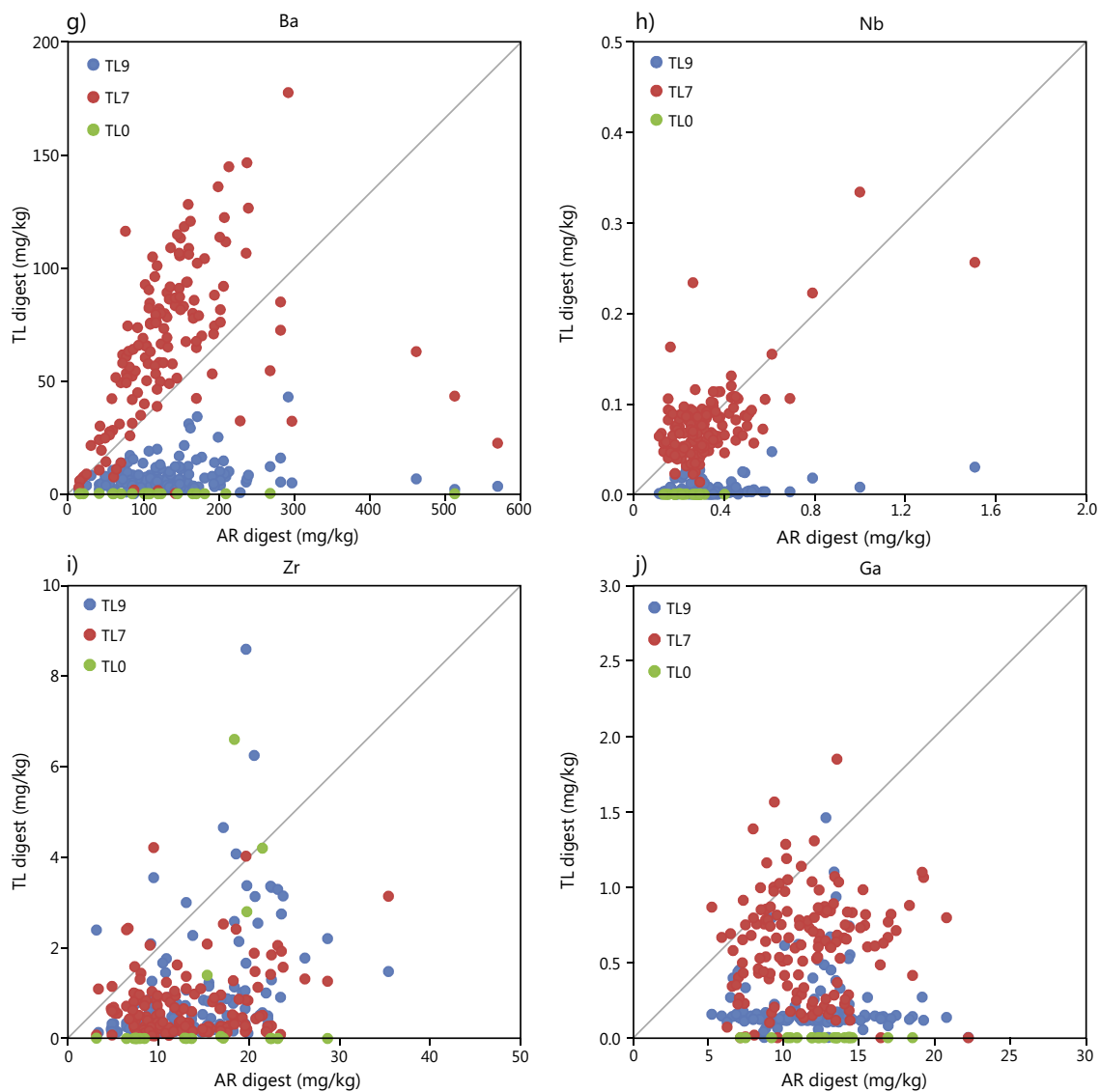
Element	AR			TL7			TL9			TL0		
	Unit	LLD	Median	Unit	LLD	Median	Unit	LLD	Median	Unit	LLD	Median
Ag	mg/kg	0.05	<LLD	µg/kg	0.5	29.4	µg/kg	2	<LLD	µg/kg	0.05	0.51
As	mg/kg	1	6.00	µg/kg	5	249	µg/kg	20	425	µg/kg	0.5	8.70
Au	µg/kg	1	6.00	µg/kg	0.1	0.86	µg/kg	0.5	1.20	µg/kg	0.05	0.22
Ba	mg/kg	1	119	mg/kg	0.01	67.5	mg/kg	0.05	5.40	µg/kg	0.3	31.3
Be	mg/kg	0.05	1.09	µg/kg	5	333	µg/kg	20	96.0	µg/kg	0.5	<LLD
Bi	mg/kg	0.01	0.21	µg/kg	1	52.6	µg/kg	5	<LLD	µg/kg	0.02	0.02
Cd	mg/kg	0.05	<LLD	µg/kg	1	39.2	µg/kg	5	<LLD	µg/kg	0.1	0.40
Ce	mg/kg	0.01	42.5	µg/kg	0.1	32183	µg/kg	0.5	1467	µg/kg	0.01	8.27
Co	mg/kg	0.1	14.4	µg/kg	5	7098	µg/kg	20	286	µg/kg	0.5	2.75
Cr	mg/kg	2	125	mg/kg	0.2	9.85	mg/kg	0.2	2.50	mg/kg	0.05	<LLD
Cu	mg/kg	1	30.0	mg/kg	0.05	13.0	mg/kg	0.2	6.25	mg/kg	0.05	<LLD
Dy	mg/kg	0.01	2.80	mg/kg	0.1	1894	µg/kg	0.5	347	µg/kg	0.01	1.04
Er	mg/kg	0.01	1.42	µg/kg	0.05	1191	µg/kg	0.2	154	µg/kg	0.005	0.60
Eu	mg/kg	0.01	0.91	µg/kg	0.05	836	µg/kg	0.2	132	µg/kg	0.005	0.25
Ga	mg/kg	0.05	11.2	µg/kg	1	647	µg/kg	5	132	µg/kg	0.1	0.60
Gd	mg/kg	0.01	3.34	µg/kg	0.05	2992	µg/kg	0.2	458	µg/kg	0.005	0.99
Ge	mg/kg	0.05	<LLD	µg/kg	5	10.0	µg/kg	20	<LLD	µg/kg	0.5	<LLD
Hf	mg/kg	0.01	0.31	µg/kg	0.2	14.6	µg/kg	1	6.00	µg/kg	0.02	0.10
Hg	mg/kg	0.2	<LLD	µg/kg	5	34.5	µg/kg	20	<LLD	µg/kg	0.5	<LLD
Ho	mg/kg	0.01	0.53	µg/kg	0.05	442	µg/kg	0.2	63.5	µg/kg	0.005	0.15
In	mg/kg	0.01	0.05	µg/kg	0.1	8.72	µg/kg	0.5	<LLD	µg/kg	0.01	<LLD
La	mg/kg	0.01	21.1	µg/kg	0.1	15033	µg/kg	0.5	1588	µg/kg	0.01	4.31
Li	mg/kg	0.1	23.8	µg/kg	2	891	µg/kg	10	201	µg/kg	0.3	6.90
Lu	—	—	—	µg/kg	0.05	135	µg/kg	0.2	18.1	µg/kg	0.005	0.05
Mo	mg/kg	0.1	0.50	µg/kg	20	49.0	µg/kg	0.1	<LLD	µg/kg	0.3	<LLD
Nb	mg/kg	0.02	0.28	µg/kg	0.2	69.2	µg/kg	1	3.00	µg/kg	0.02	0.09
Nd	mg/kg	0.01	20.2	µg/kg	0.01	17914	µg/kg	0.5	2118	µg/kg	0.01	5.09
Ni	mg/kg	1	54.0	mg/kg	0.05	7.82	mg/kg	0.2	1.10	mg/kg	0.05	<LLD
Pb	mg/kg	1	12.0	mg/kg	0.02	5.88	mg/kg	0.1	<LLD	µg/kg	3	<LLD
Pd	µg/kg	10	<LLD	µg/kg	20	<LLD	mg/kg	0.1	<LLD	µg/kg	0.05	0.11
Pr	mg/kg	0.005	5.50	µg/kg	0.05	4403	µg/kg	0.2	454	µg/kg	0.005	1.52
Pt	µg/kg	5	<LLD	µg/kg	0.5	<LLD	µg/kg	2	<LLD	µg/kg	0.05	<LLD
Rb	mg/kg	0.02	40.6	—	—	—	—	—	—	—	—	—
Sb	mg/kg	0.02	0.20	µg/kg	0.5	6.90	µg/kg	2	9.00	µg/kg	0.05	0.07
Sc	mg/kg	1	12.0	mg/kg	0.1	0.20	mg/kg	0.1	<LLD	mg/kg	0.05	<LLD
Se	mg/kg	1	<LLD	µg/kg	20	165	mg/kg	0.1	<LLD	µg/kg	3	11.0
Sm	mg/kg	0.01	4.34	µg/kg	0.1	3477	µg/kg	0.5	532.15	µg/kg	0.01	1.03
Sn	mg/kg	0.05	1.70	µg/kg	5	185	µg/kg	20	<LLD	µg/kg	0.5	<LLD
Sr	mg/kg	0.02	107	—	—	—	—	—	—	—	—	—
Ta	mg/kg	0.01	<LLD	µg/kg	0.1	1.20	µg/kg	0.2	0.50	µg/kg	0.02	<LLD
Tb	mg/kg	0.005	0.48	µg/kg	0.05	411	µg/kg	0.2	64.5	µg/kg	0.005	0.12
Te	mg/kg	0.05	<LLD	µg/kg	5	15.0	µg/kg	20	<LLD	µg/kg	0.5	<LLD
Th	mg/kg	0.01	10.5	µg/kg	0.2	313	µg/kg	1	147	µg/kg	0.02	0.59
Tl	mg/kg	0.01	0.22	µg/kg	0.5	18.3	µg/kg	2	4.50	µg/kg	0.05	0.06
Tm	mg/kg	0.01	0.19	µg/kg	0.05	158	µg/kg	0.2	19.6	µg/kg	0.005	0.06
U	mg/kg	0.01	0.79	µg/kg	0.2	351	µg/kg	1	203	µg/kg	0.02	1.33
V	mg/kg	2	76.0	mg/kg	0.2	12.5	mg/kg	0.2	3.10	mg/kg	0.05	<LLD
W	mg/kg	0.05	0.06	µg/kg	1	30.5	µg/kg	5	17.0	µg/kg	0.1	2.25
Y	mg/kg	0.02	14.0	µg/kg	0.2	11630	µg/kg	1	1642	µg/kg	0.02	4.72
Yb	mg/kg	0.01	1.23	µg/kg	0.1	969	µg/kg	0.5	123	µg/kg	0.01	0.47
Zn	mg/kg	1	40.0	µg/kg	1	5003	µg/kg	1	712	µg/kg	1	<LLD
Zr	mg/kg	0.1	12.5	µg/kg	1	495	µg/kg	1	326	µg/kg	0.1	3.15

NOTES: — not determined
AR aqua regia
TL9 TerraLeach9
TL7 TerraLeach7
TL0 TerraLeach0
LLD Lower limit of detection

Appendix 4

Bivariate plots of concentrations following TerraLeach (TL) and aqua regia (AR) digestions for elements As, Sb, Co, Ni, Ce, Gd, Ba, Nb, Zr, and Ga. TL9, TL7, and TL0 are described in Table 3.





JS59

02/04/14

This Record is published in digital format (PDF) and is available as a free download from the DMP website at
<www.dmp.wa.gov.au/GSWApublications>.

Further details of geological products produced by the Geological Survey of Western Australia can be obtained by contacting:

Information Centre
Department of Mines and Petroleum
100 Plain Street
EAST PERTH WESTERN AUSTRALIA 6004
Phone: (08) 9222 3459 Fax: (08) 9222 3444
www.dmp.wa.gov.au/GSWApublications

